exosat esa

EXOSAT EXPRESS

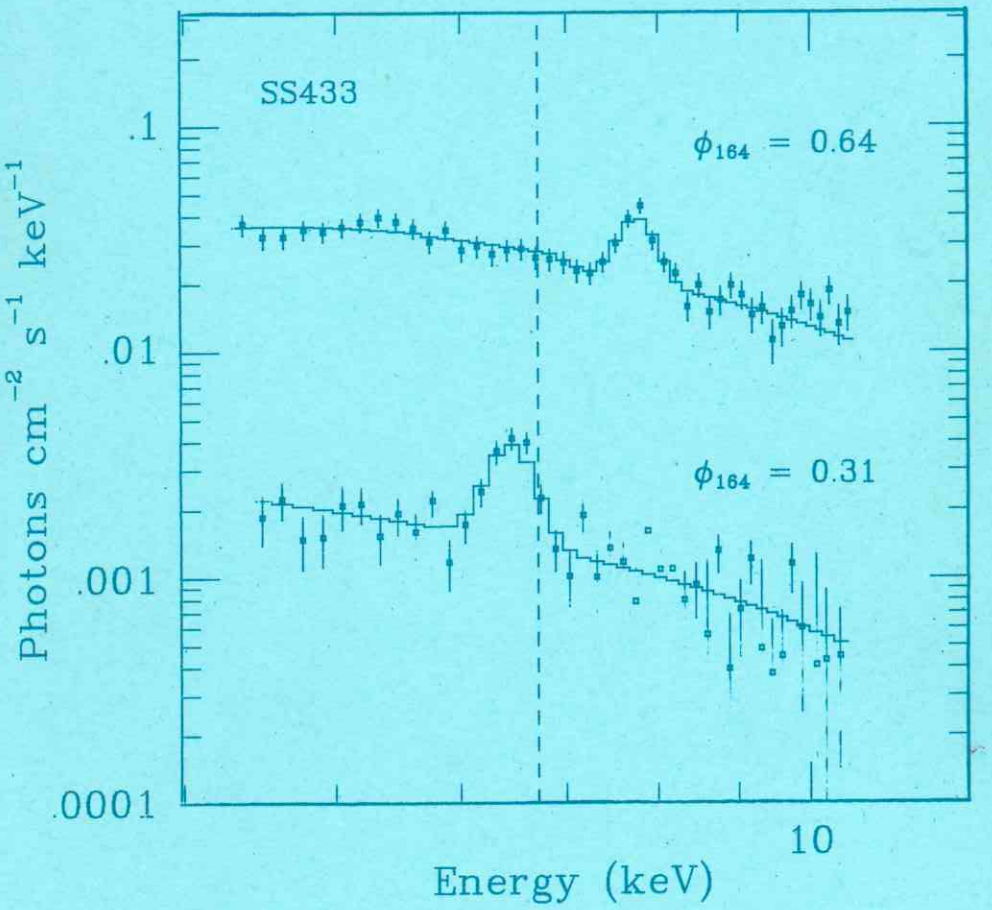

EXOSAT
EUROPEAN X-RAY ASTRONOMY SATELLITE

No. 12 August 1985

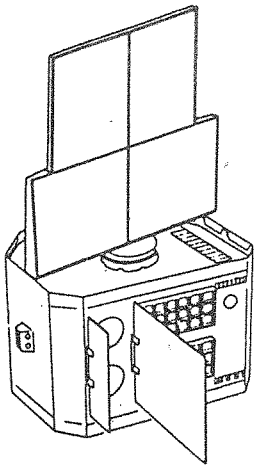

esa

EXOSAT EXPRESS

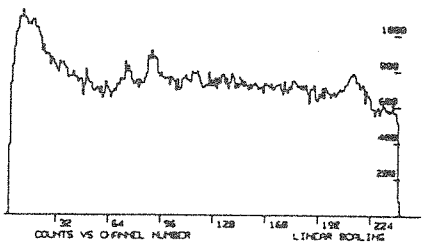

TABLE OF CONTENTS

NO. 12 AUGUST 1985

Front Cover

Photon spectra derived from GSPC observations of SS433 made at two phases of the 164 day cycle (0.64 phase spectrum shifted by 1 decade in intensity). The emission feature evident at 6.5 keV (phase 0.31) and at 7.6 keV (0.64) corresponds with that expected from 6.7 keV iron emission (the rest wavelength is indicated by the vertical dashed line) doppler-shifted according to the ephemeris of the blue-shifted optical line.

Courtesy: G.C. Stewart, M.G. Watson, W. Brinkmann

FOREWORD

AO-4 was issued in August 1985 with a response required by 1st January 1986. The observing programme, which will have a duration from March 1986 to the end of the mission, will be by recommended to the Agency by the Committee on Observation Proposal Selection (COPS) in February next year. Attention is drawn to the note on p.2 concerning advance time lines during the period of orbit manoeuvres (Jan 86 to the end of mission) and the increased likelihood of changes with little warning.

Several articles on aspects of the LE1 telescope calibration and data analysis are published in this issue of the Express. Of particular interest are the discussions of CMA sensitivity (p.33) and EXOSAT source position determination (p.53). Inclusion of a number of factors in the IA analysis software has cumulatively given an improvement of several arc seconds in correlation between EXOSAT positions and known optical/radio positions of a sample of sources. Note that there are presently no plans to modify the automatic analysis software to include these effects, although it is highly probable that the majority of the images will at some future date be re-analysed to determine the best positions of both known and serendipitous sources.Observers primarily interested in very accurate position determination are requested to contact the Observatory and/or apply to use the IA system.

Release of data from the EXOSAT data archive has started. Some 60 requests for data have been received, representing a few hundred FOT's. With a few exceptions, release has been authorised and the tapes are now being despatched from ESOC.

An announcement is given on p.84 of a Cambridge Discussion Meeting on EXOSAT results to be held on 5/6 November 1985. Notice is given on pp.85/88 of current vacancies within ESA's Space Science Department and readers are kindly requested to display a copy of the advertisements or bring them to the attention of any suitable candidates.

EXOSAT EXPRESS

Editor: David Andrews

Published by: EXOSAT Observatory,
ESOC,
Robert Bosch Str.5,
6100 Darmstadt,
W. Germany.

Tel: 06151-886-705
Telex: 419453/49441
Telefax: 886/622/611

OBSERVATORY STATUS AS OF 31.8.85

The AO-3 programme of observations is 38% complete with many of the important galactic centre observations carried out in the last two months. Because of the planned modifications to EXOSAT's orbit in order to extend the mission lifetime, advance time lines for both the AO-3 programme post-January 14th 1986 and the approved AO-4 observations will be more liable to real time changes. In principle, an orbit modification per orbit may be executed and PI's are advised that observation times may change with little prior notice, although the Observatory Team will strive to minimise the subsidiary effects of any unavoidable changes, particularly in respect of co-ordinated observations.

1. Hardware

There have been no changes in the status of the spacecraft hardware.

On day 232 (August 20th 1985) at 01.02Z, the monitored HT's of ME detector C suddenly decreased from 2195V to 2048V for the Argon supply and from 2003V to 1926V for the Xenon supply. Both HT's were immediately switched off. Subsequent tests indicate that the Detector C monitored HT's are stable at 77V and 147V below the nominal values for Xenon and Argon respectively. Background energy spectra in the Argon and Xenon ranges suggest normal proportional counter operation at a gas gain about a factor of 5 lower than nominal, not consistent with the above reduced voltages on the detector anodes. Further investigation and analysis of data is in progress, however Detector C is currently not operated. The other seven detectors of the ME experiment continue to function satisfactorily.

2. Performance and Operations

Tables 1 and 2 on p.5/6 give the current performance parameters of the EXOSAT instruments.

New star tracker calibration reference data (Local Lord Points) has been implemented on 30.7.85 and subsequent measurements indeed show an improvement in star separation errors. A sample of X-ray objects with accurately known optical/radio positions has been analysed to include the improved calibration data together with a number of other effects such as the 5" offset of the Y-axis limit-cycle (ref. Express No. 4 p.34) - refer to the article on p.53. A clear improvement in the correlation between EXOSAT position and known RA, DEC has been demonstrated and EXOSAT source positions can now generally be quoted to an accuracy of about 5 or 6 arcseconds.

Some observers have reported anomalies in the power spectra of data obtained with the GSPC experiment and the OBC in DIRECT mode, specifically spikes in the spectra at the software cycle frequency and at associated harmonics. This is believed to result from use of an SDS set-up which samples the GSPC E channel at 2K s^{-1} and 'misses' two sample slots/SWC (ref. Express No. 5 p.38) separated by 0.5 x SWC. In spectral analysis (arguably the GSPC's prime function), this minor loss of samples can be ignored whereas for timing analysis when data is summed over 100.000's of SWC's, corrections must be incorporated arbitrarily into the transform. All SDS configurations have been modified to avoid this problem and PI's who wish to use the GSPC DIRECT mode for timing studies should contact the Observatory.

Minor loss of observing time has occurred on a number of occasions for a variety of reasons, viz: power failure at VILSPA (day 193, $\sim$ 1 hr), solar activity (day 198, LE1 only operated for $\sim$18 hrs), antenna problems (day 213/214, $\sim$ 2 hrs) and real time graphics computer hardware faults (day 223/224, LE1 not operated because no real time monitor of the detector gain was possible).

3. On-board Software

Attention is drawn to the note on p.76 giving details of the use of MHER7, which processes the ME experiment data and provides high time resolution (sub-millisecond) intensity samples with an option of limited energy resolution.

Specification, development and initial testing of MHTR4, a further high time resolution ME application program, has been completed. Operational use of MHTR4 will start as soon as realistic tests have been carried out on a bright X-ray source. A detailed specification and operational procedures will be given in the next issue of the Express, but in the meantime PI's with observations for which this mode may be suitable (eg. bright sources, for which extremely high time resolution is required or when the use of MHER7 is CPU-limited) should contact A. Parmar at the Observatory. Basically, MHTR4 processes ME energy data and sets a single bit to '1' or '0' per sample corresponding to the presence or absence of a photon within a defined selectable energy range. In its expected normal mode of operation, it will provide 0.25 msec time resolution data and use 58% of the available telemetry.

4. Future Plans

Given the current estimates of the remaining attitude control gas and the natural decay of the EXOSAT orbit in April 1986, the strategy for raising the orbit perigee height to extend the lifetime beyond its natural termination will consist of the following:

- review of fuel situation at beginning of 1986.
- Delta V manoeuvre of 10 ms^{-1} (maximum possible) on 14.1.86.
- Delta V manoeuvre of 10 ms^{-1} on 14.2.86.
- review of fuel situation in March 1986 and scheduling of further Delta V's.

These two 'Delta V's' in January and February will extend the mission lifetime by about 6 weeks to the end of May 1986 and will provide realistic figures of attitude gas usage for stabilisation during the manoeuvre, an important input to the planning of any further orbit changes.

Now that regular gauging exercises are carried out to estimate attitude gas usage, it should prove possible by recognising changes in thermal inertial of the propane at the liquid/gas transition to identify with some confidence a point in time when approximately 1 kg of gas remains, sufficient for about 4 months of operation. At this stage a programme of observations with the LE1 grating will be assessed and attempts made to position the grating correctly in the FOV of the X-ray beam in order to devote the final few orbits of the mission to important grating observations.

One final major update of the FOT Handbook is planned and should be complete by the end of the year. It will consist mainly of detailed specifications of new OBC modes (e.g. MHER7, MHTR4 etc.) and descriptions of the recent calibrations and CCF modifications - most of this information has already been published in various issues of the Express. Users who received update no.2 or collected it at the Observatory will automatically receive the relevant pages of update no. 3.

TABLE 1

PERFORMANCE CHARACTERISTICS (LE)

LE1	Characteristics			
Energy Range	0.04-2 keV (6-300 A) CMA*			
	0.3 - 2 keV PSD			
Energy resolution	Five filters are available for broad-band spectroscopy (CMA)			
	$(\Delta E/E) = 41/E(keV)^{0.5}$ %FWHM (PSD)			
Field of view	2.2° diameter (CMA) 1.5° diameter (PSD)			
Effective area (cm^2)	Thin Lexan Filter	Al/P Filter	Boron Filter	Open position (PSD)
.05 keV	0.4	2.6	-	-
.1 keV	11.1	0.4	-	-
.5 keV	4.5	3.3	0.4	1.9
1.0 keV	3.2	2.5	2.0	13.5
1.5 keV	2.2	1.6	1.8	9.7
2.0 keV	0.6	0.5	0.6	1.9
Spatial resolution (Line spread function HEW)				
On axis :	18 arc sec (CMA)		3 arc min (PSD)	
20 arc minutes off-axis:	40 arc sec (CMA)		3.5 arc min (PSD)	
Average steady residual background**	1.8 cnts/sec/cm^2 (CMA)			
	0.7 cnts/sec/cm^2/kev (PSD)			

* Subject to UV contamination between 900 - 2600 Å
** Background rate subject to flaring

TABLE 2

PERFORMANCE CHARACTERISTICS (ME & GSPC)

Medium Energy Experiment	Characteristics
Total effective area	1500 cm^2 (all quadrants co-aligned)
Effective energy range	1-20 keV (Argon proportional counters) 5-50 keV (Xenon proportional counters)
Energy resolution ($\Delta E/E$)	$51/E\ (kev)^{1/2}$ % FWHM (Argon counters) 18% for 10 keV$\leq E \leq$ 30 keV (Xenon counters)
Field of view	45 arc minutes FWHM, triangular response with a 3' flat top
Total residual background	4 cnts/sec/keV (2-10 keV Argon counters co-aligned)
Gas Scintillation Counter (GSPC)	
*Total effective area	100 cm^2
Effective energy range	2-18 keV or 2-40 keV, depending on gain setting
Energy resolution ($\Delta E/E$)	$27/E\ (kev)^{1/2}$ % FWHM
Field of view	45 arc minutes FWHM triangular response with a 3' flat top
Total residual background rate	1.3 cnts/sec/keV (2-10 keV)

* depends on E and burst length window setting

LIST OF AO-3 OBSERVATIONS 1.7.85 - 30.8.85

Day (85)	Time	Target	RA	Dec	SAA	Duration h m	Principal Investigator	
181	22.05	Her X-1	16 55 49	+35 26 10	116	14 49	Voges	AO-2
182	16.40	2S 0921-630	09 21 01	-63 04 15	91	33 39	Mason	
184	07.19	2223-052	22 23 14	-05 09 57	125	3 33	McHardy	
184	14.24	NGC 5675	14 30 22	+36 30 58	95	9 58	Reichert	
185	15.49	NGC 4593	12 36 55	-05 04 58	88	11 11	Clavel	
186	06.28	Z Cha	08 09 25	-76 24 30	99	6 4	TOO	
186	17.00	NGC 5548	14 15 31	+25 21 34	96	6 0	Branduardi	AO-2
187	00.43	1402+04	14 02 10	+04 15 43	103	5 47	TOO	
187	07.52	PG1426+015	14 26 24	+01 29 49	109	5 49	Zamorani	
187	18.20	IRAS 1833+326	18 33 03	+32 40 58	124	2 52	Ops	
187	22.49	E1821+643	18 21 27	+64 21 08	92	5 1	Stanger	
188	06.45	E1615+061	16 15 08	+06 11 03	129	5 15	Piro	
188	14.44	1E1352+182	13 52 01	+18 20 23	93	4 31	Giommi	
189	12.00	1E1352+182	13 51 59	+18 19 50	92	5 31	Giommi	
189	19.50	E1615+061	16 15 05	+06 10 37	128	6 18	Piro	
190	10.42	GT Peg	22 49 30	+31 32 28	105	6 51	Shafer	
191	19.52	FF AND	00 40 00	+35 13 30	83	5 34	Shafer	
191	03.48	EXO 2030+37	20 30 28	+37 25 35	117	5 13	TOO	
191	11.55	HD 146361	16 12 32	+33 58 59	108	1 15	Brinkman	AO-2
193	14.36	Cen X-3	11 18 36	-60 21 31	94	32 54	Tennant	
195	05.02	IRAS 1833+326	18 32 58	+32 40 46	123	2 28	Ops	
195	11.00	NGC 5548	14 15 28	+25 20 43	89	4 59	Branduardi	AO-2
195	18.44	EX Hya	12 49 29	-28 59 57	91	13 02	Mason	
196	17.55	EX Hya	12 49 29	-28 59 34	90	7 45	Mason	
197	03.44	Nova Muscae	11 49 04	-66 56 13	99	6 39	Krautter	AO-2
197	18.12	4U1631-64	16 31 11	-64 20 28	126	11 23	White	
198	10.07	EX Hya	12 49 29	-28 59 32	88	7 53	Mason	
198	19.29	PK 318+41.1	13 37 45	-19 38 48	95	2 47	de Korte	AO-2
199	04.09	III ZW 2	00 08 04	+10 44 49	108	6 21	Pounds	
199	13.05	MKN 335	00 03 49	+19 58 22	105	5 34	Pounds	
199	21.12	II Peg	23 52 32	+28 24 13	103	5 22	White	
200	18.33	EXO 0748-67	07 48 45	-67 39 15	88	4 35	TOO	
201	03.35	II Peg	23 52 29	+28 23 55	104	12 25	White	
201	19.08	SS433	19 09 20	+04 53 53	151	10 53	Watson	AO-1
202	08.46	CM Dra	16 33 05	+57 14 27	91	5 3	Jensen	
202	18.00	MKN 335	00 03 49	+19 58 22	108	19 34	Pounds	
203	15.50	II Peg	23 52 29	+28 23 55	106	6 34	White	
204	10.50	II Peg	23 52 29	+28 23 56	107	6 13	White	
204	21.27	IRAS 1833+326	18 32 59	+32 39 45	122	1 43	Ops	
205	03.45	Cyg X-2	21 42 30	+38 07 47	118	11 27	Hasinger	
205	18.40	II Peg	23 52 29	+28 23 56	108	4 20	White	
206	01.50	Cyg X-2	21 42 30	+38 07 48	118	11 49	Hasinger	
206	16.15	EXO 2030+37	20 30 27	+37 25 00	122	4 5	TOO	
207	03.03	Fairall-9	01 22 03	-59 01 50	114	5 26	TOO	
207	13.05	II Peg	23 52 28	+28 23 56	110	3 47	White	
208	10.06	II Peg	23 52 30	+28 24 22	110	4 24	White	

Day (85)	Time	Target	RA	Dec	SAA	Duration h m	Principal Investigator
208	20.35	Circinus X-1	15 16 32	-57 01 30	112	22 28	Tennant
209	22.50	NGC 1097	02 44 14	-30 26 33	96	6 11	Shafer
210	09.30	4U1705-32	17 05 31	-32 15 35	132	2 15	Lewin
210	15.05	GPS 1533-556	15 33 52	-55 37 06	113	3 17	Watson
210	21.42	IRAS 1509-211	15 08 55	-21 09 27	104	5 18	Ward
211	07.40	IRAS 1833+326	18 32 57	+32 39 45	120	12 8	Ops
211	20.23	IRAS 1833+326	18 32 58	+32 39 25	120	12 57	Ops
212	14.00	IC 4329A	13 46 39	-30 02 00	88	8 15	TOO
213	00.19	PKS 1510-098	15 10 18	-08 53 10	99	10 51	Petre
213	13.41	X1728-169	17 28 59	-16 55 00	133	10 2	Parmar
214	05.35	H1405-451	14 06 10	-45 01 00	95	10 24	Osborne
214	19.10	ESO 103-G35	18 33 10	-65 25 20	127	3 35	Pounds
215	01.15	G308.7+0.0	13 38 23	-61 59 59	97	5 41	Smith
215	15.46	A0538-66	05 37 23	-67 04 00	91	3 13	TOO
215	22.10	NGC 526A	01 21 47	-35 17 08	118	6 9	Pounds
216	07.26	UV Cet	01 36 31	-18 10 34	113	8 24	Pallavicini
216	20.50	Circinus X-1	15 16 33	-57 00 49	107	14 11	Tennant
217	12.08	G312.4	14 09 00	-61 30 05	99	7 1	Peacock
218	00.20	BD+6 189	01 14 22	+06 35 12	113	3 0	Cecchini
218	06.40	EQ Peg	23 29 20	+19 42 16	128	7 49	Pallavicini
218	19.24	MXB 1636-53	16 36 45	-53 41 20	116	6 15	Van Paradijs
219	11.11	MXB 1636-53	16 36 42	-53 41 32	116	78 39	Van Paradijs
223	16.00	IRAS 1833+326	18 32 59	+32 38 37	117	2 50	Ops
223	21.30	E1821+643	18 21 18	+64 19 02	93	5 34	Stanger
224	05.35	LE Cal	19 56 15	+35 04 12	125	5 31	LE Cal
224	14.40	Circinus X-1	15 16 33	-57 01 15	101	22 45	Tennant
225	17.43	EXO 2030+37	20 30 26	+37 25 00	126	1 31	TOO
225	22.50	ESO 103-G35	18 33 24	-65 31 04	121	3 29	Pounds
226	04.55	RCW103	16 13 37	-50 57 23	107	17 38	Peacock AO-2
227	11.47	MXB 1735-44	17 35 11	-44 27 10	120	77 22	Trümper
230	18.15	MXB 1735-44	17 35 09	-44 27 32	117	14 14	Trümper
231	11.50	4U1820-30	18 20 27	-30 23 17	128	20 28	Stella
232	11.05	X1813-140	18 13 02	-14 04 57	125	19 11	Parmar
233	10.36	IRAS 1833+326	18 32 59	+32 38 48	113	2 38	Ops
233	16.37	TT Ari	02 04 04	+15 01 38	114	8 22	Hudec
234	15.51	V471 Tau	03 47 38	+17 08 16	90	27 2	Jansen
235	2250	NGC 526A	01 21 48	-35 17 54	130	5 13	Pounds
236	07.45	Sco X-1	16 16 57	-15 32 30	94	7 18	PriedhorskyAO2
236	16.21	GL 644AB	16 52 40	-07 51 00	101	9 1	Butler
236	05.25	EXO 2030+37	20 30 10	+37 28 21	125	3 32	TOO
237	13.00	Sco X-1	16 16 57	-15 32 31	93	9 15	PriedhorskyAO2
238	09.05	Sco X-1	16 16 56	-15 33 09	92	4 53	PriedhorskyAO2
238	8.05	GL735	18 52 56	+08 18 44	125	8 3	Butler
239	04.54	Sco X-1	16 16 56	-15 33 09	91	8 48	PriedhorskyAO2
239	15.45	1758-250	17 57 56	-25 06 52	115	22 2	Van Paradijs
240	18.03	1730-33	17 30 06	-33 01 15	108	14 42	TOO
241	10.40	1758-250	17 57 56	-25 06 52	114	6 0	Van Paradijs

OUTSTANDING AO-1/AO-2 POINTINGS

AO-1 (6)

Target	Proposal No.	Comments
SC 0627-54	CLU F10	To be scheduled
3C345	AGN F50	TOO Status waiting for outburst
U Gem	LLX G17	" " " "
GX340+0	OCC G1	Occultation - on hold
GX349+2	OCC G4	" "
PKS 1934-63	EXG F36	Scheduled Oct. '85

AO-2 (31)

Target	Proposal No.	Comments
Decided by PI	AGN 024	
NGC 7172	AGN 036	Scheduled Oct. '85
NGC 1808	AGN 057	To be scheduled
Abell 2235	CLU 006	" "
3A1006+475	MIS 011	" "
IH2236-372	MIS 011	Scheduled Oct. '85
N63A	SNR 028	To be scheduled
G41.1-0.3	SNR 030	Scheduled Oct. '85
G39.9+0.0	SNR 041	To be scheduled
U Gem	LLX 105	TOO status waiting for outburst (2 observations)
GL 754	LLX 171	Scheduled Oct. '85
3A1954+319	HLX 039	To be scheduled
AO538-66	HLX 053	TOO Status (5 observations)
NGC 6553	HLX 055	Scheduled Sept. '85
AM Her	HLX 063	Partially complete (1 observation remaining)
AO535+26	HLX 154	Scheduled Mar.86 (5 observations)
2S1636-536	HLX 046	Scheduled Sept. '85
Fornax	AGN 075	To be scheduled (partially completed)
IHO422-086	MIS 011	Scheduled Sept. '85
Cyg X-1	HLX 044	Scheduled Oct. 85
H1615+09	MIS 019	To be scheduled
RCW 86	SNR 039	Partially complete;to be scheduled

EXOSAT X-RAY SOURCES

'New' X-ray sources are discovered by EXOSAT serendipitously in the FOV of the telescope or in the offset quadrants of the ME or from an analysis of ME/GSPC 'background' data recorded during manoeuvres. We intend to maintain a list of published 'new' sources and readers are encouraged to report 'discoveries'.

EXOSAT Source Nomenclature

Source Position: RA 02H 30m 20.5s (1950)
DEC -02D 20m 33.2s

Name : EXO 023020-0220.5

EXO 074824-6737.4:	IAU Telegram No. 4039
EXO 184639-0307.5:	IAU Telegram No. 4051
EXO 174725-2124.7:	IAU Telegram No. 4058
EXO 203021+3727.9:	IAU Telegram No. 4066
EXO 063111+1801.9:	IAU Telegram No. 4081
EXO 041604-5504.9:	IAU Telegram No. 4097
EXO 125653+2809.9:	Space Science Reviews, 40, 1985, 648.
EXO 125757+2840.3:	" "
EXO 125905+2807.0:	" "
EXO 125921+2828.2:	" "
EXO 125938+2803.1:	" "

IAU (EXOSAT) TELEGRAMS

Circular No.	Title	Comment	Authors
3841	Hercules X-1	Anomalous X-ray behaviour	EXOSAT Team
3842	Supernova in NGC 5236	Multi-waveband observations	W. Wamsteker
3850	GK Persei	351s periodicity during an outburst	M. Watson, A. Smith EXOSAT Team
3854	MXB 1730-335	Active, type 1 bursts	G. Pollard, N. White P. Barr, L. Stella
3858	4U 1543-45	Accurate position, ultra-soft spectrum	R. Blissett, EXOSAT Team
3872	GX 1+4	Unexpected low X-ray state: $\lesssim$ 4 UFU	R. Hall, J. Davelaar EXOSAT Team
3882	4U1755-33	Periodic dips in intensity	N. White, A. Parmar K. Mason
3887	4U2129+47 = V1727 Cygni	Unexpected low X-ray and optical state	W. Pietsch, H. Steinle M. Gottwald
3893	V0332+53	Accurate position, and flux	J. Davelaar, R. Blissett, L. Stella M. McKay, N. White, J. Bleeker
3902	V0332+53	Discovery of 4.4s period	L. Stella, N. White
3906	V0332+53	Unexpected brightening	A.N. Parmar R.J. Blissett T. Courvoisier L. Chiappetti
3912	V0332+53	Orbital parameters determination	N. White, J.Davelaar, A.N. Parmar, L. Stella M. van der Klis

Circular No.	Title	Comment	Authors
3923	Her X-1	Her X-1 'on' again at 80 Uhuru flux units, 1.24s pulsations (March 1.5 - 1.8)	J. Trümper, P. Kahabka H. Ögelmann, W. Pietsch, W. Voges, M. Gottwald, A. Parmar
3932	2S1254-690	Discovery of type 1 Burst and an absorption 'event'.	T. J.-L. Courvoisier, A. Peacock, M. Pakull
3935	AN URSAE MAJORIS	Serendipitous observation: soft X-ray flux suggests a return to the 'bright' state.	J.P. Osborne
3939	VW HYDRI	Discovery of X-ray pulsations during superoutburst	J. Heise, F. Paerels, H. van der Woerd
3952	2S1254-690	Discovery of a 3.9hr period in the X-ray light curve	T. J.-L. Courvoisier A. Parmar, A. Peacock
3961	4U1323-62	Type 1 Burst discovered	M. van der Klis, F.A. Jansen, J. van Paradijs, W.H.G. Lewin
3980	TV Columbae	X-ray periodicity discovered in range 1-7 keV.	A.C. Brinkman, J. Schrijver
3996	2S 0142+61	1456 sec Modulation of the X-ray flux	N.E. White, P. Giommi, A.N. Parmar, F.E. Marshall
4033	1E1402.3+0416	Rapid variability in BL Lac Objects.	P. Giommi, P. Barr
4038	PG0834-488	Detection of a hard X-ray flux	M.C. Cook
4039	EXO 0748-676	Discovery of a bright transient X-ray source which shows bursts, irregular intensity dips and periodic total eclipses	A.N. Parmar, N.E. White, P. Giommi F. Haberl.
4043	GX 5-1	Quasi periodic oscillation in the 1-10 keV flux	M. van der Klis, F. Jansen, J. van Paradijs, W. Lewin, J. Trümper, M. Sztajno
4044	4U 1323-62	Periodic dips in the 1-10 keV flux	M. van der Klis, A. Parmar, J. van Paradijs, F. Jansen, W. Lewin
4044	NGC 3031	Flux increases and variablity in the 0.1-6 keV range	P. Barr, P. Giommi

Circular No	Title	Comment	Authors
4049	RS OPHIUCHI	Intense X-ray emission detected; spectrum soft & absorbed.	F.A. Cordova, K.O. Mason, M.F. Bode, P. Barr
4051	EXO 1846-031	Detection of a new bright X-ray transient; non-variable flux .2 Crab.	A.N. Parmar, N.E.White
4051	4U1624-49	Periodic intensity dips discovered in the 2-10 keV flux.	M.G. Watson, R. Willingale, R. King I.E. Grindlay, J. Halpern
4054	NGC 4051	Quasi-periodic flux variations observed.	A. Lawrence, M. Elvis K. Pounds, M. Watson
4057	EXO 0748-676	Still active at 0.01 Crab - 21 type I bursts in total.	A.N. Parmar, M. Gottwald, F.Haberl N.E. White
4058	EXO 1747-214	New transient X-ray source Intensity 0.07 Crab, Type I bursts seen.	A.N. Parmar, N.E.White P. Giommi, L. Stella M. Sweeney
4060	SCO X-1	Quasi-periodic fast variability between 4 and 9 Hz during quiescent state.	J. Middleditch, W. Priedhorsky
4065	Nova Vul 1984 No. 2	Detected at 3 σ level in 0.04-2 keV range soon after outburst.	J. Krautter, H. Ögelman,
4066	EXO 2030+375	Discovery of a bright, uncatalogued, transient X-ray pulsar period 41.83s.	A.N. Parmar, L. Stella P. Ferri, N.E. White
4068	SCO X-1	Intensity dependent quasi-periodic oscillations in 5-35 KeV data.	M. van der Klis, F. Jansen, N. White, L. Stella, A. Peacock
4070	CYG X-2	Intensity dependent quasi-periodic oscillations in 1-10 KeV flux.	G. Hasinger, A. Langmeier, M. Sztajno, N. White,
4081	EXO 063111+ 1801.9	Improved position of an Einstein serendipitous source - tentative optical counterpart	G.F. Bignami, P.A. Caraveo, L. Salotti, G.G.C. Palumbo
4082	AG-DRA	Detection of X-ray emission at minimum phase.	L. Piro, A. Cassatella L. Spinoglio, R.Viotti A. Altamore

Circular No	Title	Comment	Authors
4083	R. AQ	Weak X-ray emission at maximum suggests non-correlation with MIRA-type variations.	R. Viotti, L. Piro, M. Friedjung, A.Cassatella
4083	1E1048.1-5937	X-ray pulsations with a period 6.44s; power law spectrum, high obscuration.	A.P. Smale, P. Charles R.H.D. Corbet, F.D. Seward.
4096	BR CIRCINI	Extreme high-state flux (> 3 Crab) observed	A.F. Tennant, R. Shafer
4097	EXO 041604-5504.9	Discovery of a new soft X-ray source; X-ray flux variable, 70% changes on a timescale of 1 month. Possible optical counterpart - A5 type star.	D. Alloin, D. Pelat, S. D'Odorico

RECENT EXOSAT Preprint List

This list of recent EXOSAT preprints refers to all papers, with an Observatory Team member as author, which have been accepted for publication. Once the paper is published in the literature, it will be removed from this list.

4. The Structure of Low-Mass X-ray Binaries.
White, N.E., Mason, K.

5. The Contributions of the EXOSAT Observatory to the 18th ESLAB Symposium.
Observatory Team.

7. EXOSAT Observations of broad Iron-K line emission from Sco X-1.
White, N.E., Peacock, A., Taylor, B.G.

9. Simultaenous X-ray and optical observations of the X-ray dip source X1755-338.
Mason, K.O., Parmar, A.N., White, N.E.

10. An EXOSAT Observation of Quiescent and Flare Coronal X-ray Emission from Algol.
White, N.E., Culhane, J.L., Parmar, A.N. Kellett, B.J., Kahn, S., van den Oord, G.H.J., Kuijpers, J.

13. The Discovery of low-level Iron K line emission From Cyg X-1
Barr, P., White, N.E., Page, C.G.

14. A Study of the Continuum and Iron K line emission from low mass X-ray binaries.
White, N.E., Peacock, A., Hasinger, G. Mason, K.O., Manzo, G, Taylor, B.G. Branduardi-Raymong, G.

15. The orbital periods of the low mass X-ray Binaries.
White, N.E.

16. X-rays from the Magnetic White Dwarf PG 1658+441.
Pravdo, S.H., Marshall, F.E., White, N.E. Giommi, P.

Copies of these preprints are available on request to the Observatory Secretary.

EXOSAT BIBLIOGRAPHY

Hardware

Pre-Launch

A simple method of obtaining high background rejection in large area proportional counters. Bailey, T.A., Smith, A., and Turner, M.J.L. Nucl. Instrum. and Methods 115, 177 (1978).

Efficiency and resolution measurements of gratings between 7.1 and 304 Angstroms. Brinkman, A.C., Dijkstra, J.H., Geerlings, W.F.P.A.L., van Rooijen, F.A., Timmermann, C., and de Korte, P.A.J. Appl. Opt. 19, 1601 (1980).

X-ray scattering from epoxy replica surfaces. de Korte, P.A.J. SPIE Proceedings Space Optics - Imaging X-ray Optics Workshop 184, 189 (1979).

The X-ray imaging telescopes on EXOSAT. de Korte, P.A.J., Bleeker, J.A.M., den Boggende, A.J.F., Branduardi-Raymont, G., Brinkman, A.C., Culhane, J.L., Gronenschild, E.H.B.M., Mason, I. and McKechnie, S.P. Space.Sci.Rev. 30, 495 (1981).

X-ray imaging telescope on EXOSAT. Lainé, R., Giralt, R., Zobl, R., de Korte, P.A.J., and Bleeker, J.A.M. SPIE Proceedings Space Optics - Imaging X-ray Optics Workshop 184, 181 (1979).

The gas scintillation proportional counter on EXOSAT. Peacock,A., Andresen, R.D., Manzo, G., Taylor, B.G., Re, S., Ives, J.C., and Kellock, S. Space.Sci.Rev. 30, 525 (1981).

The parallel-plate imaging proportional counter and its performance with different gas mixtures. Sanford, P.W., Mason, I.M., Dimmock, K. and Ives, J.C. IEEE Trans.Nucl.Sci., NS-26 (1) 169 (1979).

The EXOSAT Mision. Taylor, B.G., Andresen, R.D., Peacock, A. and Zobl, R. Space.Sci.Rev. 30, 479 (1981).

The Medium Energy Instrument on EXOSAT. Turner, M.J.L., Smith,A., and Zimmermann, H.U. Space.Sci.Rev. 30, 513 (1981).

Post-Launch

The in-orbit performance of the EXOSAT Gas Scintillation Proportional Counter. Peacock, A., Taylor, B.G., White, N.E., Courvoisier, T., Manzo, G. IEEE Trans. Nucl. Sci., Vol. NS-32, No. 1, 1985.

The EXOSAT imaging X-ray detectors. Mason, I.M., Branduardi-Raymont, G., Culhane, J.L., Corbet, R.H.D., Sanford, P. IEEE Trans. Nucl. Sci., Vol. NS-31, No. 1, 1984.

The suppression of destructive sparks in parallel plate proportional counters. Cockshott, R.A., Mason, I.M. IEEE Trans. Nucl. Sci., NS-31, No. 1, 1984.

High Luminosity X-ray sources (HLX)

Spectral and temporal features in bursts from 2S1636-536 observed with EXOSAT. Turner, M.J.L. and Breedon, L.M. M.N.R.A.S. (1984), 208, 29p.

Evidence for 4.4 hour periodic dips in the X-ray flux from 4U1755-33. White, N.E., Parmar, A.N., Sztajno, M., Zimmermann, H.U., Mason, K.O., Kahn, S.M. Ap.J., 238, L9-12, 1984.

An extended X-ray low state from Hercules X-1. Parmar, A.N., Pietsch, W., McKechnie, S., White, N.E., Trümper,J. Voges, W., Barr, P. Nature 313 (1985), 119.

The Discovery of 4.4 second X-ray pulsations from the rapidly variable X-ray transient V0332+53. Stella, L., White, N.E. Davelaar, J., Parmar, A.N., Blissett, R.J., and van der Klis, M. Ap.J., 288, L45-49 (1985).

Transient quasi-periodic oscillations in the X-ray flux of Cygnus X-3. Van der Klis, M., Jansen, F.A. Nature 313 (1985), p.768-770.

Evidence for variation in the phase-dependent ionisation structure of the stellar wind in VELA X-1. Van der Klis, M., Hammerschlag-Hensberg, G. Proc. 4th European IUE Conference 15-18 May 1985, Rome. ESA SP(218), 443.

Spectral Studies of Low Mass X-ray Binaries Observed by EXOSAT. Sztanjno, M., Trümper, J,. & Langmeier, A. Proceedings Int. Symposium on X-ray Astronomy, Bologna, 1984, p.111.

Discovery of Regularities in the Cycle-to-Cycle Variability of Cygnus X-3. van der Klis, M., Jansen, F. Proceedings Int. Symposium on X-ray Astronomy, Bologna, 1984, p.115.

EXOSAT Observation of 4U1705-44. Langmeier, A., Sztajno, M., & Trümper, J. Proceedings Int. Symposium on X-ray Astronomy, Bologna, 1984, p.121.

EXOSAT Observations of 1636-536. Breedon, L.M., Turner, M.J.L. Proceedings Int. Symposium on X-ray Astronomy, Bologna, 1984, p.145.

Recent Results of EXOSAT observations of 2S1254-690. Courvoisier, T. J.-L., Parmar, A.N., Peacock, A. Proceedings Int. Symposium on X-ray Astronomy, Bologna, 1984, p.153.

Pulse Phase Spectroscopy of Her X-1 with EXOSAT. Kahabka, P., Pietsch, W., Trümper, J., Voges, W., Kendziorra, E., and Staubert, R. Proceedings Int. Symposium on X-ray Astronomy, Bologna, 1984, p.193.

EXOSAT Observations of the 35 days Intensity Variations of Her X-1. Oegelman, H., Kahabka, P., Pietsch., W., Trümper, W., Voges, W., Kendziorra, E, & Staubert, R. Proceedings Int. Symposium on X-ray Astronomy, Bologna, 1984, p.197.

EXOSAT Observations of 3A1954+319. Cook, M.C., Warwick, R.S., and Watson, M.G. Proceedings Int. Symposium on X-ray Astronomy, Bologna, 1984, p.225.

EXOSAT Observations of the X-ray Transient V0332+53. Davelaar,J., White, N.E., Parmar, A.N., Blissett, R.J., van der Klis, M., and Schrijver, H. Proceedings Int. Symposium on X-ray Astronomy, Bologna, 1984, p.235.

Observations of LMC X-3 with EXOSAT. Treves, A., Bonnet-Bidaud, J.M., Chiappetti, L., Maraschi, L., Stella, L., Tanzi, E.G., and van der Klis, M. Proceedings Int. Symposium on X-ray Astronomy, Bologna, 1984, p.259.

EXOSAT Observations of the Andromeda Nebula. McKechnie, S.P., Jansen, F.A., de Korte, P.A.J., Hulscher, F.W.H., van der Klis,M. Bleeker, J.A.M., and Mason, K.O. Proceedings Int. Symposium on X-ray Astronomy, Bologna, 1984, p.373.

X-ray observation of VELA-X. Smith, A., Zimmermann, H.U., Adv. Space Res., Vol. 5 No. 3, p.33, 1985.

Is Cygnus X-3 a low-mass X-ray binary? Van der Klis, M., Jansen, F. Adv. Space Res., Vol. 5, No. 3, p.109, 1985.

EXOSAT observation of the galactic bulge X-ray source GX17+2. Sztajno, M., Trümper, J., Zimmermann, H.U., Langmeier, A. Adv. Space Res., Vol. 5, No. 3, p.121, 1985.

Optical and X-ray observations of 4U2129+47/V1727 Cyg in a quiescent state. Pietsch, W., Steinle, N., Gottwald, M. Adv. Space Res., Vol. 5, No. 3, p.117, 1985.

Search for millisecond rotational periods in some low-mass X-ray binaries observed by EXOSAT. Langmeier, A., Sztajno, M., Trümper, J. Adv. Space Res., Vol. 5, No. 3, p.121, 1985.

Cygnus X-3: The dependence of the Iron-line parameters on orbital phase. van der Klis, M. Proc. Japan-US Seminar on Galactic and Extragalactic compact X-ray sources. Tokyo, 1985. p.195.

* EXOSAT MEDA obsevations of Cyg X-3. Willingale, R., King, A.R., Pounds, K. M.N.R.A.S. (1985) 215, 295-314.

* EXO 0748-676: An exciting new X-ray transient. Parmar, A.N., Gottwald, M., Haberl, F., Giommi, P. and White, N.E., Proc. ESA Workshop. Recent results on Catacylsmic Variables, Bamberg 17-19 April 1985 (ESA SP-236, June 1985) p.119.

* The spectral and temporal variability of GX 13+1. Stella, L., White, N.E., and Taylor, B.G. Proc. ESA Workshop. Recent results on Catacylsmic Variables, Bamberg 17-19 April 1985 (ESA SP-236, June 1985) p.125.

* EXOSAT Observations of the X-ray source in the Globular Cluster Terzan 2. Belli, B.M., D'Antona, F., Molteni, D., and Morini, M. Proc. ESA Workshop. Recent results on Catacylsmic Variables, Bamberg 17-19 April 1985 (ESA SP-236, June 1985) p.263.

* Intensity-dependent quasi-periodic oscillations in the X-ray flux of GX5-1. Van der Klis, M., Jansen, F., Van Paradijs, J., Lewin, W.H.G., van den Heuvel, E.P.J., Trümper, J.E., Sztajno, M. Nature, 316, (1985), p.225.

* The Big Dipper: 4U1624-49. Watson, M.G., Willingale, R., King, A.R., Grindlay, J.E. and Halpern, J. Space Science Reviews, 40 (1985), Nos. 1-4, p.195.

* Spectral Variability of Scorpius X-1, as observed with EXOSAT. Brinkman, A.C., Mewe, R., Langerwerf, T., Heise, J., Peacock,A. and White, N. Space Science Reviews, 40 (1985), Nos. 1-4, p.201.

* High and Medium Resolution Spectroscopy of the X-ray Transient 4U1543-47. Chiappetti, L., White, N.E., Kahn, S.M., and Shafer,R. Space Science Reviews, 40 (1985), Nos. 1-4, p.207.

* An Investigation into the Nature of the 4.4 hr Periodic Source 4U1755-33. Parmar, A.N., White, N.E., Sztajno, M. and Mason, K.O. Space Science Reviews, 40 (1985), Nos. 1-4, p.213.

* An EXOSAT Observation of the peculiar X-ray Binary 2S 0921-630 during optical eclipse. Mason, K.O., Cordova, F.A., Corbet, R.H.D. and Branduardi-Raymont, G. Space Science Reviews, 40 (1985), Nos. 1-4, p.225.

* EXOSAT medium energy observations of Cyg X-2. Hasinger, G., Langmeier, A., Pietsch, W. and Sztajno, M. Space Science Reviews, 40 (1985), Nos. 1-4, p.233.

* Co-ordinated Optical-EXOSAT-Tenma observations of a Burst from 2S1636-536. Turner, M.J.L., Breedon, L.M., Ohashi, T., Courvoisier, T., Inoue, H., Matsuoka, M., Pederson, H., van Paradjis, J. and Lewin, W.H.G. Space Science Reviews, 40 (1985), Nos. 1-4, p.249.

* EXOSAT and Optical observations of the X-ray Burst Source 4U/MXB1636-53. Trümper, J., Van Paradijs, J., Sztajno, M., Lewin, W.H.G., Pietsch, W., Krautter, J., Stollman, G., and van der Klis, M. Space Science Reviews, 40 (1985), Nos. 1-4, p.255.

* EXOSAT observations of Bursts from 2S1636-536: Burst Morphology. Turner, M.J.L., Breedon, L.M. and Ohashi, T. Space Science Reviews, 40 (1985), Nos. 1-4, p.263.

* The Quiescent Spectrum of 2S1636-536. Breedon, L.M., Turner, M.J.L., King, A., and Courvoisier, T. Space Science Reviews, 40 (1985), Nos. 1-4, p.269.

* EXOSAT results on the X-ray Burster 2S1254-690. Courvoisier, T., Parmar, A.N., Peacock, A. Space Science Reviews, 40 (1985), Nos. 1-4, p.275.

* Coordinated EXOSAT and Optical observations of the X-ray Burster 4U1735-44. Smale, A.P., Corbet, R.H.D., Charles, P.A., Menzies, J.W. and Mack, P. Space Science Reviews, 40 (1985), Nos. 1-4, p.281.

* First detection of an X-ray Burst from a one hour intensity dip in 4U1323-62. van der Klis, M., Jansen, F., van Paradijs, J. and Stollmann G. Space Science Reviews, 40 (1985), Nos. 1-4, p.287.

* Detection of Iron Lines in the persistent emission of some X-ray Burst sources observed by EXOSAT. Sztajno, M., Trümper, J., Hasinger, G. and Langmeier, A. Space Science Reviews, 40 (1985), Nos. 1-4, p.293.

* The Variable Iron Line in Cygnus X-3. van der Klis, M., Peacock, A. Smith, A., White, N.E., Mason, K. and Manzo, G. Space Science Reviews, 40 (1985), Nos. 1-4, p.297.

* Temporal intensity fluctuations of Her X-1 around 100 sec time-scales. Voges, W., Kahabka, P., Ögelman, H., Pietsch, W. and Trümper, J. Space Science Reviews, 40 (1985), Nos. 1-4, p.339.

* 35 day cycle and the rotation period of Her X-1. Ögelman, H., Kahabka, P., Pietsch, W., Trümper, J., and Voges, W. Space Science Reviews, 40 (1985), Nos. 1-4, p.347.

* EXOSAT Observations of the iron line emission of Her X-1 during a 35 day cycle. Kahabka, P., Ögelman, H., Pietsch, W., Trümper, J. and Voges, W. Space Science Reviews, 40 (1985), Nos. 1-4, p.355.

* Spectra and time variability of GX 5-1. Kendziorra, E., Collmar, W., Brunner, H., Staubert, R. and Pietsch, W. Space Science Reviews, 40 (1985), Nos. 1-4, p.361.

* EXOSAT observations of the Bright X-ray source GX9+1. Langmeier, A., Sztajno, M., Trümper, J. and Hasinger, G. Space Science Reviews, 40 (1985), Nos. 1-4, p.367.

* LMC X-4: 13.5 pulsations and an X-ray flare observed by EXOSAT. Pietsch, W., Pakull, M., Voges, W. and Staubert, R. Space Science Reviews, 40 (1985), Nos. 1-4, p.371.

* LMC X-4, A0538-66 and surrounding X-ray sources observed with EXOSAT. Pakull, M., Brunner, H., Pietsch, W., Staubert, A., Beuermann, K., van der Klis, M. and Bonnet-Bidaud, J.M. Space Science Reviews, 40 (1985), Nos. 1-4, p.379.

* The discovery of low-level iron line emission from Cyg X-1. Barr, P., White, N.E., and Page, C. Space Science Reviews, 40 (1985), Nos. 1-4, p.383.

* Study of rapid variability in Cygnus X-1. Page, C.G. Space Science Reviews, 40 (1985), Nos. 1-4, p.387.

* The spectral and temporal variability of the X-ray Transient 4U1630-47. Parmar, A.N., Stella, L. and White, N.E. Space Science Reviews, 40 (1985), Nos. 1-4, p.391.

* EXOSAT observations of the X-ray Pulsar 4U1145-619. Warwick, R.S., Watson, M.G. and Willingale, R. Space Science Reviews, 40 (1985), Nos. 1-4, p.429.

* A high quality low state observation of Cir X-1. Tennant, A.F. Space Science Reviews, 40 (1985), Nos. 1-4, p.433.

* A new view of the Galactic Plane with EXOSAT. Turner, M.J.L., Warwick, R.S., Watson, M.G. and Willingale, R. Space Science Reviews, 40 (1985), Nos. 1-4, p.437.

Low Luminosity X-ray sources (LLX)

EXOSAT Observation of the candidate X-ray counterpart of Geminga. Caraveo, P.A., Bignami, G.F., Giommi, P., Mereghetti, S., and Paul, J.A. Nature 310, 481-483 (1984).

EXOSAT Observations of H2215-086: detection of the X-ray pulse period. Cook, M.C., Watson, M.G., McHardy, I.M. M.N.R.A.S (1984), 210, 7p.

Further Evidence on the Increasing One Minute Period in the X-ray Data of Geminga (1E0630+178). Bignami, G.F., Caraveo, P.A., and Salotti, L. Proceedings Int. Symposium on X-ray Astronomy, Bologna, 1984, p.209.

EXOSAT Observation of "Geminga". Caraveo, P., Bignami, G.F., and Mereghetti, S. Proceedings Int. Symposium on X-ray Astronomy, Bologna, 1984, p.213.

The detection of X-rays from Nova Muscae 1983 with the EXOSAT Satellite. Ögelman, H., Beuermann, K., Krautter, J., Ap.J., 287, L31-34, 1984.

EXOSAT soft X-ray Observations of EX HYDRAE. Cordova, F.A., Mason, K.O., Kahn, S.M. M.N.R.A.S. (1985), 212, 447-461.

An X-ray corona in SS Cygni. King, A.R., Watson, M.G., Heise, J. Nature 313 (1985), p.290-291.

The old Nova GK Per: discovery of the X-ray pulse period. Watson, M.G., King, A.R., Osborne, J. M.N.R.A.S. (1985), 212, 917-930.

Preliminary results of co-ordinated optical UV and X-ray observations of magnetic white dwarfs in binaries. Maraschi, L., Beuermann, K., Bonnet-Bidaud, J.M., Charles, P.A., Chiappetti, L. Hammerschlag, G., Howarth, I., Motch, C., Mouchet, M., Osborne,J. Stella, L., Treves, A., Van Paradijs, J., Willis, A.J., Wilson,R. Proc. 4th European IUE Conference 15-18 May 1985, Rome. ESA SP(218), 427.

EXOSAT hard X-ray observations of EX Hydrae. Beuermann, K., and Osborne, J. Proceedings, Int. Symposium on X-ray Astronomy, Bologna, 1984. p.23.

X-ray observations of the AM Her Star CW1103+254. Beuermann, K., Stella, L., and Krautter, J. Proceedings Int. Symposium on X-ray Astronomy, Bologna, 1984. p.27.

EXOSAT Observations of late-type stars: Preliminary Results. Landini, M., Monsignori-Fossi, B.C., and Pallavicini, R. Proceedings Int. Symposium on X-ray Astronomy, Bologna, 1984. p.31.

X-ray Emission from the Planetary Nebulae NGC 1360. de Korte, P.A.J., Claas, J.J., Jansen, F.A., McKechnie, S.P. Proceedings Int. Symposium on X-ray Astronomy, Bologna, 1984. p.35.

The soft X-ray superoutburst of VW Hydri: 14 second periodicity. van der Woerd, H., Heise, J., and Paerels, F. Proceedings Int. Symposium on X-ray Astronomy, Bologna, 1984. p.55.

EXOSAT Observations of Am Her objects: Preliminars Results. Osborne, J., Maraschi, L., Beuermann, K., Bonnet-Bidaud, J.M., Charles, P.A., Chiappetti, L., Motch, C., Mouchet, M., Tanzi, E.G., Treves, A., and Mason, K.O. Proceedings Int. Symposium on X-ray Astronomy, Bologna, 1984. p.59.

EXOSAT observations of Intermediate Polars: Preliminary Results. Osborne, J., Mason, K.O., Bonnet-Bidaud, J.M., Beuermann, K., and Rosen, S. Proceedings Int. Symposium on X-ray Astronomy, Bologna, 1984. p.63.

Simultaneous EXOSAT and optical observations of the pulsing X-ray binary H2252-035/AO Psc. Pietsch, W., Pakull, M., Tjemkes, S., Voges, W., Kendziorra, E., and van Paradijs, J. Proceedings Int. Symposium on X-ray Astronomy, Bologna, 1984. p.67.

X-ray emission from the planetary nebula NGC 1360. de Korte, P.A.J., Claas, J.J., Jansen, F.A., McKechnie, S.P. Adv. Space Res., Vol. 5, No. 3, p.57, 1985.

Soft X-ray characteristics of White Dwarfs observed by EXOSAT. Heise, J., Bleeker, J.A.M., Brinkman, A.C., Gronenschild, E., Paerels, F., Grewing., M., Wulf-Mathies, C., Beuermann, K. Adv. Space Res., Vol. 5., No. 3, p.61, 1985.

Spectral and temporal studies of various late-type stars. Brinkman, A.C., Gronenschild, E., Mewe, R., McHardy, I., Pye, J.P. Adv. Space Res., Vol. 5, No. 3, p.65, 1985.

A simultaneous X-ray and radio observation of a flare from ALGOL. Parmar, A.N., Culhane, J.L., White, N.E., van den Oord, G.H.J. Adv. Space Res., Vol. 5, No. 3, p.65, 1985.

A search for X-ray emitting coronal structures in ALGOL. Culhane, J.L., White, N.E., Kahn, S., Parmar, A.N., Blisset, R.J., Kellett, B. Adv. SPace Res., Vol. 5, No. 3, p.73, 1985.

Einstein and EXOSAT observations of Geminga (1E0630+1748). A summary of the short- and medium-term variability data. Bignami, G.F., Caraveo, P.A., Mereghetti, S., Salotti, L. Adv. Space Res., Vol. 5, No. 3, p.145, 1985.

The identification of H2311+77 with HD220140: A probable RS CVn. Pravdo, S., White, N.E., Giommi, P. M.N.R.A.S. (1985), 215, 118.

* Orbital and fast variability of the AM Her System H1405-45 in the X-ray and Optical ranges. Bonnet-Bidaud, J.M., Beuermann, K., Charles, P., Maraschi, L., Motch, C., Mouchet, M., Osborne, J., Tanzi, E. and Treves. A. Proc. ESA Workshop. Recent results on Catacylsmic Variables, Bamberg 17-19 April 1985 (ESA SP-236, June 1985) p.155.

* X-ray optical and UV observations of the AM Her object E2003+225. Osborne, J.P., Mukai, K. Bonnet-Bidaud, J.M., Charles, P., Corbet, R., Henry, P., Hill, G., Kahn, S., van der Klis, M., Maraschi, L., Treves, A., and Vrtilek, S. Proc. ESA Workshop. Recent results on Catacylsmic Variables, Bamberg 17-19 April 1985 (ESA SP-236, June 1985) p.161.

* EF Eri: Structure of the X-ray light curve. Watson, M.G., King, A.R., Williams, G., Heise, J., Beuermann, K. Proc. ESA Workshop. Recent results on Catacylsmic Variables, Bamberg 17-19 April 1985 (ESA SP-236, June 1985) p.169.

* Geometry and Magnetic field of the AM Her star H0139-68. Schwope, A. and Beuermann, K. Proc. ESA Workshop. Recent results on Catacylsmic Variables, Bamberg 17-19 April 1985 (ESA SP-236, June 1985) p.173.

* X-ray observations of classical novae during the outburst stage by EXOSAT. Ögelman, H., Beuermann, K., Krautter, J. Proc. ESA Workshop. Recent results on Catacylsmic Variables, Bamberg 17-19 April 1985 (ESA SP-236, June 1985) p.177.

* Multi-frequency observations of Dwarf Novae - outbursts. Skzody, P. Proc. ESA Workshop. Recent results on Catacylsmic Variables, Bamberg 17-19 April 1985 (ESA SP-236, June 1985) p.

* X-ray emission from the catacylsmic variable PG 0834+488. Cook, M.C. M.N.R.A.S. (1985), 215, 81p-84p.

* An X-ray study of AM Herculis I Discovery of a new mode of soft X-ray emission. Heise, J., Brinkman, A.C., Gronenschild, E., Watson, M., King, A.R., Stella, L., Keiboom, K. Astronomy & Astrophys. 148, L14-16 (1985).

* Magnetic Activity in Cool Stars. Schrijver, C.J. Space Science Reviews, 40 (1985), Nos. 1-4, p.3.

* An EXOSAT observation of the morphology of the coronal X-ray emission from Algol. White, N.E., Culhane, J.L., Parmar, A.N., Kellett, B., Kahn, S., van den Oord, G.H.J. and Kuijpers, J. Space Science Reviews, 40 (1985), Nos. 1-4, p.25.

* Observation of an X-ray outburst and quiescent emission from the RS CVn binary HR1099. Barstow, M.A. Space Science Reviews, 40 (1985), Nos. 1-4, p.35.

* EXOSAT observations of late-type stars: The application of Coronal Loop Models. Landini, M., Monsignori-Fossi, B.C. and Pallavicini, R. Space Science Reviews, 40 (1985), Nos. 1-4, p.43.

* X-ray observations of Active Chromosphere Stars. Bedford, D.K., Elliott, K.H. and Eyles, C.J. Space Science Reviews, 40 (1985), Nos. 1-4, p.51.

* EXOSAT observation of the compact binary VW Cephei. Vilhu, O. and Heise, J. Space Science Reviews, 40 (1985), Nos. 1-4, p.55.

* The extremely X-ray bright Wolf-Rayet star HD193793. Pollock, A.M.T. Space Science Reviews, 40 (1985), Nos. 1-4, p.63.

* EXOSAT observations of M Dwarfs. Schmitt, J.H.M.M. and Sztajno,M. Space Science Reviews, 40 (1985), Nos. 1-4, p.69.

* EXOSAT observations of active stellar coronae in the Cygnus Loop, T Tau & NGC 2264 regions. Charles, P.A., Corbet, R.H.D., Mukai, K., Smale, A.P., Kahn, S.M., Kuhi, L.V. and Brown, A. Space Science Reviews, 40 (1985), Nos. 1-4, p.73.

* X-ray emission from isolated hot white dwarfs. Heise, J. Space Science Reviews, 40 (1985), Nos. 1-4, p.79.

* X-ray and optical variability at the hour timescale for 1E 0630+178 (Geminga) and its proposed optical counterpart. Vigroux, L., Paul, J.A., Delache, P., Bignami, G.F., Caraveo, P.A. and Salotti, L. Space Science Reviews, 40 (1985), Nos. 1-4, p.91.

* X-ray emission from Catacylsmic Variables. Mason, K.O. Space Science Reviews, 40 (1985), Nos. 1-4, p.99.

* Hard X-ray observations of the eclipsing binary EX Hydrae. Beuermann, K. and Osborne, J. Space Science Reviews, 40 (1985), Nos. 1-4, p.117.

* 2A 0526-328: The White Dwarf rotation period revealed. Schrijver, J., Brinkman, A.C., van der Woerd, H., Watson, M.G., King, A.R., van Paradijs, J. and van der Klis, M. Space Science Reviews, 40 (1985), Nos. 1-4, p.121.

* SS Cygni in outburst and quiescence. Watson, M.G., King, A.R. and Heise, J. Space Science Reviews, 40 (1985), Nos. 1-4, p.127.

* EXOSAT/Opticial observations of the AM Her star H0139-68. Beuermann, K., Schwope, A., Weissieker, H. and Motch, C. Space Science Reviews, 40 (1985), Nos. 1-4, p.135.

* X-ray variability of the AM Her star CW1103+254. Beuermann, K. and Stella, L. Space Science Reviews, 40 (1985), Nos. 1-4, p.139.

* New EXOSAT results from the intermediate polar V1223 Sgr. Osborne, J., Rosen, R., Mason, K.O. and Beuermann, K. Space Science Reviews, 40 (1985), Nos. 1-4, p.143.

* X-ray, optical & UV observations of the AM Her system E2003+225. Mukai, K., Bonnet-Bidaud, J.M., Bowyer, S., Charles, P.A., Chiappetti, L., Clarke, J.T., Corbet, R.H.D., Henry, J.P., Hill, G.J., van der Klis, M., van Paradijs, J. and Vrtilek, S.D. Space Science Reviews, 40 (1985), Nos. 1-4, p.151.

* X-ray and optical observations of Nova Muscae 1983 during its Nebular stage. Krautter, J., Beuermann, K. and Ögelman, H. Space Science Reviews, 40 (1985), Nos. 1-4, p.156.

* The discovery of a 25 min regular modulation in the X-ray flux from 2S0142+61. White, N.E., Giommi, P., Parmar, A.N., Marshall, F.E. and Mason, K.O. Space Science Reviews, 40 (1985), Nos. 1-4, p.157.

* The decay of Dwarf Nova outbursts. van der Woerd, H. and Heise,J. Space Science Reviews, 40 (1985), Nos. 1-4, p.163.

Active Galactic Nuclei (AGN)

EXOSAT Observations of Active Galactic Nuclei. Branduardi-Raymont G. MPE Report 184. X-ray and UV Emission from Active Galactic Nuclei. October 1984, p.88.

EXO1102.8+2539, an X-ray Variable AGN. Beuermann, K. MPE Report 1984. X-ray and UV Emission from Active Galactic Nuclei. October 1984, p.111.

Multi-frequency observations of active galactic nuclei. Tanzi, E.G., Chiappetti, L., Danziger, J., Palomo, R., Maccagni, D., Maraschi, L., Treves, A., Wamsteker, W. Proc. 4th European IUE Conference 15-18 May 1985, Rome. ESA SP(218), 111.

X-ray timing and spectral observations of active galactic nuclei. McHardy, I.M. Proceedings: 'Non-thermal and very high temperature phenomena in X-ray Astronomy, Rome, 1983. p.117.

EXOSAT Observations of Active Galactic Nuclei. Pounds, K.A., McHardy, I.M., Stewart, G., and Warwick, R.S. Proceedings Int. Symposium on X-ray Astronomy, Bologna, 1984. p.409.

EXOSAT Observations of Three Bright BL Lac objects. Warwick, R.S. McHardy, I.M., Pounds, K.A. Proceedings Int. Symposium on X-ray Astronomy, Bologna, 1984. p.467.

IUE-EXOSAT Observations of NGC 4151. Perola, G.C., Altmore, A., Boksenberg, A., Bromage, G.E., Clavel, J., Elvius, A., Penson, M.V., Pettini, M., Piro, L., Snijders, M.A.J., Tarenghi, M., and Ulrich, M.H. Proceedings Int. Symposium on X-ray Astronomy, Bologna, 1984. p.475.

The Soft X-ray emission from OI 235 and MK766. Maccagni, D., Garilli, B., Rampini, A., Chiappetti, L., & Giommi, P. Proceedings Int. Symposium on X-ray Astronomy, Bologna, 1984. p.479.

EXOSAT observation of the Perseus Cluster. Branduardi-Raymont, G., Kellett, B., Fabian, A.C., McGlynn, T., Manzo, G., Peacock, A. Adv. Space Res., Vol. 5, No. 3, p.133, 1985.

EXOSAT observation of Active Galactic Nuclei. Branduardi-Raymont, G., Bell-Burnell, S.J., Kellett, B., Fink, H., Molteni, D., McHardy, I. Adv. Space Res., Vol. 5, No. 3, p.129, 1985.

Broad band X-ray spectra and time variability of selected Active Galactic Nuclei observed with EXOSAT. Pounds, K. Proceedings Japan-US Seminar on Galactic and Extragalactic compact X-ray sources. Tokyo, 1985, p.26.

EXOSAT observations of a 2000s intensity dip in Seyfert Galaxy NGC 4151. Whitehouse, D.R., Cruise, A.M. Nature, 315(1985) p.554.

* The Soft X-ray spectrum of NGC 4151. Pounds, K.A., Warwick, R.S., Culhane, J.L., and de Korte, P. Space Science Reviews, 40 (1985), Nos. 1-4, p.585.

* Simultaneous EXOSAT-IUE observations of NGC 4151. Perola, G.C., Altamore, A., Boksenberg, A., Bromage, G.E., Clavel, J., Elvius, A., Penston, M.V., Pettini, M., Piro, L., Snijders, M.A.J., Tarenghi, M. and Ulrich, M.H. Space Science Reviews, 40 (1985), Nos. 1-4, p.593.

* EXOSAT Observations of the BL Lac object MKN 421. Warwick, R.S., McHardy, I. and Pounds, K.A. Space Science Reviews, 40 (1985), Nos. 1-4, p.597.

* X-ray variability of the Bright BL Lac object PKS 2155-304. Morini, M., Maccagni, D., Maraschi, L., Molteni, D., Tanzi, E.G., and Treves, A. Space Science Reviews, 40 (1985), Nos. 1-4, p.601.

* Variability of BL Lac objects at X-ray and other frequencies. Pollock, A.M.T., Brand, P.W.J.L., Bregman, J.L. and Robson, E.I. Space Science Reviews, 40 (1985), Nos. 1-4, p.607.

* HO332+022: Classification as a BL Lac and EXOSAT coordinated observations. Bradt, H., Baldwin, J., Geldzahler, G., Madejski, G., Massey, P., McClintock, J., McHardy, I., McMahan, R., Ohashi, T., Remillard, R., Romanishin, W., Salter, C., Schaefer, B., Schwartz, D., Tapia, S., Thorstensen, J., Urry, C.M., Wehinger, P., Wilson, A. and Wyckoff, S. Space Science Reviews, 40 (1985), Nos. 1-4, p.613.

* MR 2251-178: Preliminary results of an X-ray monitoring programme. Stewart, G.c., Pounds, K.A. and Stanger, V.A. Space Science Reviews, 40 (1985), Nos. 1-4, p.619.

* X-ray spectral variability of 3C273. Turner, M.J.L., Courvoisier, T., Staubert, R., Molteni, D. and Trümper, J. Space Science Reviews, 40 (1985), Nos. 1-4, p.623.

* EXOSAT Observation of the QSO Galaxy pair 1E0104.2+3153. Giommi, P., Gioia, I.M. and Maccacaro, T. Space Science Reviews, 40 (1985), Nos. 1-4, p.627.

* EXOSAT spectra of some Bright QSO's. McGlynn, T.A., Tennant, A.F., Shafer, R.A. and Stewart, G.C. Space Science Reviews, 40 (1985), Nos. 1-4, p.633.

* The X-ray and optical variability of the BLRG 3C390.3. Shafer, R., Ward, M., and Barr, P. Space Science Reviews, 40 (1985), Nos. 1-4, p.637.

* Optical observations of serendipitous EXOSAT Sources in the Coma Cluster. Branduardi-Raymont, G., Mason, K.O., Murdin, P.G., Martin C. and McKechnie, S.P. Space Science Reviews, 40 (1985), Nos. 1-4, p.647.

Supernova Remnants (SNR)

X-ray spectra of Supernova Remnants: observations in continuum and lines. Bleeker, J.A.M. Proceedings: 'Non-thermal and very high temperature phenomenon in X-ray Astronomy, Rome, 1983, p.77.

The X-ray structure of the Crab Nebula. Aschenbach, B., Brinkmann, W., Langmeier, A., Hasinger, G., and Bork, T. Proceedings Int. Symposium on X-ray Astronomy, Bologna, 1984. p.302. Also in Adv. Space Res., Vol. 5, No. 3, p.45, 1985.

EXOSAT Observations of SN 1006. Jones, L.R., Pye, J.P., Culhane, J.L. Proceedings Int. Symposium on X-ray Astronomy, Bologna, 1984. p.305.

Recent results on the Crab pulsar X-ray light curve. Hasinger, G. Proceedings Int. Symposium on X-ray Astronomy, Bologna, 1984. p.321.

EXOSAT observations of the Supernova Remnant Cas A. Jansen, F.A., McKechnie, S.P., de Korte, P.A.J., Bleeker, J.A.M., Gronenschild, E., Peacock, A., Manzo, G., Branduardi-Raymont, G., & Kellett, B. Proceedings Int. Symposium on X-ray Astronomy, Bologna, 1984. p.289. Also in Adv. Space Res., Vol. 5, No. 3, p.49, 1985.

* Galactic Supernova Remnants. Aschenbach, B. Space Science Reviews 40 (1985), Nos. 1-4, p.447.

* X-ray spectrum of the Tycho SNR observed with EXOSAT. Davelaar, J., Morini, M., Peacock, A., Robba, N.R. and Taylor, B.G., Space Science Reviews, 40 (1985), Nos. 1-4, p.467.

* EXOSAT PSD and CMA observations of the SNR PKS 1209-52. Kellett, B.J. Space Science Reviews, 40 (1985), Nos. 1-4, p.475.

* Mapping of the Cygnus Loop with EXOSAT. Ballet, J., Arnaud, M., Rocchia, R. and Rothenflug, R. Space Science Reviews, 40 (1985), Nos. 1-4, p.481.

* EXOSAT LE-CMA observations of the Vela Supernova Remant. Smith,A. and Zimmermann, H.-U. Space Science Reviews, 40 (1985), Nos. 1-4, p.487.

* Some crucial X-ray observations - one or two SNR(s) in Crux? Mereghetti, S., Bignami, G.F., Caraveo, P.A., Goldwurm, A. and Palumbo, G.G.C. Space Science Reviews, 40 (1985), Nos. 1-4, p.495.

* 2-10 keV spectra of Crab-like SNR's as observed by EXOSAT. Davelaar, J. and Smith. A. Space Science Reviews, 40 (1985), Nos. 1-4, p.513.

* Spectral Observation of the Composite Supernova Remnant G29.7-0.3 Koch-Miramond, L., Rocchia, R., Davelaar, J., Jansen, F.A., Becker, R.H.J., and Braun, R. Space Science Reviews, 40 (1985), Nos. 1-4, p.521.

* Thermal radiation from a radio pulsar PSR 1055-52. Brinkmann, W., Ögelman, H. and Aschenbach, B. Space Science Reviews, 40 (1985), Nos. 1-4, p.527.

Clusters (CLU)

* EXOSAT 2-10 keV observations of M87 and the Virgo Cluster. Smith, A. and Stewart, G. Space Science Reviews, 40 (1985), Nos. 1-4, p.661.

* Abell 1367 and 1060 observed with EXOSAT. Norgaard-Nielsen, H.U. Westergaard, N.J. and Hansen, L. Space Science Reviews, 40 (1985), Nos. 1-4, p.669.

* EXOSAT observations of NGC 1399 and NGC 1404: Two elliptical galaxies in the centre of the Fornax Cluster. Mason, K.O. and Rosen, S.R. Space Science Reviews, 40 (1985), Nos. 1-4, p.675.

General

First Results from the X-ray Satellite EXOSAT. Biermann, P., Mitteilungen der Astronomischen Gesellschaft Nr. 62, p.101-121, 1984 (Minden 1984).

The EXOSAT mission. Taylor, B.G. Adv. Space Res., Vol. 5, No.3, p.35, 1985.

* EXOSAT - A Service to the Astronomical Community. Sternberg,J.R. Proc. of IX Int. CODATA Conference 1984. Published in 'The Role of Data in Scientific Progress'. Elsevier (1985) Jerusalem.

* EXOSAT and Einstein high resolution images of the small Magellanic Cloud. Jones, L.R. Pye, J.P., and Fairall, A.P. Space Science Reviews, 40 (1985), Nos. 1-4, p.693.

* Denotes publications which are additions to the bibliography during the period 1.7.85 to 31.8.85.

NB: Reprints are obtainable from authors in the usual way.

THE ASTROPHYSICS OF X-RAY TIMING VARIABILITY

Recent EXOSAT results on X-ray binaries stimulated much discussion at the Workshop on X-ray timing held recently in Taos, New Mexico August 5-9th. This meeting was organised to focus attention on the need for future missions dedicated to the study of time variable phenomena from accreting compact objects. The new EXOSAT results, along with those from the Japanese satellite Tenma, illustrated that even a quite modest increase in observing capability (such as a longer satellite orbital period or a factor of two increase in energy resolution) can yield many unexpected results.

The discovery by EXOSAT of quasi-periodic oscillations (QPO) from three bright low mass X-ray binaries was discussed in detail. The QPO's first discovered by van der Klis and co-workers from GX5-1 (see Nature 316, 225) are also found to be present in Sco X-1 (Priedhorsky and Middleditch; van der Klis) and Cyg X-2 (Hasinger) at various frequencies ranging from 6 to 20 Hz. The strong correlation of frequency with intensity found for GX5-1 is also present in Cyg X-2. However in Sco X-1 the correlation between QPO frequency and intensity is only present in dips between flaring intervals. During extended quiescent periods the QPO frequency remains constant at 6 Hz. The origin of the QPO is still far from clear. Magnetospheric models were discussed in detail by F. Lamb with the QPO caused by the beat between a rapidly rotating magnetosphere and the inner Keplerian orbit of an accretion disk. While this model can explain many features of the peaks seen in the power spectra, the lack of any fundamental periodicity representing the pulsar spin was clearly a concern to many present.Middleditch argued strongly that some residual pulse should still be seen. Other possible models were not yet sufficiently developed to be tested against the data. The general feeling was that the planned observations of these sources by EXOSAT this summer, in particular those designed to measure the energy dependence of the QPO, were essential to further understanding of this new phenomenon. Re-examination of HEAO 1 and 2 data has now shown that QPO were also present in Cyg X-2 (Wood) and GX5-1 (Weisskopf).

The orbital period distribution of the low mass X-ray binaries was considered in two presentations by Rappaport and by White. EXOSAT observations have led to the discovery of many new orbital periods, notably from the so-called dipping sources. In these systems a bulge at the edge of the accretion disk at the point of impact of the gas stream from the companion passes through the line of sight causing periodic dipping behaviour. The distribution of orbital periods allows evolutionary models to be tested. In general the periods detected are between 3 and 7 hrs,consistent with models that invoke the orbit decaying viagravitational radiation plus magnetic braking. One notable point is that no orbital periods have yet been detected from the high luminosity

galactic bulge sources. This may suggest that the periods are longer than a day and that the modulations are difficult to detect because of intrinsic variability and smearing by X-ray evaporated accretion disk coronae and winds. Long orbital periods would be consistent with evolutionary models for these systems where the orbital period increases because of the expansion of a giant companion star.

Trümper presented new EXOSAT results from Her X-1 observations which strongly suggest that the precessing disk model for the 35 day cycle is not correct. These data show major changes in the 1.28s pulse profile as a function of the 35 day cycle. In particular during the secondary on-state the profile becomes double pulsed, suggesting that the cycle is caused by the free precession of the rotating neutron star itself. The other properties of the 35 day cycle may be the result of the inner disk being distorted by the magnetosphere of the neutron star, or screening by material centrifugally held in the magnetosphere. A pre-print on this result received the notable award of "most Xeroxed pre-print" from the conference secretary.

X-ray burst sources were discussed in terms of the current theoretical and observational results. Recent theoretical work on neutron star model atmospheres and the distortion of the blackbody spectrum caused by Compton scattering, free-free and free-bound emission and absorption is in good agreement with the observed dependence between the colour temperature and apparent blackbody radius measured by both Tenma and EXOSAT (Inoue). D. Lamb discussed the current theoretical results for the expected dependence of burst properties on mass transfer rate. These calculations in general predict $\propto$, the ratio of the time averaged persistent to burst flux, to increase as the mass transfer decreases. Recent EXOSAT observations of the transient EXO 0748-676 showed that as the intensity of this source decreased by a factor of four over a three month interval, $\propto$ decreased from 120 to 25. Clearly, the theory still needs some refinement.

EXOSAT observations of X-ray bursts from Cir X-1 were presented by Tennant. These bursts show all the characteristics of Type I bursts, suggesting that thermonuclear flashes are occurring on a neutron star. This result casts serious doubt on previous speculation that the X-ray properties of Cir X-1 (which are similar to those of Cyg X-1) suggest it is a black hole candidate.

EXOSAT GSPC monitoring of the iron K line from SS433 (Watson) shows that it moves from 6.7 keV to 7.5 keV in phase with the blue shifted optical lines of the 164 day cycle (see front cover). This result indicates that most of the X-ray emission comes from the jets. There is no evidence for a red shifted component, suggesting it is hidden from view by the accretion disk.

N. White

The sensitivity of the EXOSAT Channel Multiplier Array

1. INTRODUCTION

A discussion of the sensitivity of the Channel Multiplier Array (CMA) on board the EXOSAT satellite has been given elsewhere (e.g. De Korte et al 1981, Space Science Rev. volume 30, EXOSAT Observers Guide part 2 and part III sect. 8). This was however based on pre-flight calibrations and did not take into account all the peculiarities of the in-orbit performance.

The availability of a large data base containing information from several hundreds of observations, carried out in the first two years of operations, together with the necessary sophisticated software, allows an accurate measurement of the sensitivity of the CMA. The purpose of this paper is to describe the sensitivity of the CMA to point sources over the entire field of view (FOV). Because the CMA at the focus of the second EXOSAT telescope has been operational for only a relatively small fraction of the mission, and no significant differences are expected in its performance compared to CMA 1, only data obtained with CMA1 is analysed here.

Formulae used to determine the limiting sensitivity of the instrument, are derived in sect. 2. Sections 3, 4 and 5 discuss the spatial distribution of the background, the off-axis point spread function (PSF) and the efficiency of the telescope optics as a function of the position in the FOV, conclusions are presented in section 6.

2. MATHEMATICAL FORMALISM

The X-Ray flux of a cosmic source can be calculated using the following equation:

$$\text{flux}_{[E1,E2]} = c/r * K.ss \frac{\int_{E2}^{E1} e^{\sigma(E)*NH} * dN/dE * E * dE}{\int_{E2}^{E1} e^{\sigma(E)*NH} * A(E) * dN/dE * dE} \qquad (1)$$

where A(E) is the effective area of the system comprising the telescope, the CMA and the filter, dN/dE is the source photon spectrum, c/r is the observed count rate, $\sigma(E)$ is the absorption cross section, NH the equivalent hydrogen column density in the line of sight and K.ss is a correction factor which depends on the sum signal distribution of the source photons (see EXOSAT Observers Guide part III for details). For X-ray sources which do not emit strongly in the UV, K.ss is generally very close to 1. E1 and E2 define a minimum and maximum energy outside which the effective area of the system is negligibly small. These values are generally assumed to be E1=0.05 and E2=2.0 Kev. The minimum detectable flux (fm), i.e. the limiting sensitivity of the instrument, is essentially determined by the minimum detectable count rate c/r(m) and the effective area of the system. c/r(m) depends on the exposure time (t), on the Point Spread Function (PSF), and on the mean background level (b). The exact calculation of the CMA effective area is described in detail in the EXOSAT Observers Guide part III sect. 8.1 and need not be repeated here.

It can be shown that

$$A(E)=A(x=0,y=0,E(x,y))*h(x,y)$$

where x,y is the source position in pixels, E is the energy, and h(x,y) is a function of x and y only. As a first approximation the positional dependence of E can be neglected since this is not likely to introduce large inaccuracies. In this case

$$A(E,x,y)=A(E,x=0,y=0)*h(x,y)$$

and equation (1) can now be rewritten as

$$fm(x,y)_{[E1-E2]} = c/r(m)(x,y) * K.ss/h(x,y) \frac{\int_{E2}^{E1} e^{\sigma(E)*NH} * dN/dE * E * dE}{\int_{E2}^{E1} e^{\sigma(E)*NH} * A(E,x=0,y=0) * dN/dE * dE} \quad (2)$$

which is equivalent to

$$fm(x,y)_{[E1-E2]} = fm(x=0,y=0)_{[E1-E2]} * g(x,y) \quad (3)$$

where g(x,y) is a function defined by

1) Efficiency of the optics
2) Degradation of the PSF at large offset angles
3) Background non-uniformities
4) Secondary effects such as the positional dependance of the
   a) sum signal distribution
   b) detector quantum efficiency

4a and 4b are likely to produce only very small errors and will therefore be neglected.
Eq (3) shows that the minimum observable flux at the position x,y is equal to the minimum observable flux in the centre of FOV multiplied by a function of x,y only.

Let PSF(i) be the fraction of the source net counts contained in a square box denoted by the index i and centered on the source centroid. The index i is defined such that box 0 is a square of 1 pixel in size, box i is a box whose size is 2i+1 pixels. (Note that throughout this paper, PSF(i) refers to the integral or cumulative Point Spread Function). A typical cumulative PSF in the central region of the FOV is shown in fig 1. **

**
The curve shown in fig 1 represents the typical Point Spread Function as observed with the Lexan or the Al/par filters. There is evidence that the shape of the Boron PSF is a strong function of the source energy spectrum (see EXOSAT EXPRESS no 10 page 45) and therefore, reference is always made to the Lexan or Al/par PSF.

The source count rate is generally estimated as follows

$$c/r=NET(i)/PSF(i)/t$$

where NET(i) is the source net counts in box i and t is the exposure time corrected for telemetry and sampling dead time.

$$NET(i)=TOTAL(i)-b*(2*i+1)^2*t$$

TOTAL(i) is the total number of counts found in box i and b is the average background level in units of counts/sq.pixel/sec.
Fig 2 shows the distribution of the background intensity in the central region of the FOV, as determined in the automatic analysis, for several hundreds of CMA observations. Since the LE automatic analysis excludes all periods when the background is anomalously high the distribution shown in fig 2 is representative of the CMA background under normal conditions (i.e. in the absence of what is generally referred to as 'solar activity'). The distribution is rather narrow and centered on b=9.E-6 counts/sec/sqpixel. This background value is assumed throughout this paper.
The statistical error associated with c/r is

$$\sigma_{c/r}=\frac{\sqrt{TOTAL(i)}}{PSF(i)}=\frac{\sqrt{NET(i)+b*(2*i+1)^2*t}}{PSF(i)}$$

and the signal-to-noise ratio s/n is

$$s/n=\frac{c/r*PSF(i)*t}{\sqrt{NET(i)+b*(2i+1)^2*t}} \qquad (4)$$

since the expected value of NET(i) is

$$NET(i)=c/r*PSF(i)*t$$

eq (4) becomes

$$s/n=\frac{c/r*PSF(i)*t}{\sqrt{c/r*PSF(i)*t+b(2i+1)^2*t}}=\frac{c/r*PSF(i)}{\sqrt{c/r*PSF(i)+b(2i+1)^2}}t^{1/2} \qquad (5)$$

Fig 3 shows the signal to noise ratio plotted against box number for different values of the count rate. In this example the exposure time has been assumed to be 1 EXOSAT unit (1.E4 seconds) but the graph can easily be rescaled to any value of t using eq (5). For low values of the count rates the signal to noise ratio is sufficiently high only for a rather narrow range of box sizes. Obviously, for sources near the limit of detectability it is extremely important to choose the box size that gives the best possible signal to noise ratio.
This result is strictly valid only if the PSF is perfectly known. In the central region of the FOV this is true unless the source is characterized by a very hard spectrum and/or high photoelectric cut-off (NH>1.E22). As an example, the cumulative PSFs of several bright sources, covering a wide range of spectra and photoelectric absorptions, and detected near the centre of the CMA FOV, are plotted in figure 4. The curves are all very similar and support the hypothesis that the CMA PSF is largely independent of the nature of the source. Note, however that for NH>1.E22 the PSF could be wider than those shown in figure 4. Since the PSFs plotted in fig 4 have been obtained from data collected using both lexan and Al/par filters the plots indicate that, within statistical limits, the PSFs in each filter are essentially identical.

Solving eq (5) with respect to c/r gives

$$c/r = s/n * \frac{s/n + \sqrt{s/n^2 + 4b*(2i+1)*t}}{2*PSF(i)*t} \qquad (6)$$

The minimum detectable count rate can be defined as that value of the count rate corresponding to a minimum acceptable signal-to-noise ratio; this minimum value is often taken as 5. Eq (6) has been plotted in figure 5 as a function of the exposure time t for the case of a signal to noise ratio equal to 5 (solid line). For small values of the exposure time, c/r is almost a linear function of t, corresponding to the case of the photon limited regime. In the limit of very large exposure times and/or large background values the minimum detectable count rate becomes proportional to $\sqrt{t}$. This corresponds to the case of the present generation non-imaging X-ray detectors for which the background is much higher than the minimum detectable source strength.

For X-ray images, however, a good estimate of the background can be obtained in regions close to the position of the source. Here the minimum detectable count rate can be defined as that value which would produce a number of counts such that the associated probability that the event is due to a random fluctuation of the background is sufficiently small. This condition is generally satisfied if the net counts in the box used is equal to or greater than five times the square root of the expected background.

$$c/r(m) = \frac{5*\sqrt{b*(2I+1)^2\,t}}{PSF(I)*t} = \frac{5*\sqrt{b*2(I+1)^2}}{PSF(I)}\,t^{-1/2} \qquad (7)$$

where I is the index that minimizes equation 7. The intensity of the normally expected CMA background is such that for short exposure times the expected number of background counts in the box used becomes so small that eq 7 is no longer valid and the condition that at least 10 source counts must be collected is generally substituted. Eq (7) is plotted as a dashed line in fig 5 and shows that the minimum count rate defined in this way can be more than a factor of five lower than the value obtained with eq 6 for a signal to noise ratio equal to 5.

In order to compare the minimimum detectable count rate defined by eq (6) and eq (7) to the actual data, the measured count rate of more than three hundred sources detected within 200 pixels from the centre of the CMA FOV has been plotted in figure 4. The sample has been chosen so that all the sources have been detected at least twice, either in two different filters or in the same filter but on two separate occasions and should therefore be virtually free from spurious sources. It is clear from figure 5 that the use of an over-conservative definition for the minimum detectable count rate, such as that given by eq (6) for s/n=5, leads to the loss of a significant fraction of detectable sources. Hence the minimum detectable count rate definition given by eq (7) with the restriction that the net counts must be > 10 will be adopted.

3. THE SPATIAL DISTRIBUTION OF THE BACKGROUND

As described in the EXOSAT Observers Guide part III sect 8.1, the CMA background is not uniformly distributed over the FOV. The background intensity shows a local maximum at the detector centre. It decreases at intermediate distances with roughly circular symmetry and finally increases again at the very edge of the FOV. Quantitatively, the effect is of the order of 10 percent in the central square degree.

A very deep image has been analysed (exposure time ~160.000 seconds) to illustrate in detail the spatial distribution of the CMA background. This image is free from extended sources and all point sources have been removed from it and substituted with a randomized mean background, estimated in regions near the sources. The filter used was 3000 A lexan. A comparison of this image with exposures obtained at different epochs indicates that the structure of the background does not significantly change with time. In addition, comparison with an image obtained summing exposures performed during periods of high 'solar activity' (i.e. in the presence of anomalously high particle background) shows that the spatial distribution of the CMA background depends on the overall background intensity - on average, the spatial distribution of the background during periods of high 'solar activity' differs from the distribution normally expected by an amount of the order of 5-10%.

In order to show the spatial distribution of the CMA background on the scale of a few arc minutes the image has been rebinned such that the size of each pixel is about 2 arc minutes. Figure 6 shows the background iso-intensity contours of the resulting image. The contours have been rescaled such that the central region of the image corresponds to an intensity of 100. This image can be used to calculate the CMA background in any part of the FOV, given its value in the centre.

4. THE OFF-AXIS POINT SPREAD FUNCTION

Data obtained during an in-flight raster scan performed on July 5 1983 has been analysed to study the off-axis CMA PSF. This raster scan consists of 43 observations of the X-ray source CYG X-2 carried out such that the source is detected at different locations with respect to the optical axis of the instrument. The 43 pointings cover the whole field of view and the exposure times were chosen to give at least 8-900 counts during each observation.

For each pointing the CMA Point Spread Function has been determined as follows

1) estimate the mean background in a nearby region using an area sufficiently large to guarantee a small statistical error and rescale the value thus obtained to the position of the source taking into account the background spatial distribution described in the previous paragraph.

2) calculate the source centroid X,Y

3) estimate the net counts in square boxes centered on the source centroid, subtracting from the total number of counts in the box the expected background in the same area calculated as described in point 1) and corrected for spatial non-uniformities

$$PSF(i)=(TOTAL(i)-b\#(2i+1)^2\#F(i,X,Y)\#t)/TOTAL$$

b is the average background in units of counts/sec/sqpixel, t is the exposure time and F(i,x,y) is a function which corrects for the spatial distribution of the background, and TOTAL is the total number of detected photons from the source.

The above procedure has been carried out for all pointings of the raster scan. Resulting PSFs have been grouped according to the distance from the optical axis (which, for the case of LE1 is located at X=136 Y=61 in linearized coordinates) and are shown in figure 7. Note that within a distance of roughly 200 pixels from the image centre, the PSFs remain constant in shape and essentially identical to the one shown in fig. 1. At larger distances from the centre the PSF broadens by an amount dependant on the distance. The dependance on the orientation of the source position with respect to the instrument axis is small and is probably negligible. Broadening of the PSF with distance from the optical axis is also shown in fig 8 where the index number (I(50%)) corresponding to the box containing 50% of the source photons is plotted against distance from the centre. This parameter is essentially constant for distances smaller than ~200 pixels and then increases approximately linearly with distance.

5. THE EFFICIENCY OF THE OPTICS

The dependance of the CMA effective area on position in the FOV mainly results from the variability of the efficiency of the telescope optics across the image. The exact dependance, as measured during pre-flight calibrations is given in the EXOSAT Observers Guide part III sect 8.1, fig A. A raster scan of the CRAB Nebula has been analysed to check whether the ground calibration is directly applicable to the in-orbit data. Use of the CRAB Nebula raster scan has two disadvantages.
First, the CRAB is not a point source and therefore the estimate of its count rate must be made in large boxes, therefore increasing the overall errors. This is especially true at the edge of the FOV where the Point Spread Function is very wide and where the effect of the obscuration due to the ME flap is largest (ref page 67 and the EXOSAT Observers Guide part 3 sect. 8.1)
Secondly, the CRAB raster scan did not cover the entire field of view.

For each observation, the CRAB count rate has been estimated and corrected for the efficiency of the optics at the position of the source to give the best estimate of the source count rate in the centre of the FOV. The results are summarized in Table 1, showing in Columns 1 and 2 the source position in pixels, in columns 3 and 4 the measured count rate and the relative error, in columns 5 and 6 the corrected count rate and error, and in column 7 the distance from the image centre in arc minutes.

All the values listed in column 5 are close to the mean value of 12.26 c/sec. Pointings with the source closer then approximately 20 arc minutes to the centre give a corrected count rate distribution with a standard deviation of 0.35 cts/s (~2.8% of the mean). The standard deviation increases to 0.97 c/s when only distances greater than 20 arcmin are considered and the mean value becomes 12.02. Given that minor corrections such as the dependance of the detector quantum efficiency on the position in the FOV and the corrections for the sum signal distribution have been neglected, the above result is very satisfactory.

6. CONCLUSION

In the previous sections, the formulae necessary to calculate the CMA minimum detectable count rate have been derived and examples given to illustrate the sensitivity of the instrument in the central part of FOV. The estimation of the minimum detectable count rate can now be extended to any position in the FOV by making use of eq. (7) i.e.

$$c/r(m) = 5\frac{\sqrt{b*(2I+1)^2}}{PSF(I)}\ t^{-1/2}$$

b, I, and PSF(I) all depend on the position (x,y). Near the centre of the FOV, PSF(I)~0.5 and for a generic position (x,y), PSF(I) should be calculated using the point spread functions shown in fig 7. For each PSF derived from the CYG X-2 raster scan the value of the index i (Im(x,y)) which minimizes eq (7) (i.e. the value of i for which c/r(m) is minimum) has been calculated.
The background b(x,y) is estimated assuming circular symmetry around x=136 y=61 and taking into account the spatial distribution described in sect 3.
Eq 7 can therefore be rewritten as

$$c/r(m) = 5*(2Im(x,y)+1)/PSF(Im(x,y))*b(x,y)^{1/2}*t^{-1/2} \qquad (8)$$

The minimum detectable count rate defined by eq (8) is plotted in figure 9 as a function of distance from the detector centre for the case of t=10000 seconds. Before this count rate can be converted into flux it must be corrected for the efficiency of the telescope optics at the position x,y. This correction is applied using the calibration values given in the LE current calibration file (CCF). Eq (2) now becomes

$$fm(x,y) = \frac{5*(2Im(x,y)+1)*\sqrt{b(x,y)}*K.opt(x,y)*K.ss*t^{-1/2}}{PSF(Im(x,y))} \frac{\int_{E1}^{E2} e^{\sigma(E)*NH}*dN/dE*E*dE}{\int_{E1}^{E2} e^{\sigma(E)*NH}*A(E,x=0,y=0)*dN/dE*dE}$$

where K.opt (=1/h(x,y), see eq. 2) is the correction due to efficiency of the telescope optics. Consequently eq (3) becomes

$$fm(x,y) = fm(x=0,y=0)*$$

$$*K.opt(x,y)*\sqrt{\frac{b(x,y)}{b(x=0,y=0)}}\ \frac{(2Im(x,y)+1)}{(2Im(x=0,y=0)+1)}\ \frac{PSF(Im(x=0,y=0))}{PSF(Im(x,y))}$$

i.e.

$$g(x,y)=K.opt(x,y)*\sqrt{\frac{b(x,y)}{b(x=0,y=0)}}\ \frac{2Im(x,y)+1}{2Im(x=0,y=0)+1}\ \frac{PSF(Im(x=0,y=0))}{PSF(Im(x,y))} \qquad (9)$$

g(x,y), originally defined in eq (3), describes the functional dependance of the CMA sensitivity on the position in the FOV and is plotted in figure 10 assuming circular symmetry for b(x,y) and K.opt.

It has been stressed elsewhere that the conversion of the CMA count rate to flux is a strong function of the source energy spectrum and of the total amount of equivalent hydrogen column density in the line of sight. The derived limiting sensitivity can be very different for sources characterized by different spectra and/or photoelectrc absorptions. The reader is advised to refer the EXOSAT Observers Guide part III chapter 8 where the conversion factors necessary to convert count rate in the centre of the FOV into flux in erg/cm2/sec for a wide range of spectral parameters are given. These conversion factors can esily be scaled to any position in the CMA image using eq 9 or figure 10.

Paolo Giommi

Table 1

x pixels	y pixels	measured count rate (c/s)	error (c/s)	corrected count rate (c/s)	error (c/s)	distance from centre (arcmin)
763.8	5.6	6.04	0.12	10.39	0.21	42.1
641.3	11.6	7.23	0.11	10.81	0.17	34.0
515.1	9.1	8.51	0.14	11.21	0.18	25.6
386.9	8.4	10.19	0.13	11.97	0.15	17.2
257.1	6.7	11.31	0.17	12.35	0.17	9.0
257.6	-247.9	10.19	0.15	12.87	0.19	22.2
258.3	261.0	10.00	0.15	11.68	0.18	15.7
131.6	130.2	11.26	0.16	11.68	0.17	4.6
132.4	9.1	11.54	0.17	11.86	0.17	3.5
131.9	-121.4	11.48	0.16	12.65	0.18	12.2
48.8	-121.6	11.24	0.22	12.81	0.25	13.4
49.3	-35.9	11.36	0.17	12.42	0.19	8.6
49.8	6.7	11.57	0.16	12.40	0.17	6.7
47.3	50.2	11.53	0.15	12.12	0.16	5.8
4.8	13.1	11.30	0.16	12.35	0.17	9.2
5.4	7.1	11.28	0.16	12.35	0.18	9.3
7.8	-36.3	11.43	0.15	12.74	0.17	10.6
5.1	-122.2	10.92	0.15	12.68	0.17	14.9
6.2	-250.9	10.19	0.16	12.92	0.20	22.5
8.2	-375.5	9.10	0.14	12.89	0.20	30.3
12.9	-501.3	8.23	0.13	13.29	0.21	38.3
25.0	-626.9	6.73	0.12	12.62	0.23	46.4
0.2	-743.6	5.14	0.11	11.72	0.24	54.4
-38.6	50.3	11.01	0.16	12.11	0.18	11.5
-123.6	132.5	9.95	0.14	11.82	0.17	17.8
-122.7	-120.7	10.03	0.15	12.41	0.18	21.0
-123.7	7.9	10.34	0.14	12.20	0.17	17.5
-374.4	9.3	7.73	0.11	11.57	0.16	34.1
-371.0	-246.6	7.27	0.06	11.91	0.10	39.4

FIGURE CAPTION

Figure 1

A typical CMA cumulative point spread function in the centre of the field of view

Figure 2

The distribution of the CMA background intensity in the central region of the FOV (data taken from the automatic analysis output)

Figure 3

The signal to noise ratio as a function of box number for different values of the count rate.

Figure 4

The point spread function of several cosmic X-ray sources detected by the CMA near the centre of the FOV. The nature of the sources encompass the range from very soft X-ray to extragalactic sources.
The PSFs have been obtained with both the 3000 A lexan and the Al/Par filter.

Figure 5

The minimum detectable count rate as a function of exposure time. The solid line corresponds to the case of signal to noise ratio equal to 5. The dashed line is the minimum detectable count rate defined by eq 7 with the restriction that at least 10 photons must be collected.

Figure 6

The iso-intenity contours of the LE1 CMA background for the case of no 'solar activity'.

Figure 7

The CMA integral PSF at different distances from the optical axis.

Figure 8

The index corresponding to the box containing 50% of the source photons plotted as a function of distance from the detector centre

Figure 9

The minimum detectable count rate corresponding to an exposure time of 1 EXOSAT unit (10000 sec) plotted versus distance from the detector centre.

Figure 10

The function g(x,y), which gives the ratio between the CMA sensitivity in a generic point of the field of view and the sensitivity in the centre of the detector, is plotted against distance from centre assuming circular symmetry. The solid line corresponds to g(x,y)=1

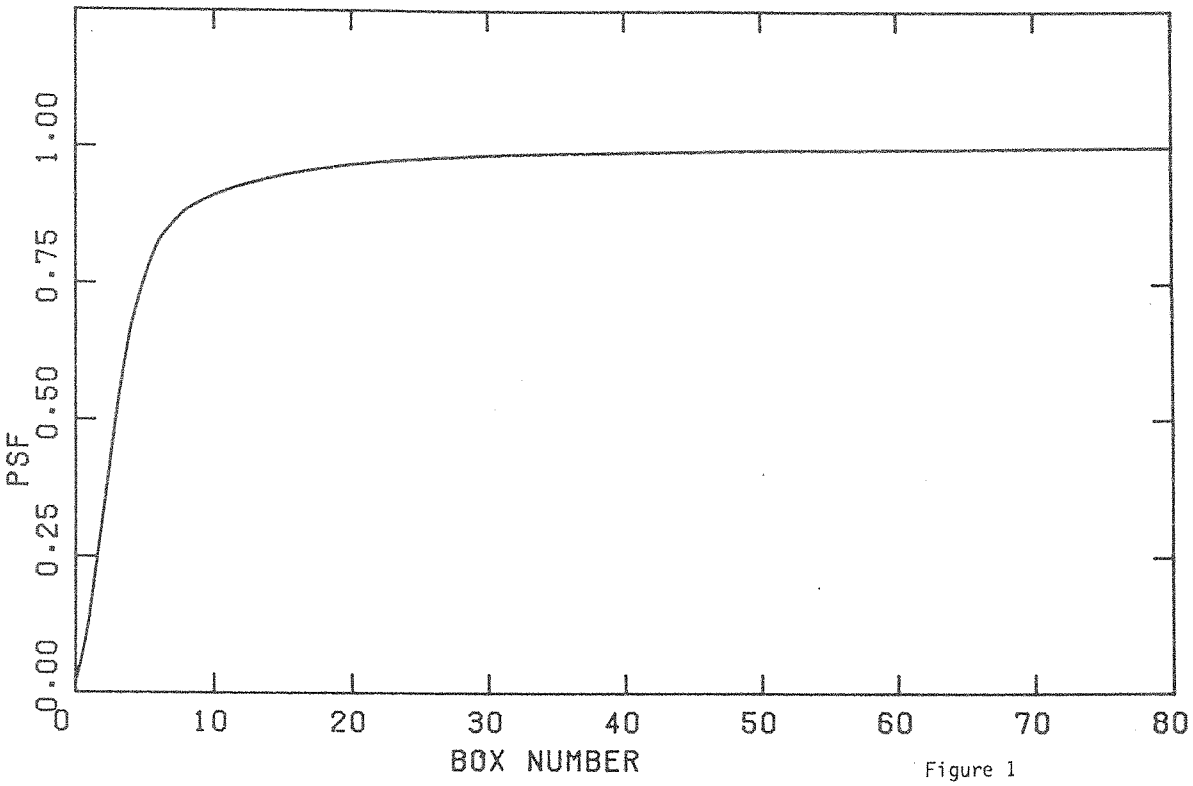

Figure 1

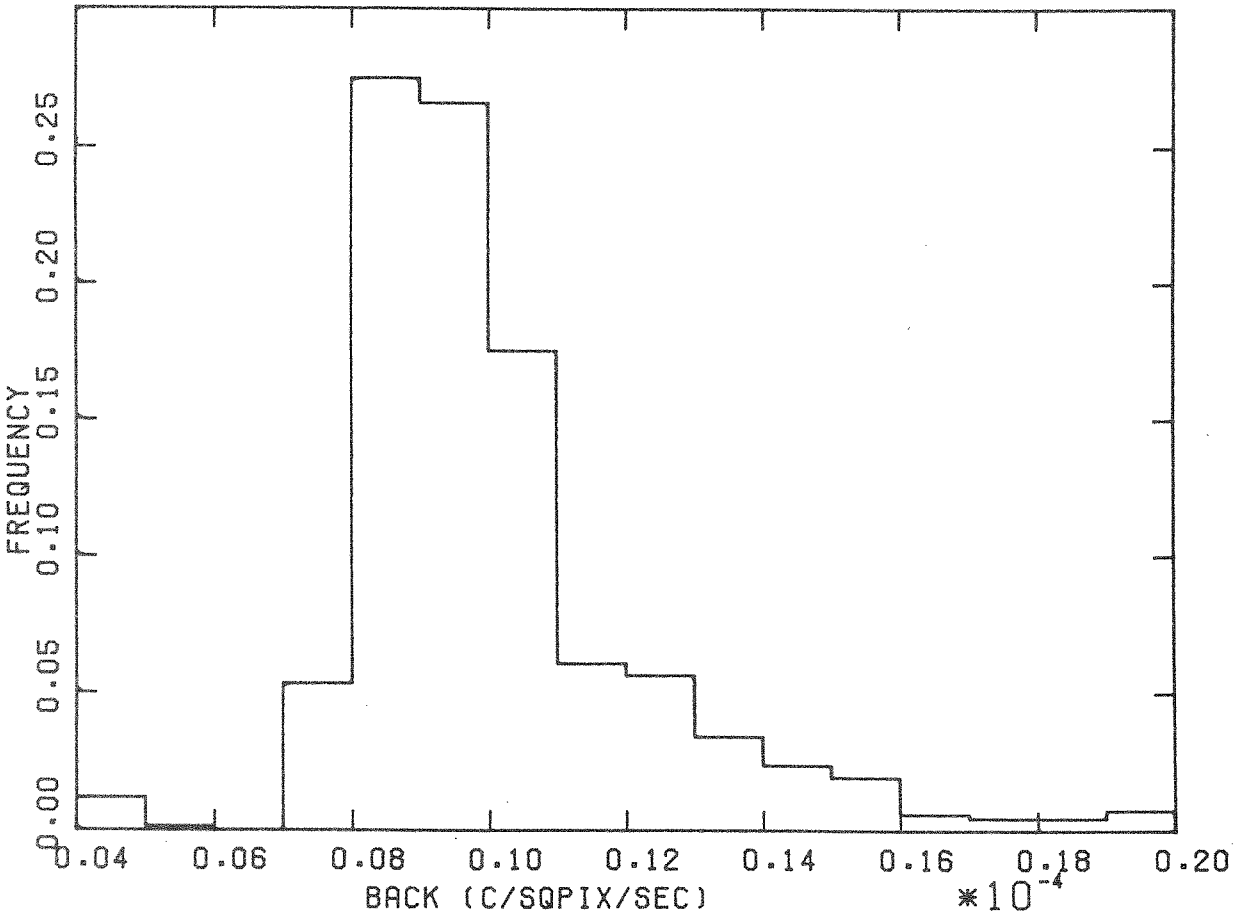

Figure 2

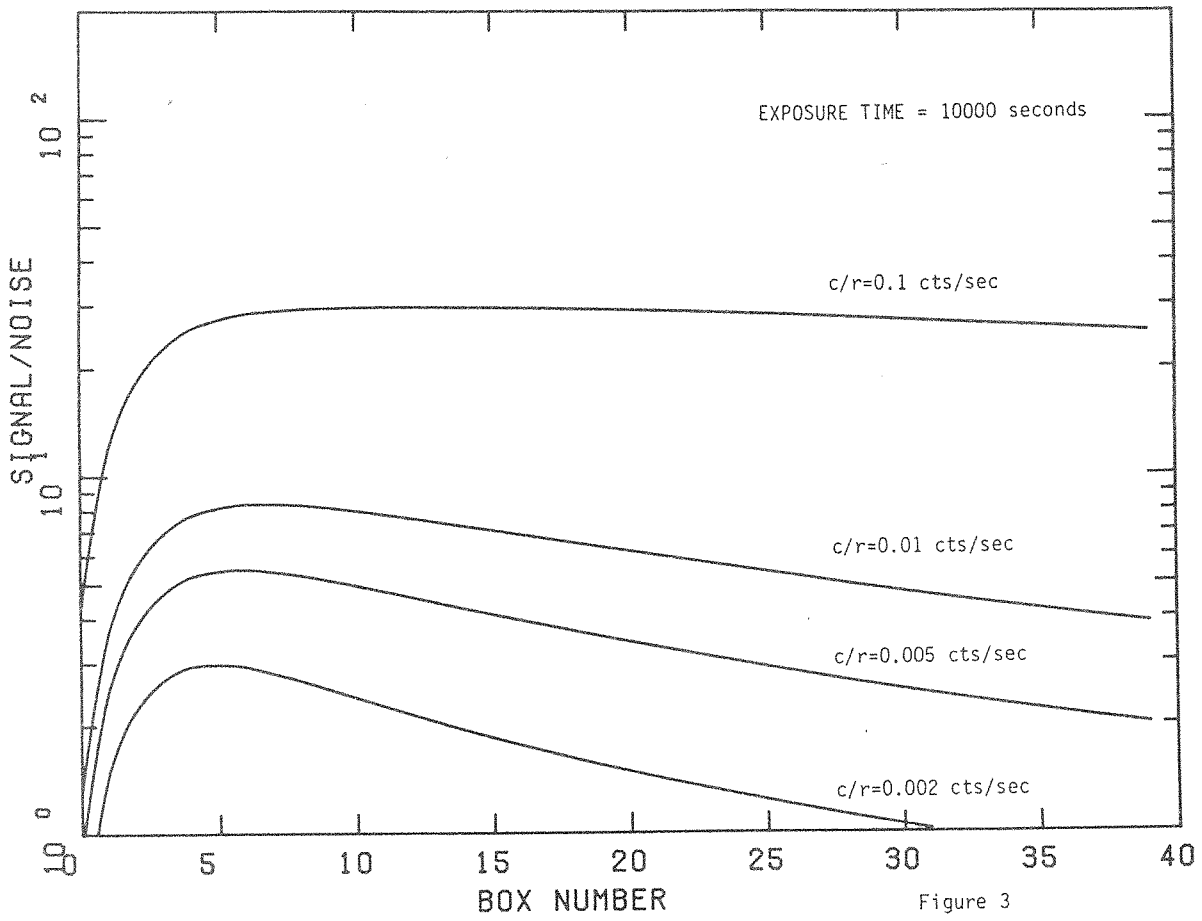

Figure 3

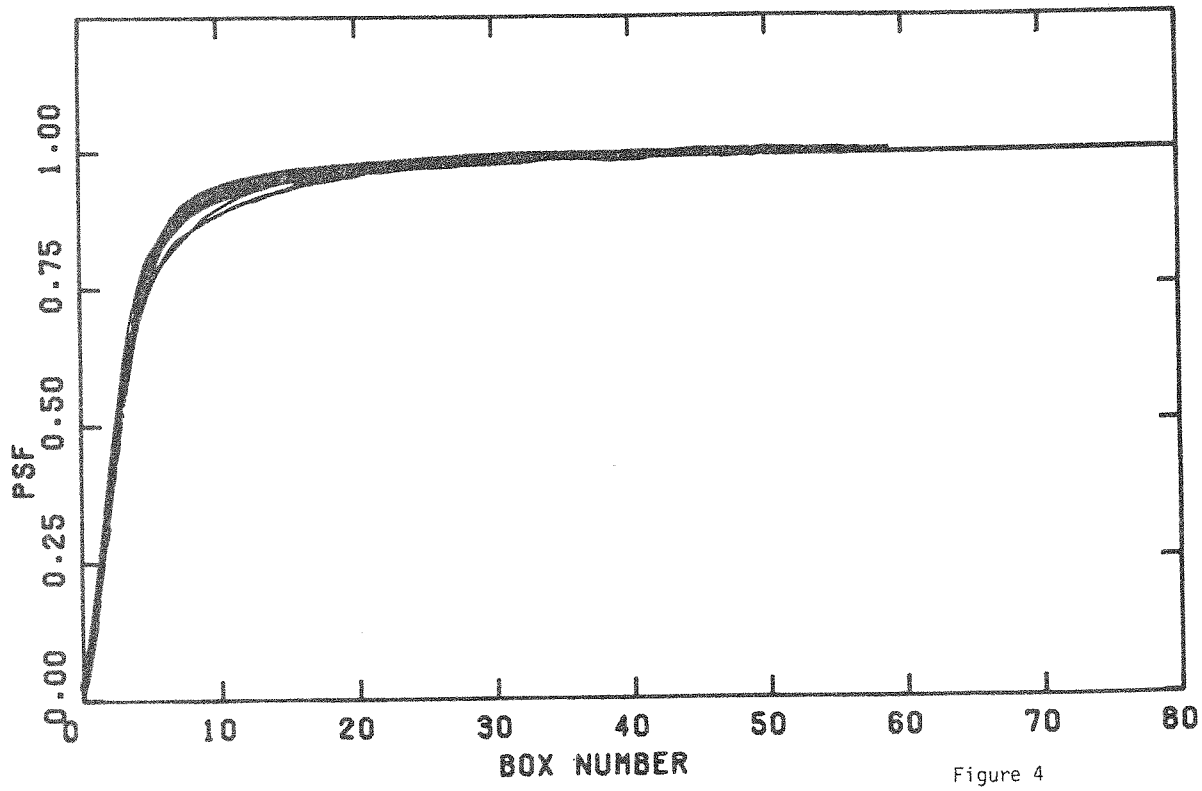

Figure 4

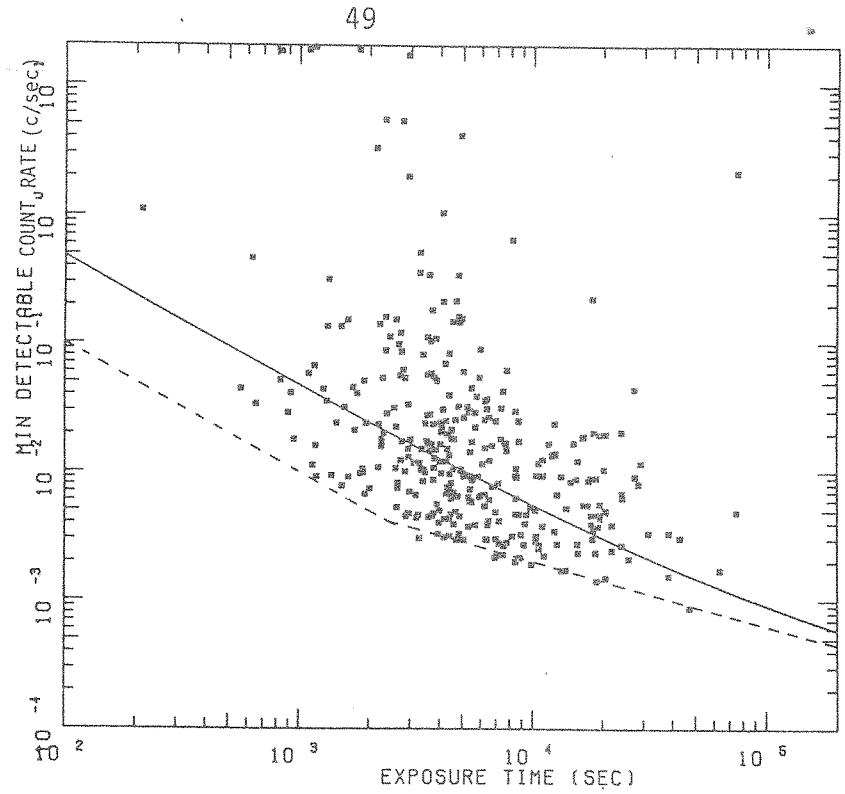

Figure 5

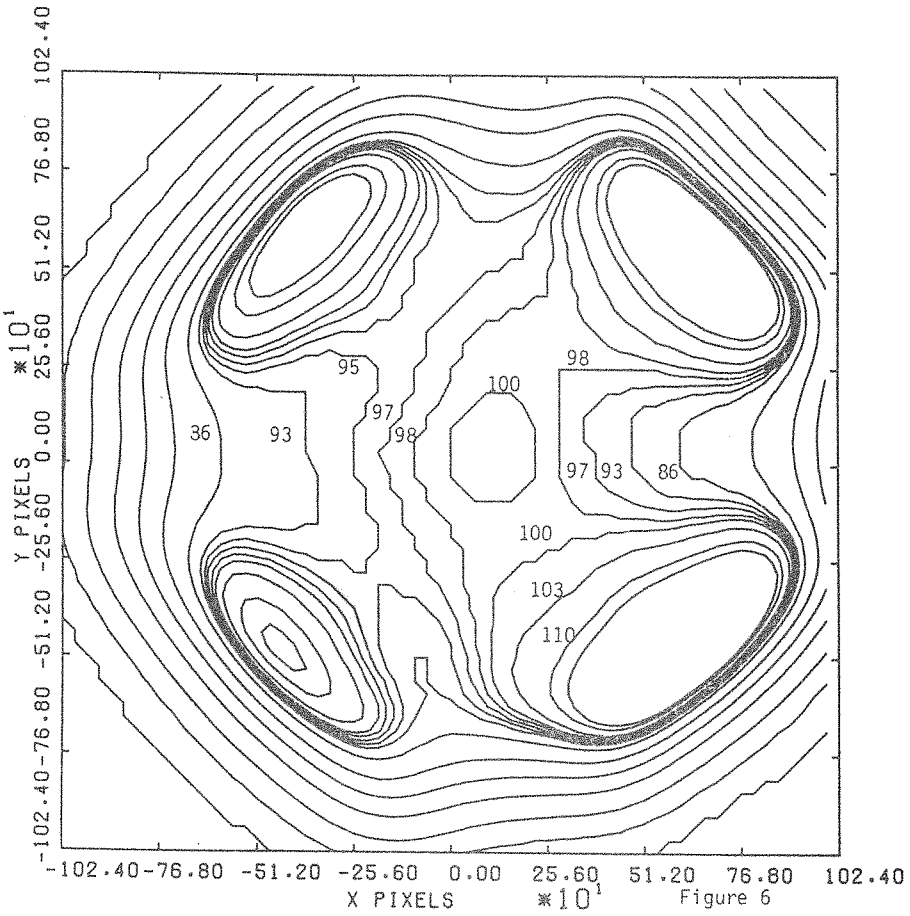

Figure 6

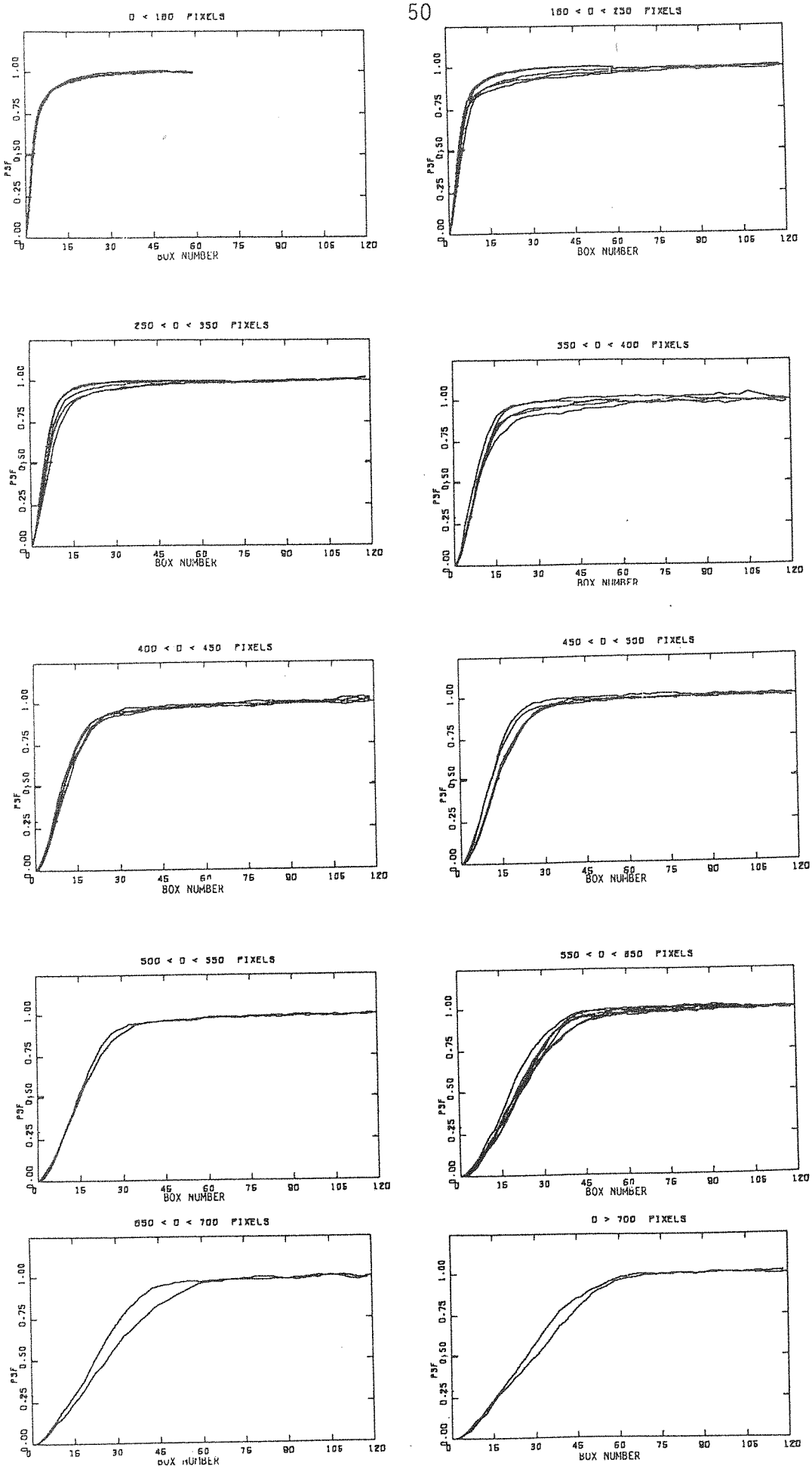
0 < 150 PIXELS
150 < 0 < 250 PIXELS
250 < 0 < 350 PIXELS
350 < 0 < 400 PIXELS
400 < 0 < 450 PIXELS
450 < 0 < 500 PIXELS
500 < 0 < 550 PIXELS
550 < 0 < 650 PIXELS
650 < 0 < 700 PIXELS
0 > 700 PIXELS
P3F
BOX NUMBER
0.00
0.25
0.50
0.75
1.00
15
30
45
60
75
90
105
120

Figure 7

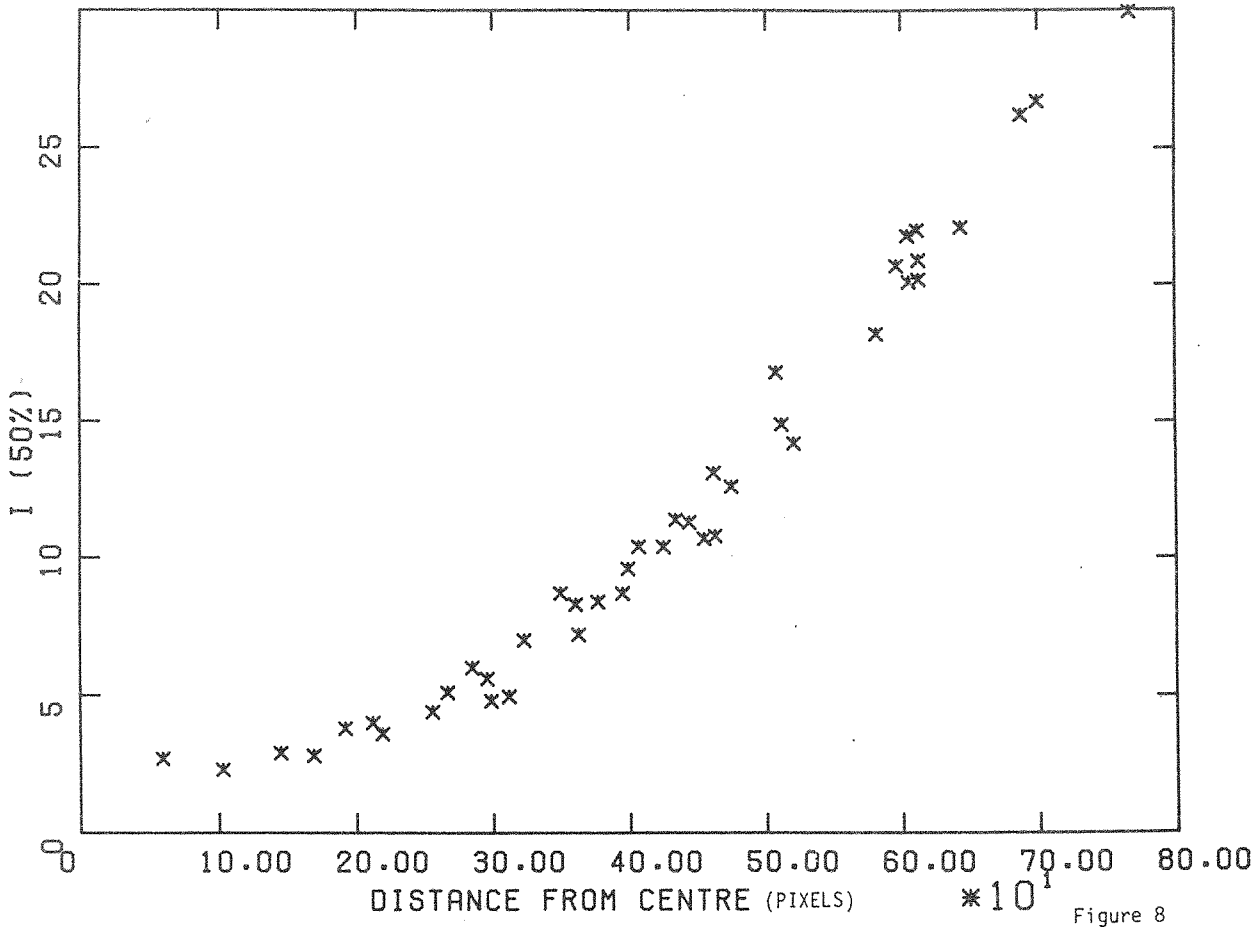

Figure 8

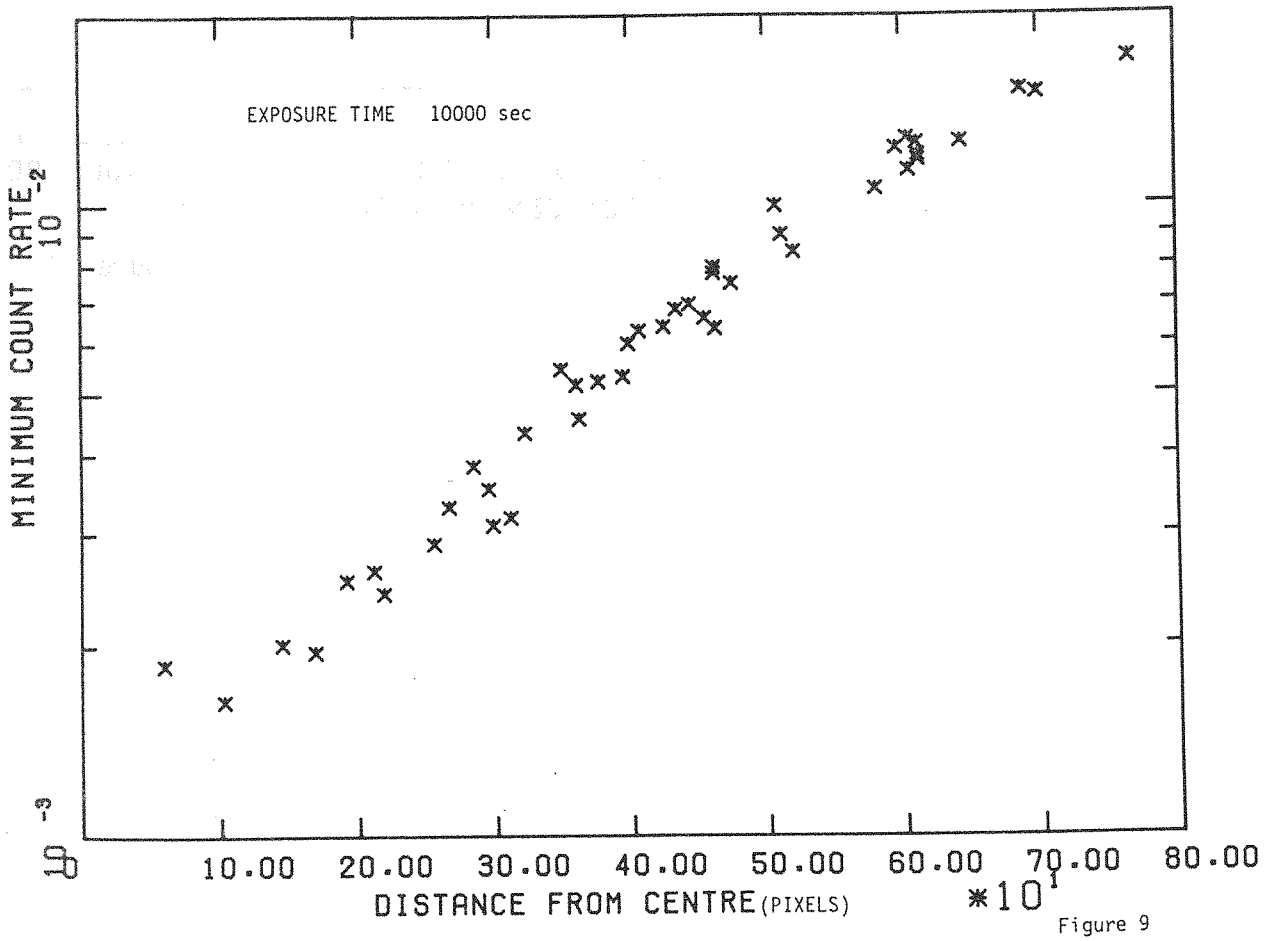

Figure 9

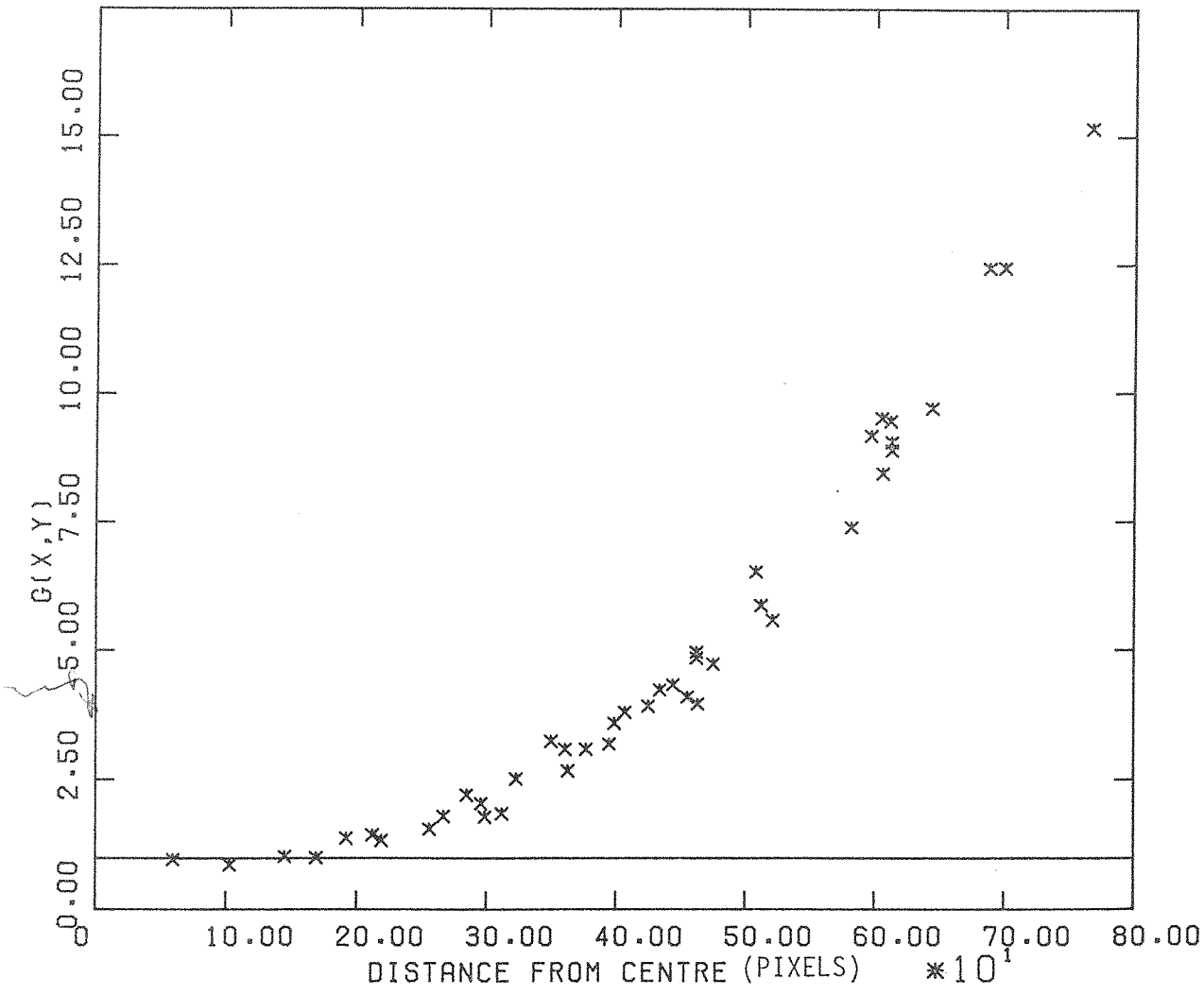
G(X,Y)
0.00
2.50
5.00
7.50
10.00
12.50
15.00
0
10.00
20.00
30.00
40.00
50.00
60.00
70.00
80.00
DISTANCE FROM CENTRE (PIXELS)
*10^1

Figure 10

EXOSAT ABSOLUTE SOURCE LOCATION

A Progress Report

1. Introduction

EXOSAT, ESA's first scientific three-axis stabilised satellite, is maintained in stable pointing with an accuracy of approximately ± 2-3 arc seconds using gyros for attitude measurement and control of a propane gas thruster system. The overall attitude measurement accuracy is about 5-6 arc seconds. A comparison of the determined EXOSAT position and the accurately known optical/radio position of a number of X-ray sources has shown systematic differences of 4 to 15 arc seconds with a mean of approximately 10". This note describes work carried out to investigate and improve the accuracy of EXOSAT source position determination.

2. Coordinate Transformations

Details of coordinate transformations, use of the attitude information and the telescope misalignment data have been given in the FOT Handbook (Sect.7.1). For completeness, the mathematics involved is presented here.

Generally, the transformation from the coordinate system (U,V,W) to a new coordinate system (X, Y, Z) involving rotation and no transition can be written as follows:

$$\begin{pmatrix} X \\ Y \\ Z \end{pmatrix} = \begin{pmatrix} X_U & X_V & X_W \\ Y_U & Y_V & Y_W \\ Z_U & Z_V & Z_W \end{pmatrix} \begin{pmatrix} U \\ V \\ W \end{pmatrix} = \underset{\sim}{T} \begin{pmatrix} U \\ V \\ W \end{pmatrix}$$

where X_U, X_V, X_W are the three components of the X unit vector with respect to U, V and W (so called direction cosines) etc.

If the coordinate frames are orthogonal then the transformation matrix T is orthogonal and the inverse of T is equal to the transpose.

$$\underset{\sim}{T}^{-1} = \underset{\sim}{T}^{T}$$

so that

$$\begin{pmatrix} U \\ V \\ W \end{pmatrix} = \underset{\sim}{T^T} \cdot \begin{pmatrix} X \\ Y \\ Z \end{pmatrix}$$

Three coordinate systems are defined as follows:

1) The star tracker reference frame (spacecraft axes): (X_{ST}, Y_{ST}, Z_{ST}).

2) The LE detector reference frame (after linearisation): (X_{LE}, Y_{LE}, Z_{LE}).

3) The Celestial Mean Equatorial (ME) 1950 reference frame: (X_{ME}, Y_{ME}, Z_{ME}).

Two transformations are required to establish the relation between the detector reference frame and the Mean Equatorial frame:

A) ME --------- ST
B) ST --------- LE

A) The auxiliary data on the FOT contain the spacecraft attitude defined as the three components of the roll, pitch and yaw axes with respect to the ME reference frame, ie:

$$\hat{roll} = (r_X, r_Y, r_Z)$$
$$\hat{pitch} = (p_X, p_Y, p_Z)$$
$$\hat{yaw} = (y_X, y_Y, y_Z)$$

The transformation ME ------ ST is then written as:

$$\begin{pmatrix} X_{ST} \\ Y_{ST} \\ Z_{ST} \end{pmatrix} = \underset{\sim}{RPY} \cdot \begin{pmatrix} X_{ME} \\ Y_{ME} \\ Z_{ME} \end{pmatrix}$$

with

$$\underset{\sim}{RPY} = \begin{pmatrix} \hat{roll} \\ \hat{pitch} \\ \hat{yaw} \end{pmatrix} = \begin{pmatrix} r_X & r_Y & r_Z \\ p_X & p_Y & p_Z \\ y_X & y_Y & y_Z \end{pmatrix} = \begin{pmatrix} AUX_1 & AUX_2 & AUX_3 \\ AUX_4 & AUX_5 & AUX_6 \\ AUX_7 & AUX_8 & AUX_9 \end{pmatrix}$$

where AUX_1 .... AUX_9 are the values in the Auxiliary data file on the FOT, record 3 bytes 8-124 (see FOT Handbook, Sect. 3.8 p.11). Note that these values are converted from the requested nominal pointing direction. The actual pointing direction is obtained from the star positions in the star tracker field of view (refer to next section). $\underset{\sim}{RPY}$ is the attitude matrix printed in the automatic analysis output.

A 5" offset is applied to the Y-axis limit cycle to overcome an operational problem of the AOCS electronics (ref. Express No.4 p.34). This affects all observations carried out from 15.9.83 at 07.00 UT (day 253, SHF time key 116924400) and pointing positions must be corrected appropriately by an additional transformation.

$$\underset{\sim}{ROT} = \begin{pmatrix} \cos(\varepsilon) & 0 & -\sin(\varepsilon) \\ 0 & 1 & 0 \\ \sin(\varepsilon) & 0 & \cos(\varepsilon) \end{pmatrix}$$

where $\varepsilon = +5"$.

B) The relationship between the ST and LE frames is given by the telescope misalignment data in the LE CCF (data type BD) The transformation ST ------ LE is written as:

$$\begin{pmatrix} X_{LE} \\ Y_{LE} \\ Z_{LE} \end{pmatrix} = \underset{\sim}{MIS} \begin{pmatrix} X_{ST} \\ Y_{ST} \\ Z_{ST} \end{pmatrix}$$

with

$$\underset{\sim}{MIS} = \begin{pmatrix} X_{MIS} \\ Y_{MIS} \\ Z_{MIS} \end{pmatrix} = \begin{pmatrix} MIS_1 & MIS_2 & MIS_3 \\ MIS_4 & MIS_5 & MIS_6 \\ MIS_7 & MIS_8 & MIS_9 \end{pmatrix}$$

where MIS_1 .... MIS_9 are given in the LE CCF (data type BD) bytes 0 - 35 (CMA) multiplied by 10^9.

The misalignment is the displacement of the LE frame with respect to the ST frame (see Fig. 1) and can be derived in terms of 3 consecutive rotational matrices about the roll, pitch and yaw axes:

$$MIS = Y_{\Delta\gamma} \; P_{\Delta\beta} \; R_{\Delta\alpha}$$

where $\Delta\alpha$, $\Delta\beta$ and $\Delta\gamma$ are the anti-clockwise rotational angles (misalignment angles) as seen from the respective positive axis in the direction of the origin (fig. 1).

$$\underset{\sim}{R}_{\Delta\alpha} = \begin{pmatrix} 1 & 0 & 0 \\ 0 & \cos\Delta\alpha & \sin\Delta\alpha \\ 0 & -\sin\Delta\alpha & \cos\Delta\alpha \end{pmatrix} \quad \text{Roll}$$

$$\underset{\sim}{P}_{\Delta\beta} = \begin{pmatrix} \cos\Delta\beta & 0 & -\sin\Delta\beta \\ 0 & 1 & 0 \\ \sin\Delta\beta & 0 & \cos\Delta\beta \end{pmatrix} \quad \text{Pitch}$$

$$\underset{\sim}{Y}_{\Delta\gamma} = \begin{pmatrix} \cos\Delta\gamma & \sin\Delta\gamma & 0 \\ \sin\Delta\gamma & \cos\Delta\gamma & 0 \\ 0 & 0 & 1 \end{pmatrix} \quad \text{Yaw}$$

yielding the following matrix elements of $\underset{\sim}{MIS}$:

$MIS_1 = \cos\Delta\beta \cdot \cos\Delta\gamma$

$MIS_2 = \cos\Delta\alpha \cdot \sin\Delta\gamma + \sin\Delta\alpha \cdot \sin\Delta\beta \cdot \cos\Delta\gamma$

$MIS_3 = \sin\Delta\alpha \cdot \sin\Delta\gamma - \cos\Delta\alpha \cdot \sin\Delta\beta \cdot \cos\Delta\gamma$

$MIS_4 = -\cos\Delta\beta \cdot \sin\Delta\gamma$

$MIS_5 = \cos\Delta\alpha \cdot \cos\Delta\gamma - \sin\Delta\alpha \cdot \sin\Delta\beta \cdot \sin\Delta\gamma$

$MIS_6 = \sin\Delta\alpha \cdot \cos\Delta\gamma + \cos\Delta\alpha \cdot \sin\Delta\beta \cdot \sin\Delta\gamma$

$MIS_7 = \sin\Delta\beta$

$MIS_8 = -\sin\Delta\alpha \cdot \cos\Delta\beta$

$MIS_9 = \cos\Delta\alpha \cdot \cos\Delta\beta$

Note the sign error in MIS_4 in the FOT Handbook (Sect. 7.1 p.49).

The misalignment angles can be extracted from the given misalignment matrix MIS as follows:

$$\Delta\alpha = -\tan^{-1}(MIS_8/MIS_9)$$

$$\Delta\beta = \sin^{-1}(MIS_7)$$

$$\Delta\gamma = -\tan^{-1}(MIS_4/MIS_1)$$

Thus, the transformation ME ------ LE is:

$$\begin{pmatrix} X_{LE} \\ Y_{LE} \\ Z_{LE} \end{pmatrix} = \underset{\sim}{MIS} \cdot \underset{\sim}{ROT} \cdot \underset{\sim}{RPY} \begin{pmatrix} X_{ME} \\ Y_{ME} \\ Z_{ME} \end{pmatrix}$$

and inversely:

$$\begin{pmatrix} X_{ME} \\ Y_{ME} \\ Z_{ME} \end{pmatrix} = \underset{\sim}{MIS}^T \cdot \underset{\sim}{ROT}^T \cdot \underset{\sim}{RPY}^T \begin{pmatrix} X_{LE} \\ Y_{LE} \\ Z_{LE} \end{pmatrix} = \begin{pmatrix} \lambda_1 & \lambda_2 & \lambda_3 \\ \mu_1 & \mu_2 & \mu_3 \\ \nu_1 & \nu_2 & \nu_3 \end{pmatrix} \begin{pmatrix} X_{LE} \\ Y_{LE} \\ Z_{LE} \end{pmatrix}$$

Fig.2 shows the orientation of the spacecraft in the ME frame and the definition of the north angle θ_o. The detector origin (= detector pointing direction) α_o, δ_o and north angle θ_o are derived as follows: the coordinates (X_o, Y_o, Zo) of the detector origin in the ME frame can be expressed in terms of α_o and δ_o:

$$X_o = \cos\alpha_o \cos\delta_o$$

$$Y_o = \sin\alpha_o \cos\delta_o$$

$$Z_o = \sin\delta_o$$

The pointing direction in the detector reference frame is given as the vector (1, 0, 0), so:

$$\begin{pmatrix} X_o \\ Y_o \\ Z_o \end{pmatrix} = \begin{pmatrix} \lambda_1 & \lambda_2 & \lambda_3 \\ \mu_1 & \mu_2 & \mu_3 \\ \nu_1 & \nu_2 & \nu_3 \end{pmatrix} \begin{pmatrix} 1 \\ 0 \\ 0 \end{pmatrix}$$

or $X_o = \lambda_1$, $Y_o = \mu_1$, $Z_o = \nu_1$

from which : $\alpha_o = \tan^{-1}(Y_o/X_o) = \tan^{-1}(\mu_1/\lambda_1)$

$\delta_o = \sin^{-1}(Z_o) = \sin^{-1}(\nu_1)$

θ_o is defined as the anti-clockwise angle between the E_x axis (the axis in the linearised detector coordinate frame, see Fig.2) which is equivalent to the $-Z_{LE}$ axis, and the north direction. From Fig.2 it follows that θ_o equals the angle between the normals to the planes QOP and NOP, ie. the angle between $-\hat{Y}_{LE}$ and $\hat{V}$ where $\hat{V}$ is given by $\hat{N} \times \hat{X}_{LE} = \sin(\pi/2-\delta_o)\hat{V} = \cos(\delta_o)\hat{V}$ (since N and X_{LE} make an angle of $\pi/2-\delta_o$). Note that $\hat{X}_{LE} = (\lambda_1, \mu_1, \nu_1)$, $\hat{Y}_{LE} = (\lambda_2, \mu_2, \nu_2)$ and $\hat{N} = (0, 0, 1)$ in the ME frame.

$$\text{Thus } \cos\theta_0 = -(\hat{Y}_{LE} - \hat{V}) = -\sec\delta_0 \left\{ \hat{Y}_{LE}.(\hat{N} \times \hat{X}_{LE}) \right\}$$

$$= -\sec\delta_0 \begin{vmatrix} \lambda_2 & \mu_2 & \nu_2 \\ 0 & 0 & 1 \\ \lambda_1 & \mu_1 & \nu_1 \end{vmatrix}$$

$$= -\sec\delta_0 \, (-\lambda_2\mu_1 + \lambda_1\mu_2)$$

$$= \frac{\lambda_2\,\mu_1 - \lambda_1\,\mu_2}{\sqrt{1 - \nu_1^2}}$$

$$\text{and } \sin\theta_0 = -\left\{ \hat{X}_{LE} .(-\hat{Y}_{LE} \times \hat{V}) \right\}$$

or

$$\sin\theta_0 = \sec\delta_0 \left\{ \hat{X}_{LE}.(\hat{Y}_{LE} \times (\hat{N} \times \hat{X}_{LE})) \right\}$$

$$= \sec\delta_0 \left\{ \hat{X}_{LE}.((\hat{X}_{LE}.\hat{Y}_{LE})\hat{N} - (\hat{N}.\hat{Y}_{LE})\hat{X}_{LE}) \right\}$$

$$= -\sec\delta_0 \; (\hat{N}.\hat{Y}_{LE}) = -\sec\delta_0.\nu_2$$

$$= \frac{-\nu_2}{\sqrt{1 - \nu_1^2}}$$

3. Results

An analysis of a number of EXOSAT X-ray sources with known optical or radio counterparts and no detectable proper motion has been carried out and the results are summarised in Table 1. Source positions were taken from the compilations of Burbridge et al. (1977), Lang (1980), Weller et al. (1980) and Clements (1981). The fourth column of Table 1 gives the day of observation and the next three columns the resulting number of counts (cts) and the position X_b, Y_b in the L1 CMA, determined as the baricentre of the distribution of the source counts corrected for background obtained from regions outside the source location.

EXOSAT RA and Dec. positions are derived using the formula given in the FOT Handbook (Sect. 7.1 p.46). The 5" offset of the Y-axis limit cycle and refinements to the accuracy of the calculation were included. Columns $\Delta\alpha_b$ and $\Delta\delta_b$ give the deviations (arcsec) of the EXOSAT position with respect to the known optical/radio position (column 2 and 3).

Secondly, a correction has been applied for the typical limit cycle of ± 2-3 arcseconds maintained during an observation. Image 'deblurring' was carried out by the simple method of calculating the mean offset (pixels) in pitch (Δ p) and yaw (Δ y) from the attitude data in the HK records and changing the positions accordingly (see Fig. 1):

$$X_d = X_b + \Delta p$$
$$Y_d = Y_b - \Delta y$$

from which the deviations $\Delta\alpha_d$ and $\Delta\delta_d$, of the order of 10", were calculated. In general, Δp and Δy are less than $\sim$2".

Two X-ray sources (3C273 and 1156+295) in the sample have twice been observed about half a year apart, with opposite orientation of the spacecraft. Fig. 3 shows the computed 'deblurred' positions for 3C273 together with the orientation of the E_X, E_Y plane of the L1 CMA. The source was observed using different filters yielding a number of positions which are within a region of about 4" diameter. A systematic error is clearly present, the two sets of observations each being located opposite the true source position and about 30" apart. Observations of 1156+295 show the same behaviour suggesting a telescope to star tracker misalignment error. This error has been calculated empirically by taking for each set of observations the difference in the E_X and E_Y direction:

3C273 :	X	=	24.3",	Y	= -18.2"
1156+205 :	X	=	23.",	Y	= -22.5"
Mean :	X	=	23.66",	Y	= -20.36"

giving the following errors in the misalignment angles (see Fig.1).

$$\Delta\beta_e = X/2 = -11.83"$$
$$\Delta\gamma_e = Y/2 = +10.18"$$

If this correction is applied to the misalignment angles, new positions and deviations $\Delta\alpha_N$ and $\Delta\delta_N$ are derived. These deviations are typically less than $\sim$7".

In July 1985, improved star tracker calibration reference data was implemented at ESOC (p.2) yielding a better knowledge of the actual pointing direction. Generally, the calculated (requested) pointing direction is within $\sim$1" of the actual one. As a final correction to the EXOSAT positions, this new calibration data gave slightly improved deviations $\Delta\alpha_{NS}$ and $\Delta\delta_{NS}$. Δ_{NS}, the corresponding distance, is now typically $\sim$ 6".

There are a few exceptions to this, some of which may be caused by the linearisation of the detector read-out positions. The linearisation for LE1 is based on an in-flight raster scan (Cyg X-2), which is less accurate than the ground-based calibration for the LE2 CMA. However, close to the detector origin, where the linearisation is most accurate, Δ_{NS} the difference between known RA, DEC and the EXOSAT position is less than 4-5".

In some cases, poor statistics ($\lesssim$ 50 cts) may yield inaccurate positions, see eg. the third pointing of MKN 421, where Y_b is about 1 pixel less than the two previous values.

4. Conclusions and Status of Analysis Software

For a small sample of X-ray sources accurate positions have been determined by including in the analysis the following factors:

- improvement in the calculation accuracy
- 5" offset applied to the Y-axis limit cycle.
- image deblurring of the 2-3" limit cycle.
- possible errors in telescope star tracker misalignment.
- improved star tracker calibration data.

Systematic errors are now negligible and generally the deviation with respect to the known optical/radio position is $\lesssim$ 6", well within the design goal of the system.

Further work is in progress to:

- implement a more sophisticated deblurring method where each photon is treated individually.

- use a correlation technique in which the source distribution is compared to the PSF based on (in-flight) calibrations.

- analyse several sets of observations separated by half a year to determine the misalignment errors accurately, together with any time dependence.

The Observatory software has been modified as a result of this work as follows:

(A) Interactive Analysis system

- 5" offset of the Y axis limit cycle included.
- improved accuracy of the calculation.
- new set of misalignment angles.

No deblurring to account for the limit cycle is presently included since in certain cases the algorithm appears to give misleading figures - the problem is under investigation.

(B) Auto analysis software

No modifications

NB: (1) the new star tracker calibration data is automatically used as from 30.7.85. Observations carried out prior to 30.7.85 have been analysed using the old reference data although any differences in derived pointing are generally small (~1") compared to the other effects described above.

(2) the misalignment angles have not been modified in the CCF, pending further study.

Users primarily interested in very accurate position determination are therefore requested to contact the Observatory Team or apply to use the IA analysis system.

E. Gronenschild

References

Burbridge, G.R., Crowne, A.H., Smith, Harding, E. Ap.J.Suppl., 33, 113 (1977).
Clements, E.D. M.N.R.A.S. (1981), 197, 829.
Lang, K.R. Astrophysical Formulae, p.195 (1980).
Weller, K.W., Johnston, K.J. M.N.R.A.S. (1980), 190, 269.

Figure Captions

Figure 1

Orientation of EXOSAT coordinate reference frames of the star tracker and the LE detector, showing the misalignment angles $\Delta\alpha$, $\Delta\beta$ and $\Delta\gamma$

Figure 2

The spacecraft attitude in the mean equatorial (ME) coordinate drame. The pointing direction is given by the vector X_{LE}, the detector origin by α_o and δ_o. The north angle θ_o is defined as shown.

Figure 3

The observations of 3C273. Two sets of observations were carried out, separated by half a year. The first set yielded positions in the lower right-hand corner, the second set in the upper left-hand corner (numbers refer to the sequence of pointings givien in Table 1). The orientation of the detector reference frame E_X, E_Y is also indicated. Final source positions (index NS) after deblurring, incorporation of the new misalignment angles and taking the actual pointing positions based on a new star tracker calibration are now close to the true source position.

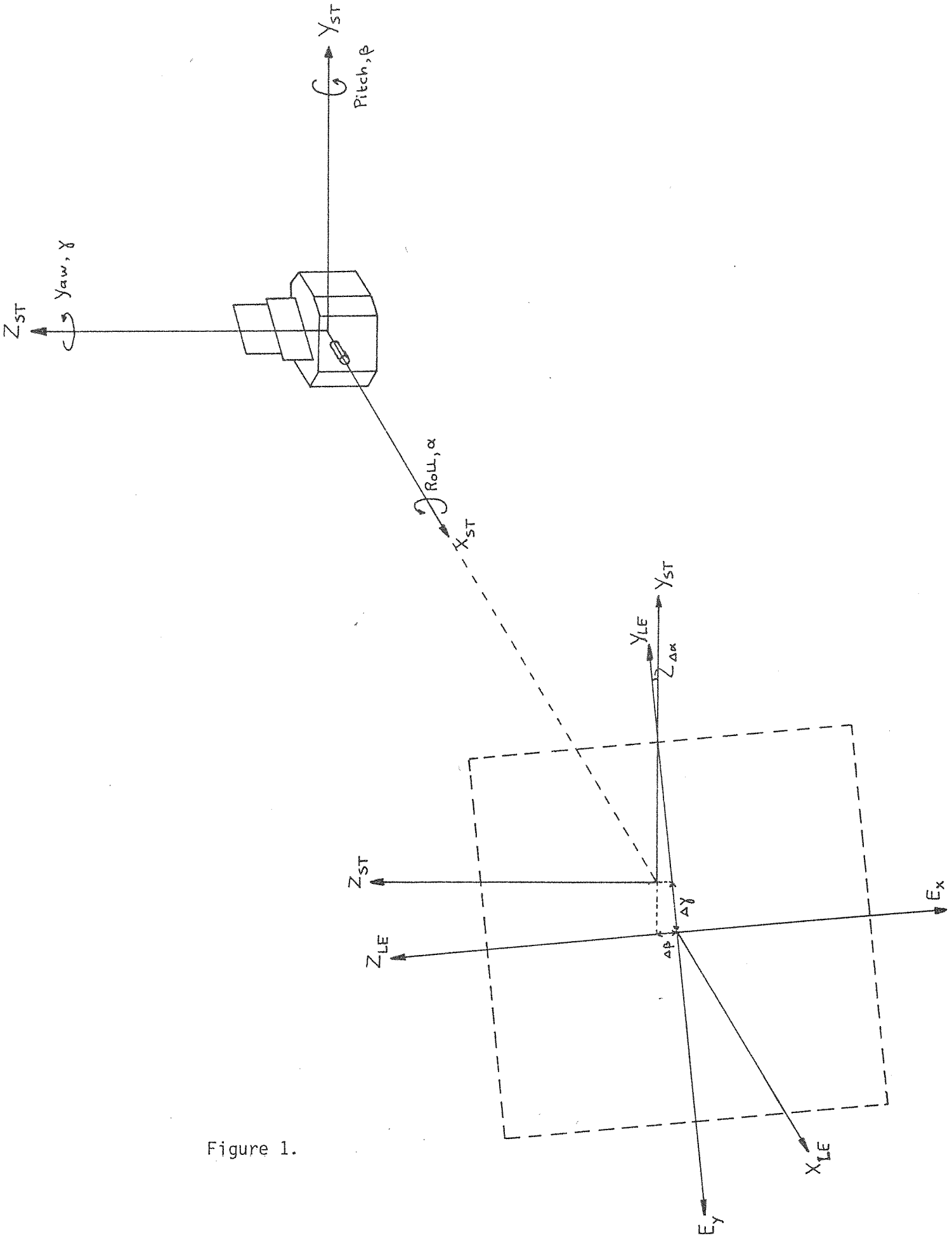
Y_{ST}
Pitch, β
Yaw, γ
Z_{ST}
Roll, α
X_{ST}
Y_{ST}
Y_{LE}
$\Delta\alpha$
Z_{ST}
E_x
$\Delta\gamma$
Z_{LE}
$\Delta\beta$
X_{LE}
E_y

Figure 1.

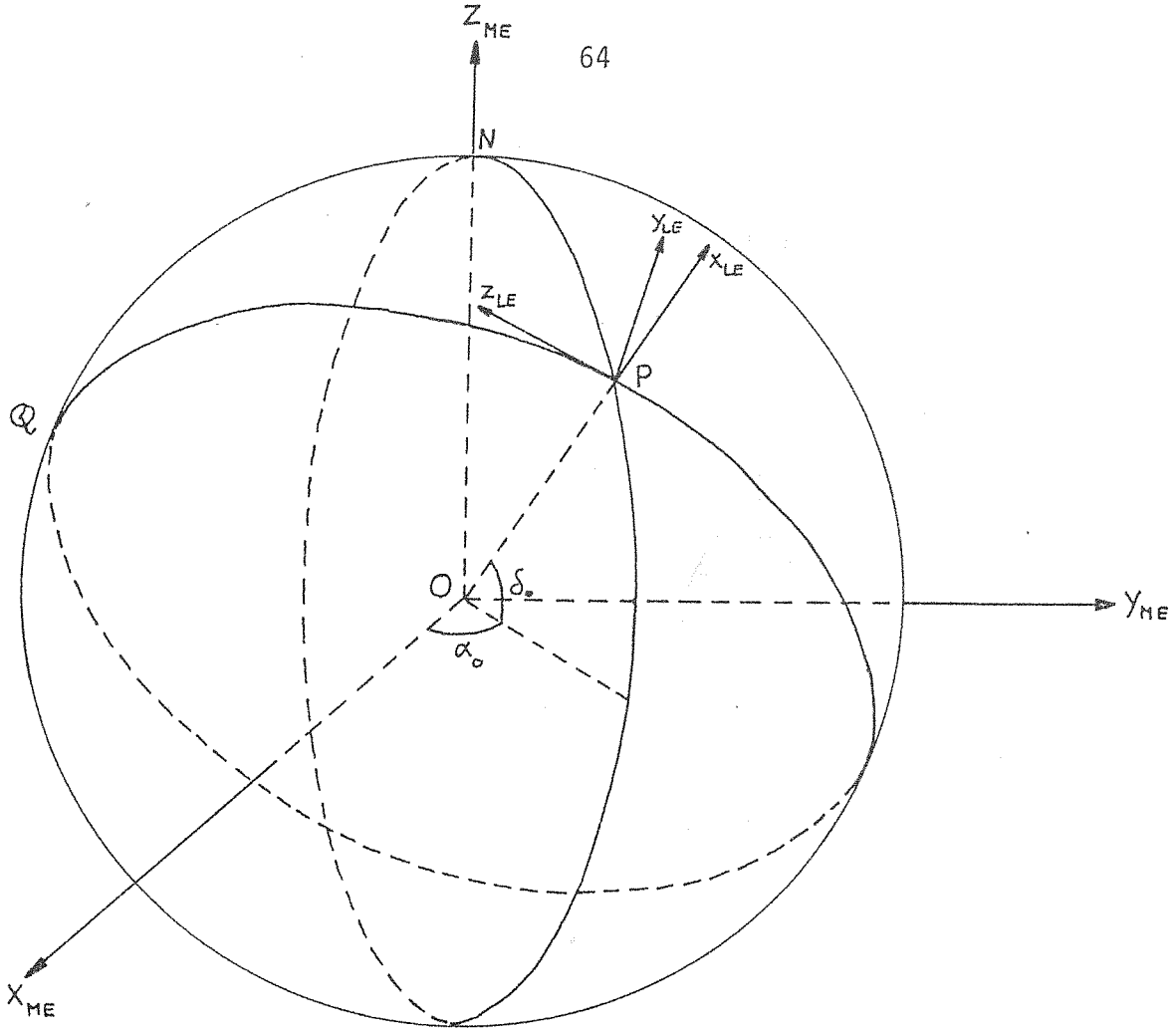
Z_{ME}
N
Y_{LE}
X_{LE}
Z_{LE}
P
Q
O
δ_o
α_o
Y_{ME}
X_{ME}

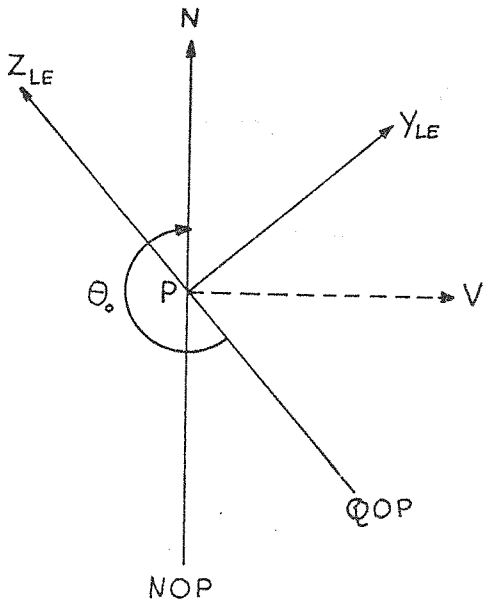
N
Z_{LE}
Y_{LE}
θ_o
P
V
QOP
NOP

Figure 2.

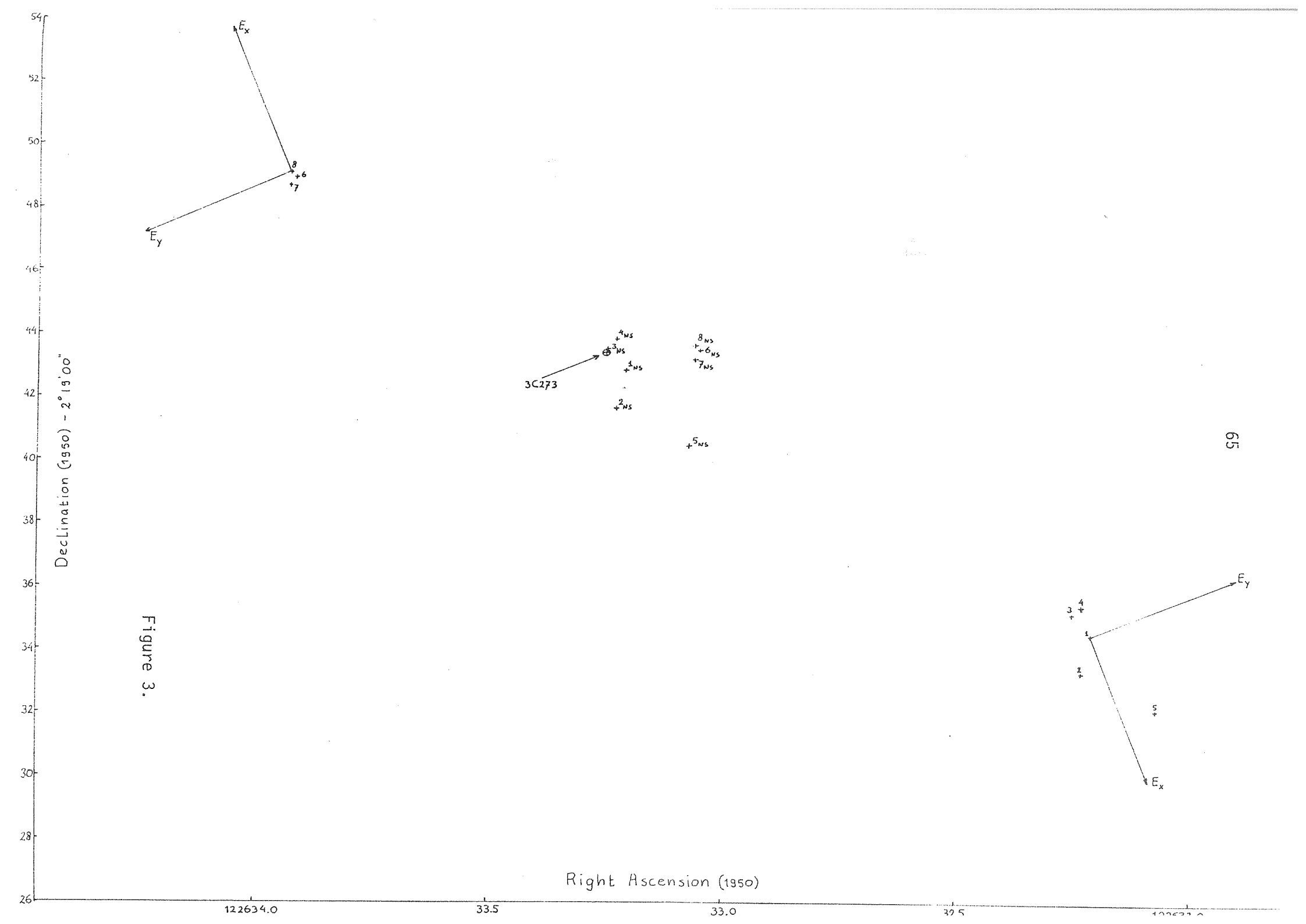
54
52
50
48
46
44
42
40
38
36
34
32
30
28
26
Declination (1950) - 2°19'00"
Right Ascension (1950)
122634.0
33.5
33.0
32.5
E_x
E_y
8
6
7
3C273
4 NS
3 NS
1 NS
2 NS
5 NS
8 NS
6 NS
7 NS
E_y
E_x
3
4
1
2
5

Figure 3.

Source	RA	DEC	DAY	cts	X_b	Y_b	$\Delta\alpha_b$	$\Delta\delta_b$	$\Delta\alpha_d$	$\Delta\delta_d$	$\Delta\alpha_N$	$\Delta\delta_N$	$\Delta\alpha_{NS}$	$\Delta\delta_{NS}$	Δ_N
3C120	043031.61	+051459.79	83/305	198	-40.09	-110.59	-5.6	-9.0	-5.9	-9.5	7.8	-2.0	6.2	-1.8	6.5
"	"	"	"	157	-39.42	-109.36	-11.1	-9.8	-11.3	-9.6	2.3	-2.0	0.7	-1.8	1.9
"	"	"	84/008	96	0.81	2.92	-1.4	14.6	-2.7	13.6	-6.2	-1.6	-6.3	-1.8	6.6
"	"	"	"	32	0.60	3.20	0.0	14.4	-0.6	14.4	-4.1	-0.8	-4.2	-1.0	4.3
MKN79	073847.34	+495540.88	84/090	271	-0.94	3.46	12.6	7.1	11.3	5.6	-1.5	-3.3	-2.2	-4.2	4.7
"	"	"	"	61	-2.47	4.11	13.5	0.6	12.5	-1.0	-0.3	-9.9	-1.0	-10.8	10.9
"	"	"	"	23	-0.94	4.25	15.6	6.3	14.7	4.7	1.8	-4.2	1.1	-5.1	5.2
EX0751-674	074824.90	-673732.30	85/046		0.08	-1.16	-0.4	13.6	-0.4	13.6	4.7	-1.1	4.9	-1.4	5.1
"	"	"	/050		-0.35	0.73	-5.5	15.0	-5.0	14.5	-1.0	-0.6	1.3	-1.2	1.8
"	"	"	/057		-1.05	1.40	1.7	16.1	2.1	15.7	4.1	0.3	4.2	0.0	4.2
"	"	"	/069		41.83	2.00	-5.3	21.8	-5.3	21.2	-6.6	5.7	-6.4	5.4	8.4
"	"	"	/088		74.52	-10.68	7.5	20.3	7.5	19.7	1.5	5.3	4.1	4.4	6.0
"	"	"	/099		61.11	10.53	5.2	25.0	5.2	24.3	-3.6	11.4	-1.4	10.8	10.9
MKN421	110140.57	+382843.00	84/037	1432	-7.42	-6.66	-1.0	-9.6	-0.5	-10.3	0.6	5.3	3.4	2.5	4.2
"	"	"	"	577	-7.19	-6.70	-0.3	-10.3	0.5	-10.8	1.6	4.7	4.4	1.9	4.8
"	"	"	"	53	-7.06	-7.84	3.7	-8.0	3.9	-8.7	5.0	6.8	7.8	4.0	8.8
1156+295	115658.10	+293124.00	83/336	58	-28.68	-15.12	-23.0	-13.7	-21.4	-12.2	-6.7	-7.0	-5.5	-6.3	8.4
"	"	"	84/151	44	0.64	4.96	8.6	-3.6	9.5	-3.3	-5.1	-8.4	-4.0	-7.7	8.7
"	"	"	"	35	0.74	5.26	9.9	-3.8	10.7	-3.5	-3.9	-8.7	-2.8	-8.0	8.5
2A1219+305	121851.77	+302714.00	84/037	1017	-46.23	-63.20	-7.1	-17.0	-5.8	-16.0	2.6	-2.8	3.1	-3.2	4.5
"	"	"	"	486	-46.11	-63.33	-6.5	-17.4	-5.2	-16.4	3.2	-3.3	3.7	-3.7	5.2
"	"	"	"	57	-45.19	-64.09	-3.0	-20.6	-2.0	-19.5	6.4	-6.4	6.9	-6.8	9.7
3C273	122633.25	+021943.38	84/006	671	1.27	1.46	-15.0	-7.4	-15.5	-8.9	-1.5	-1.9	-0.4	-0.5	0.6
"	"	"	"	151	1.53	1.28	-14.8	-8.7	-15.3	-10.1	-1.3	-3.1	-0.2	-1.7	1.7
"	"	"	"	379	1.07	1.38	-14.4	-6.8	-14.9	-8.2	-1.0	-1.2	0.1	0.2	0.2
"	"	"	"	698	1.77	1.47	-15.8	-9.3	-15.2	-7.9	-1.2	-1.0	-0.1	0.4	0.4
"	"	"	"	636	2.02	1.72	-17.1	-9.8	-17.6	-11.3	-3.6	-4.3	-2.5	-2.9	3.8
"	"	"	84/180	2501	3.06	-5.93	10.4	6.6	10.1	5.6	-3.9	-1.3	-2.8	0.1	2.8
"	"	"	"	1007	2.94	-5.84	10.6	6.0	10.3	5.4	-3.8	-1.5	-2.7	-0.1	2.7
"	"	"	"	351	3.02	-5.87	10.6	6.3	10.3	5.8	-3.8	-1.1	-2.7	0.0	2.7
MKN501	165211.73	+395026.00	84/036	1741	-43.50	33.23	-12.4	6.0	-10.1	3.1	4.5	8.7	3.3	8.5	9.1
"	"	"	"	886	-43.86	32.98	-10.8	6.8	-8.9	4.0	5.6	9.6	4.4	9.4	10.4
"	"	"	"	109	-43.52	33.02	-11.6	5.7	-9.5	2.8	5.1	8.4	3.9	8.2	9.1
3C390.3	184537.57	+794306.52	84/153	27	-2.39	-5.79	7.4	-8.2	4.9	-9.4	0.0	5.4	-1.6	5.5	5.7
"	"	"	"	33	-3.72	-5.80	2.9	-5.5	0.6	-6.8	-4.3	7.9	-5.9	8.0	9.9
PKS2155-304	215558.20	-30.2751.80	83/304	6167	-0.45	1.83	4.1	7.5	7.4	8.4	3.5	-6.7	4.1	-6.0	7.3
"	"	"	"	2799	-0.45	1.36	2.4	6.6	5.7	7.6	1.9	-7.6	2.5	-6.9	7.3
"	"	"	"	389	-0.97	0.88	1.6	3.9	5.0	4.8	1.2	-10.3	1.8	-9.7	9.9

Table 1.

IMAGE OBSCURATION IN THE LE TELESCOPES

1. Summary

Ray tracing studies have been performed to clarify the origin of unexpected structural features observed in the images of both EXOSAT low energy telescopes. A comparison of observed and simulated images covering the total field of view suggests that the ME flap has opened by an angle of 94.5 ± 0.5 degrees, thereby obstructing the aperture of LEIT1 and LEIT2 and reducing the effective telescope throughput to 0.721 of its nominal value for on-axis sources. Several other possible causes of the image obscuration have been investigated and rejected, viz: LE flap not fully opened, transmission grating ring not entirely in "out" position, filter wheel position shift, selective degradation of mirror coating material, field stop position shift and entrance aperture position shift.

Although 'over-opening' of the ME flap can explain the anomalous features observed in the LEIT images, MBB (the satellite prime contractor) comment that there is no evidence that the mechanical design was in any sense marginal and that qualification tests in vacuum demonstrated in a fully representative fashion the performance of the hardware and its conformity with design.

2. Diagnosis of observed images

Note that two different coordinate systems are commonly used in describing the EXOSAT system: the spacecraft coordinate system and the LE image coordinate system. +y of the image system is practically equivalent to -y of the spacecraft system and +x of the image system to -z of the spacecraft system. Unless stated, reference is made to the image system coordinates.

An analysis of a number of images at different positions in the field of view of both telescopes has been carried out using data from a raster scan observation of Cyg X-2 (day 186, 1983). 40 positions in the LEIT1 FOV and 7 in the LEIT2 FOV have been used. Fig. 1 shows typical images (LEIT1) in each quadrant at approximately 25 arc min from the centre of the FOV.

A number of conclusions can be drawn from an analysis of the images:-

1. For all field positions outside a radius of about 15 arcmin around the centre, the image shows a cut-out wedge of nearly zero brightness.

2. Each wedge is symmetric with respect to the y-axis and opens towards the +y direction.

3. The opening angle of each wedge is between 95° and 120°.

4. Images at opposite y positions tend to show a change in opening angle but in general the characteristics of the wedges in each of the four quadrants of the field of view are identical.

5. Images with a relatively high surface brightness reveal a wedge not of zero brightness but containing counts clearly in excess of the ambient background.

6. LEIT1 and LEIT2 images show identical wedges for each field of view position.

7. Close to the centre of the field of view, ie. at a radial distance of less than about 15 arcmin, the images appear elongated, being longer in the x than in the y direction.

3. Ray Tracing in the EXOSAT LE Telescopes

EXOSAT carries two identical low energy imaging X-ray telescopes of the Wolter type 1 configuration, ie. a confocal and co-axial mounting of a grazing incidence paraboloid and hyperboloid. Each telescope comprises two nested systems. The telescope optical axis is oriented in the +x direction (in spacecraft coordinates). The field of view is limited by field stops in the paraboloid and hyperboloid section. For stray light baffling, an aperture plate is mounted in front of the telescope. It has a free opening slightly larger than would be required for the field of view. Flaps, which covered the ME detectors (ME flap) and both telescopes (LE flap) during the ground calibration and launch phases, were opened in flight to act as telescope and star tracker light baffles and are positioned towards +y and -y respectively (spacecraft coordinates) with their surface planes parallel to the x-z plane.

The following items have been specifically modelled in the program:-

- mirror surface geometry.
- size and position of field stops in the paraboloid and hyperboloid sections.
- size and position of entrance aperture plate.
- position of grating hinges.
- size and position of grating ring.

- size and position of filter wheel opening.
- position of LE flap hinges.
- size and position of LE flap.
- position of ME flap hinges.
- size and position of ME flap.

A dedicated ray tracing program has been used to simulate the X-ray images formed by the EXOSAT LE telescopes. The code generates X-ray events randomly distributed across the aperture area for any given angle of incidence and determines their paths to the focal plane, checking for the proper intersection requirements with the mirror surfaces and for any obstruction.

Because perfect mirror surfaces introduce additional features in the images, the program includes local axial slope errors of the surfaces, according to the measurements on the EXOSAT qualification model (P. de Korte et al. App.Optics, 20, 1080 (1981)).

4. Origin of the Image Distortions

Since the wedge in the X-ray images is always in the +y direction, the location of the obscuring object is in one specific hemisphere. Extreme ray paths for the inner and outer shells of the telescope system define the envelope of the ray bundle within which rays can be focussed by the telescope. Figure 2 gives a close-up view of this envelope in the region of the focal plane and shows that rays entering the telescope at the highest y-values are imaged into a region of lowest y-values and vice versa. This property is important because any image distortion can then be attributed directly to the relevant hemisphere of the telescope and the origin of the distortion investigated along the ray path in this particular hemisphere.

Because the wedges appear at +y, the obscuring body has to be in the -y hemisphere as seen from the telescope's optical axis. This conclusion is valid (see figure 2) if the detector is located close to the nominal focal plane. (Only a shift of more than 7 mm towards the mirror system would give the reverse signs. Such a de-focussing would however produce a significantly broadened on-axis image - which is not observed). The following items can therefore be excluded as possible obstructions of the ray path because they both are located in the +y hemisphere.

- the transmission grating ring (not fully in "out" position).
- the LE flap (not fully opened).

4 candidate obscuring mechanisms, all associated with the -y hemisphere, have been studied and rejected as follows:

A shift of the filter wheel in the y direction - obscuration at +y and -y cannot be reproduced.

Deterioration of the gold coating of the mirror surfaces over a sector angle of about 100 degrees, such that the reduced reflectivity produces a wedge of lower surface brightness in the X-ray image - a significant flux would be expected even if the gold were totally removed and this is not observed.

A shift of the field stops inside the mirror assembly in the y direction - it is not possible to produce the observed image structure.

A shift of the entrance aperture plates, located about 100mm in front of the telescopes - the blocking effect is asymmetric with respect to the y direction.

The effect of a rotation of the ME flap of more than 90° (88° is the nominal opening angle), such that the upper part of the flap shadows the entrance aperture of both telescopes by the same amount, has been studied. A series of simulated images has been produced at a variety of different source positions within the field of view. Figure 3 shows typical EXOSAT and simulated images for the same FOV position. A comparison of all observed and simulated images suggests that the ME flap is within the field of view of LEIT1 and LEIT2. Furthermore, under this assumption each property of the structural features listed in Section 2 can be reproduced in the simulated images.

5. Conclusion

Agreement between the observed and simulated images has been found by setting the opening angle of the ME flap at 94.5° ± 0.5°, 6.5° greater than its nominal value.

Based upon the value of 94.5° the effective throughput of the telescope is 0.721 of its nominal value for on-axis source positions, a figure in good agreement with the value of 0.735 ± 10% determined from calibration measurements of the Crab Nebula and currently used by the Observatory software for flux determination.

(This article is a summary of a report prepared by Dr B. Aschenbach of MPE, Garching, describing work carried out by him under contract to MBB, München. - D. Andrews)

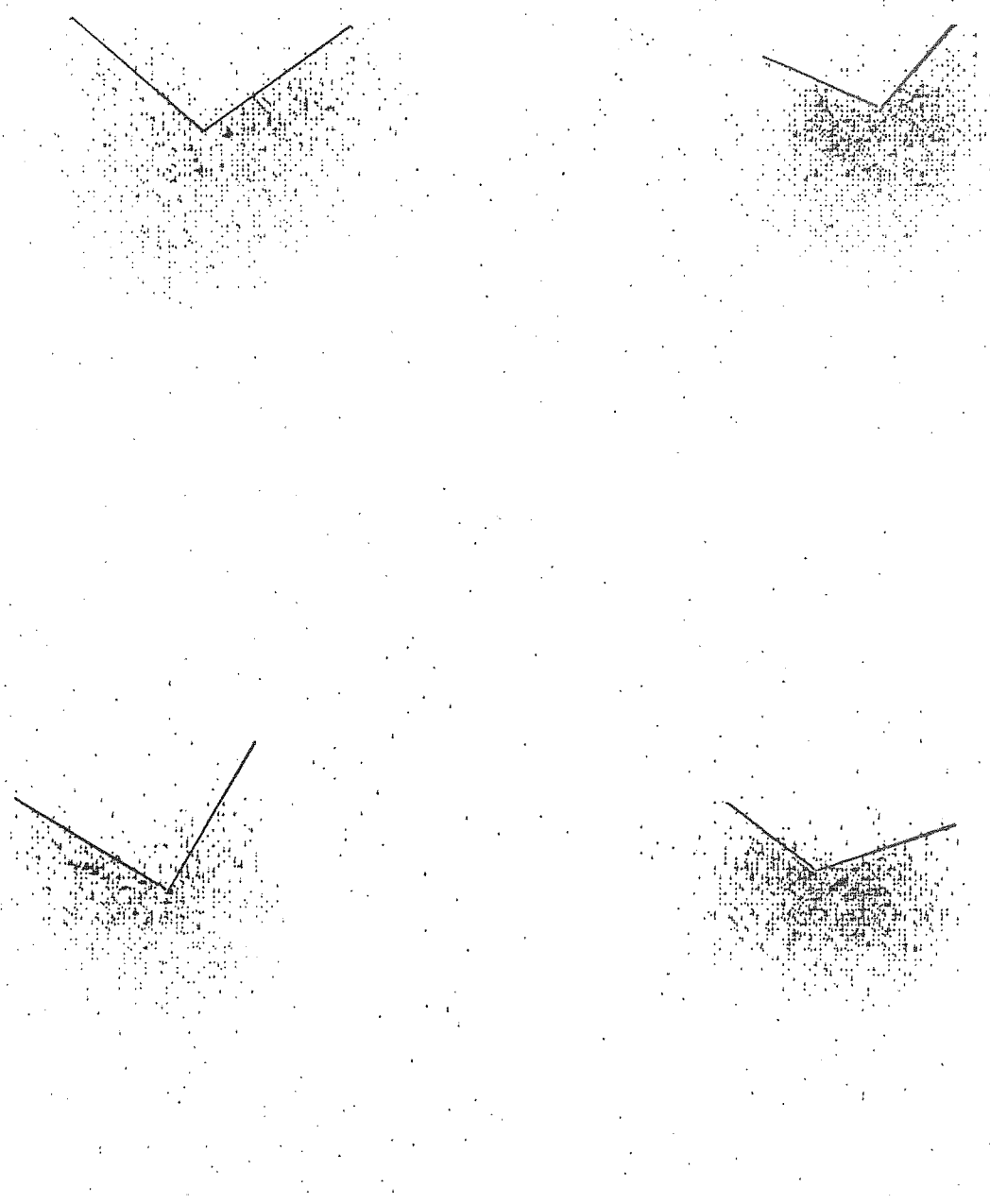

Figure 1: Typical EXOSAT LEIT1 Images showing image obscuration

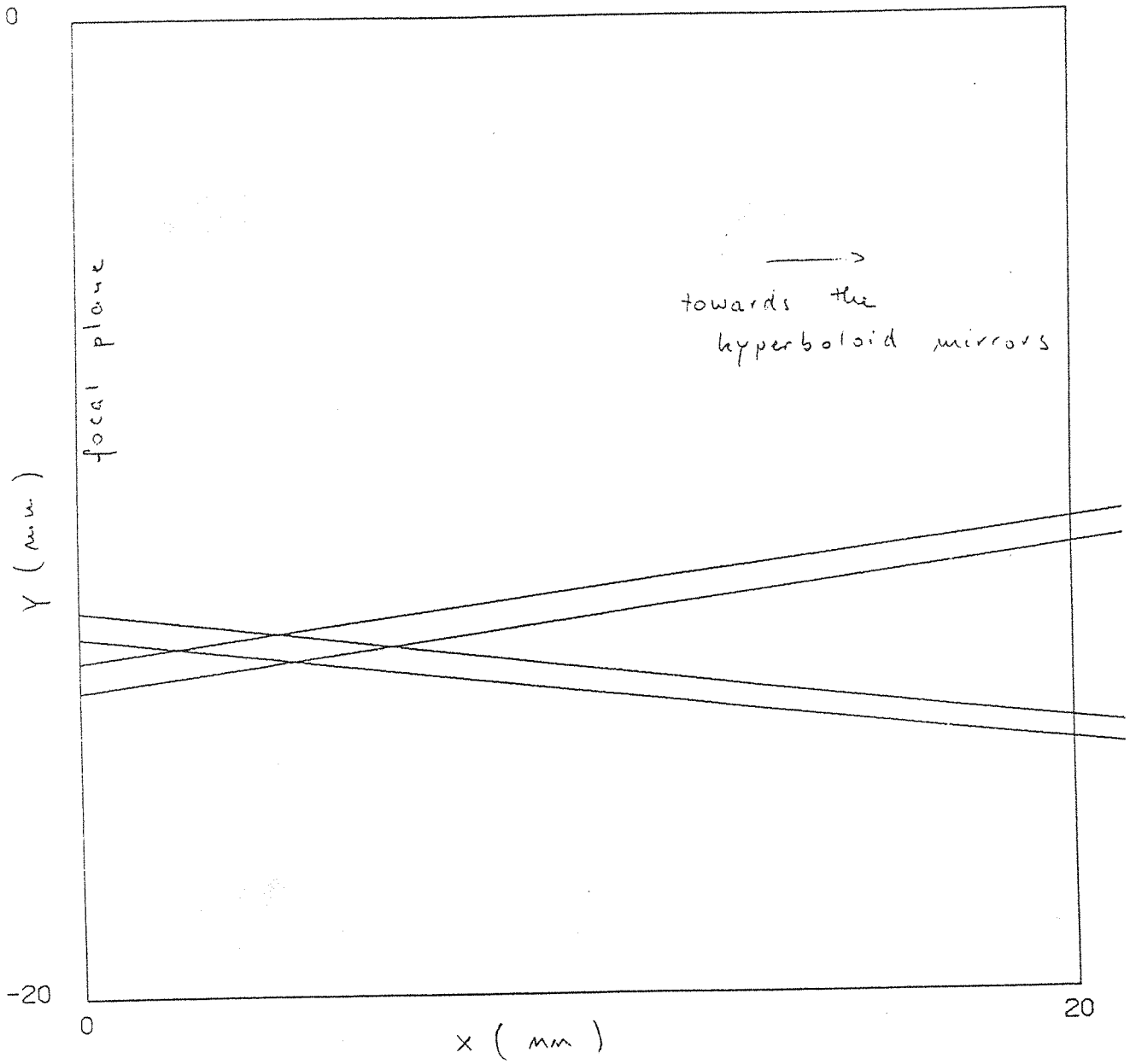

Figure 2: Off-axis X-ray light path in the outer shell of the nested mirror system

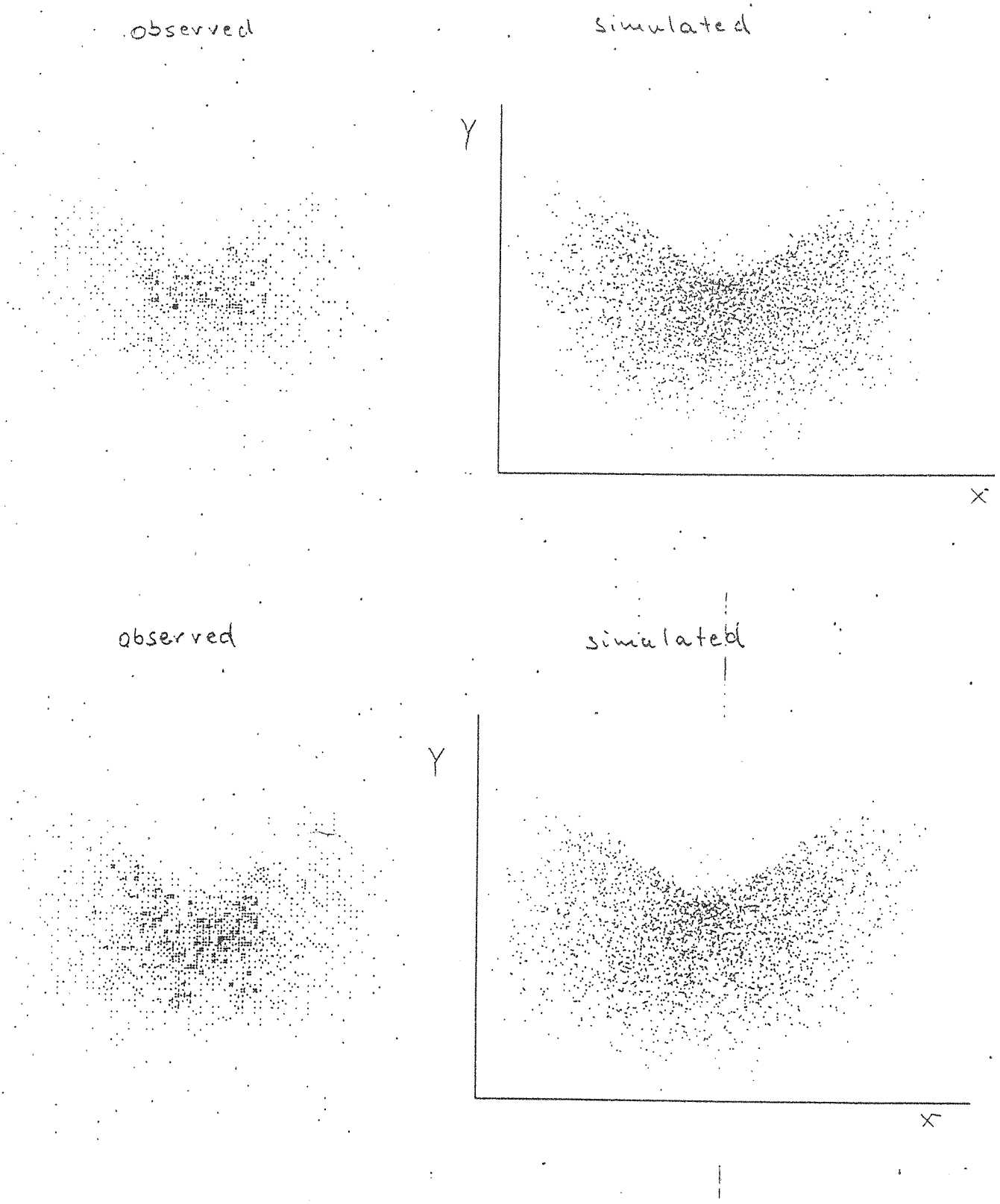

Figure 3: Comparison of observed and simulated images at same FOV position

MODIFICATION OF GSPC CALIBRATION DATA

The new effective areas as given in EXPRESS No. 11, p.66 and the coefficients for the analytical expression for the burst length efficiency (same EXPRESS p.64) have been added to the GSPC CCF.

The new data reside in the newly defined data type EA which replaces data types E1, E2.

EA contains 84 pairs of energy/area (E_i/EA_i) for burst length window open together with 5 energies E_j* and 13 coefficients P1j, P2j for the transformation to burst length windows 89-107 and 89-104.

Record 1:

Bytes 0-3	E_1
4-7	EA_1
8-11	E_2
.	
.	
248-251	E_{32}
252-255	EA_{32}

Record 2:

Bytes 0-3	E_{33}
4-7	EA_{33}
8-11	E_{34}
.	
.	
248-251	E_{64}
252-255	EA_{64}

Record 3:

Bytes 0-3	E_{65}
4-7	EA_{65}
8-11	E_{66}
.	
.	
142-145	E_{84}
146-149	EA_{84}
150-255	spare

Record 4:

Bytes 0-3	E_1*
4-7	E_2*
8-11	E_3*
12-15	E_4*
16-19	E_5*
20-23	spare
24-27	burst length window 1 lower limit
28-31	" " " 2 upper "
32-35	$P1_1$
36-39	scaling factor $S1_1$
40-43	$P1_2$
.	
.	
.	

128-131	$P1_{13}$
132-135	$S1_{13}$
136-143	spare
144-147	burst length window 2 lower limit
148-151	" " " upper "
152-155	$P2_1$
156-159	$S2_1$
.	
.	
.	
248-251	$P2_{13}$
252-255	$S2_{13}$

Units: E_i = 0.01 keV
EA_i = 0.001 cm^2
Ej* = 1.0 keV
P1, P2 = 0.001

The coefficients POL1, POl2 (subroutine GSAXE) are given by:

$$POL1_j = P1_j/10^{S1j}$$
$$POL2_j = P2_j/10^{S2j}$$

M. Gottwald

A GUIDE TO THE USE OF MHER7

As noted in Express No. 11 p.3 MHER7 is a new OBC program, developed in response to the discovery of quasi-periodic oscillations from some X-ray binary sources, which provides high time resolution (sub-millisecond) intensity samples and an option of limited energy resolution for the ME experiment data.

MHER7 gives 4-bit intensity samples, summed over a selectable time interval, in 1, 2 or 4 selectable energy ranges. The intensity is determined by counting valid events ($E \neq 0$) within the specific energy and time range (defined as a number of samples of the E channel). Since 4-bit counters are used, the maximum counts/sample is 15 and the integration time should be selected to give a count rate/sample of significantly less than 15. This can be achieved quite simply by setting the integration period to $\leq$ 14 E channel samples ($\lesssim$14 events, irrespective of input count rate). Energy ranges can be defined arbitrarily within the total spectral range from ADC channel 0 in Argon to ADC channel 127 in Xenon.

There is no selection according to detector ID and MHER7 is therefore more suited to co-aligned observations.

When configuring MHER7 care is necessary to avoid CPU overload (and the attendant problem of safety mode monitoring during an OBC 'crash' - ref. Express No.9 p.4) and TM overflow when discontinuous data would result. CPU overload errors are possible if MHER7 is running in conjunction with other CPU-intensive programs such as MHER5, or MHER4. A limit of 82% CPU usage is set by the operations team to ensure that such errors do not occur and this has the following implications:

- With MHER4 and GHEBL4 in nominal configuration and LDIR2 not running, an incident count rate of $\sim$1300 s^{-1} (summed over all Argon and Xenon detectors) will produce 82% CPU usage. With LDIR2 active, the figure drops to $\sim$1200 s^{-1}.

- Assuming a background of 600 s^{-1}, a source rate of $\sim$700 s^{-1} can therefore be accommodated.

- By processing only Argon data (ie. ignoring $\sim$ 500 s^{-1} of Xenon background) data from brighter ($\sim$1200 s^{-1}) sources can be analysed. Note that this is achieved by a switch in the ME electronics and is not a program facility.

- The incident count rate could be further reduced by operating in an offset configuration, although HTR3 may, in this case, be a better alternative.

As a guide to the use of MHER7, a typical configuration is as follows (used for an observation of EXO 0748-676):

MHER7: 0.75 msec time resolution intensity samples.
no spectral resolution

MHER5: 32 channel Argon spectrum every 1s.
32 " Xenon " " 4s.

GHEBL4: 256 channel spectrum every 8s.

LDIR2: Diamond filter

This used 95% telemetry and 80% CPU for a source strength of 100 cts s^{-1}.

Telemetry use by HER7 can be determined according to:

$$\% \text{ TM} = \frac{956 \times N}{\text{WSP2} \times \text{WSP3}}$$

where N is the number of energy ranges selected (1, 2 or 4), WSP2 is the offset between E samples (4 at 4k sampling) and WSP3 is the number of E samples summed to produce 1 intensity sample, eg. for 2 energy ranges with 4k sampling and a time resolution of 2 ms (WSP3 = 8) the telemetry used is $\sim$60%.

Note that the normal sampling of the ME energy channel for use in MHER7 is 4k s^{-1}. In principle, 8k s^{-1} would be feasible although the non-experiment sequencer samples (ref. Express No.5 p.38) at slots 1 and 257 would lead to non-uniform dead times throughout the software cycle and difficulty in interpretation of the data. Use of an 8k sample rate is therefore strongly discouraged.

D. Andrews
A. Parmar

INTERACTIVE ANALYSIS SYSTEM

There has recently been an increased demand for use of the interactive system to analyse data from an on-going observation or from one just completed. Because of the difficulty of accommodating this within the current booking system (the exact times of an observation may change at short notice), the following changes in procedures will be made:

a. One terminal on HP4 will be available for analysis of the most recent 24 hours of data. The limit of 24 hours will be strictly adhered to and data will be deleted after the interval. Formal booking is not necessary, and real time data will have an identifier RT, rather than the observer's initials: nevertheless observers must inform us by telex if they wish to use the facility. Files created during the analysis (eg. rates buffers) will be deleted overnight. In the event of a computer failure, the real time analysis may be unavailable, and this risk must be accepted by visitors, although so far the reliability of the system has been excellent.

b. One other terminal on HP4 will be for interactive analysis of FOT's. Time should be booked through S. Ernst as at present, at least 2 weeks in advance, and every booking is for only one of the periods 0800-1500 or 1500-2300. Only users with previous experience of the system will be booked for the second period. Extensions of bookings (while an observer is present at ESOC) are not automatic and must also be made through S. Ernst.

c. If, exceptionally, an observer asks for access to HP4 more than 24 hours after his observation, this must be booked in advance as in b, and not as in a.

Note that no support is provided between 2300 and 0800.

To accommodate more users simultaneously on HP4, the amount of disc storage will be increased from October 1985.

J.R. Sternberg

F O R M A T O F P R I N T E D L I N E O F A R C H I V E

The information in the data archive list is from 3 sources:

A = auxiliary data (=manoeuvre history)
F = FOT request file
- = manual (via editor) insertion

description of field	data source	printout format
start time of stable pointing	A	yy/ddd hhmm
end " " " "	A	..ddd hhmm
right ascension (of star tracker)	A	hh mm ss
declination (" " ") (RA & dec are in 1950 epoch; note that these are not the target coordinates - normally target is offset from star tracker by about 2 arc mins)	A	+/-dd mm.m
target name (left justified) (no special convention for names; the + sign to indicate a trim is always the 16th character, if present)	A	up to 16 characters
proposal code : divided into 2 fields, - class of proposal(PV ,TOO,LLX,AGN, OPS,CAL,HLX,CLU,SNR,OCC,EXG, or MIS)	F	up to 8 characters
- identification of proposal	F	
miscellaneous footnotes: 11 = solar aspect angle < 90 degs. 13 = partial data loss 19 = OBC problem or crash * = 1st pointing of multi-pointing FOT		12 = unstable attitude 18 = ME/HER4 data problem 21 = raster scan C = continuation of a '*' FOT
principal investigator (a number > 0 pointing to a table of PI's names and addresses. 0 means 'Observatory'.)	F	
4 flags for whether FOTs exist : (space means corresponding FOT doesn't exist)	F	L = LE1 available K = LE2 " M = ME " G = GS "
P.I. name (from FOT request; a blank space is shown if the request was for the Observatory, e.g. for data from performance verification phase; PI name will not be in final log, only the PI number plus list of names)	F	

EXOSAT DATA ARCHIVE

1984 day 181 to day 241 inclusive

84/232	16ØØ	232	1948	ØØ 18 28	+37 41.6	HD 1671	LLX ØØ8			134	L	MG	Praderie, F.
84/229	1Ø12	23Ø	ØØ37	ØØ 22 32	+63 51.5	TYCHO SNR	SNR G1			Ø	L	MG	
84/198	Ø157	198	1121	ØØ 26 37	+12 59.1	PG ØØ26+129	AGN 113			85	L	MG	Treves, Dr. A.
84/199	1526	199	1736	ØØ 27 28	+26 .4	PGØØ27+26Ø	LLX F132			36	L	MG	Mason, Dr. K.O.
84/212	2239	213	Ø149	ØØ 32 39	-Ø3 52.Ø	HD 3196	LLX F12Ø			81	L	MG	Bedford, Dr. D.K.
84/234	1715	234	19Ø7	ØØ 34 39	+35 7.3	HD3421	LLX ØØ8		*	134	L	MG	Praderie, F.
84/2Ø5	19Ø1	2Ø6	1229	ØØ 43 44	+2Ø 14.7	A98	CLU F1Ø			5	L	MG	Molteni, Dr. D.
84/2ØØ	1448	2ØØ	2Ø14	ØØ 5Ø 57	+12 25.7	I ZW I	AGN F21			16	L	MG	Bergeron, Dr. J.
84/23Ø	1456	232	1321	Ø1 Ø4 13	+31 53.7	LE BACK CAL	CAL			Ø	L	M	
84/234	213Ø	235	Ø126	Ø1 Ø7 Ø7	+19 23.4	HD69Ø3	LLX ØØ8		C	134	L	MG	Praderie, F.
84/21Ø	1918	211	ØØØ7	Ø1 Ø8 29	+1Ø 5.8	PG Ø1Ø8+1Ø1	LLX -1Ø1			147	L	MG	Wulf-Mathies, C.
84/224	Ø226	224	Ø957	Ø1 Ø9 25	+22 29.Ø	GCØ1Ø9+224	AGN F25			88	L	MG	Maccagni, Dr. D.
84/2Ø1	1844	2Ø1	2129	Ø1 Ø9 44	+11 8.1	PG Ø1Ø9+111	LLX 1Ø1			147	L	MG	Wulf-Mathies, C.
84/2Ø3	Ø1Ø8	2Ø3	1146	Ø1 11 21	-15 6.1	MKN 1152	AGN Ø36			8	L	MG	Pounds, Prof. K.A.
84/198	18Ø8	198	2217	Ø1 15 43	-73 42.6	SMC X-1	HLX G8			91	L	MG	Robba, Dr. R.
84/236	Ø925	236	121Ø	Ø1 2Ø 19	+Ø7 9.2	HD 8357	TOO			Ø	L	MG	
84/2Ø9	Ø6Ø5	2Ø9	1742	Ø1 33 4Ø	+2Ø 42.3	3C47	CAL			42	L	MG	Smith, Dr. A.
84/212	1642	212	1958	Ø1 39 35	-68 8.4	HØ139-68	LLX 154			63	L	MG	Beuermann, Dr. K.
84/24Ø	1355	241	Ø222	Ø1 42 55	+61 3Ø.3	4UØ142+61	HLX Ø89			Ø	L	MG	
84/224	2158	225	Ø314	Ø1 49 51	+35 54.2	A 262	CLU Ø19			119	L	MG	Mushotzky, R. F.
84/218	Ø847	218	1123	Ø1 51 29	+35 59.8	IHØ151+359	MIS Ø33			124	L	MG	Wood, Dr. K. S.
84/232	2217	233	1229	Ø2 Ø4 2Ø	+23 13.7	HD12929	LLX ØØ8			134	L	MG	Praderie, F.
84/214	Ø322	214	Ø749	Ø2 35 51	+16 24.1	Ø235+164	AGN -Ø85	11		19	L	MG	McHardy, Dr. I.
84/213	2Ø5Ø	214	Ø1Ø3	Ø3 2Ø 3Ø	-53 49.4	LB 1663	LLX -Ø95			61	L	MG	Heise, Dr. J.
84/237	Ø2Ø1	237	Ø459	Ø4 18 53	-55 3.4	NGC 1566	AGN Ø43			1Ø9	L	MG	Alloin, D.
84/225	2Ø26	226	Ø313	Ø5 36 28	-68 5Ø.4	PSRØ54Ø-69	SNR Ø23			6	L	MG	Schnopper, Prof. H.W.
84/197	171Ø	197	223Ø	1Ø 41 1Ø	-64 7.9	IC 26Ø2	LLX F14			6	L	MG	Schnopper, Prof. H.W.
84/198	1354	198	1529	11 1Ø 14	-57 59.8	4U1111Ø-58	HLX F42			55	L	MG	Van Paradijs, Dr. J.
84/187	1615	187	18ØØ	11 45 3Ø	-61 56.Ø	4U1145-619	+ HLX Ø48		*	162	L	MG	Willingale, R.
84/183	1419	183	1734	11 45 34	-61 56.1	4U1145-619	HLX Ø48			162	L	MG	Willingale, R.
84/189	1833	189	22ØØ	11 45 35	-61 56.Ø	4U1145-619	HLX Ø48			162	L	MG	Willingale, R.
84/196	2347	197	13Ø	11 49 37	-66 55.5	NOVA MUSCAE	LLX 162			152		MG	Krautter, J.
84/2Ø7	2333	2Ø8	Ø253	12 23 22	-63 17.9	ALPHA CRUC.	LLX Ø82			143	L	MG	Swank, J. H.
84/181	12ØØ	181	1257	12 26 33	+Ø2 19.Ø	3C273	AGN G16	11		25		MG	Turner, Dr. M.J.L.
84/183	ØØ55	183	Ø637	12 37 Ø5	-Ø5 4.6	NGC 4593	AGN Ø3Ø			1Ø8	L	MG	Clavel, J.
84/219	2115	22Ø	1353	12 54 2Ø	-69 1.1	2S 1254-69Ø	HLX 122			169	L	MG	Courvoisier, T.
84/2Ø1	1315	2Ø1	16ØØ	12 58 1Ø	-61 2Ø.3	GX 3Ø4-1	HLX 1Ø9			56	L	MG	Pietsch, Dr. W.
84/22Ø	1515	22Ø	182Ø	12 58 1Ø	-61 2Ø.Ø	GX 3Ø4-1	HLX 1Ø9	11		56	L	MG	Pietsch, Dr. W.
84/212	1Ø28	212	1349	12 58 13	-61 2Ø.1	GX 3Ø4-1	HLX 1Ø9			56	L	MG	Pietsch, Dr. W.
84/193	Ø531	193	Ø94Ø	13 21 46	-Ø2 3.Ø	H1325-Ø2	MIS Ø35		C	13	L	MG	Lawrence, Dr. A.
84/211	2314	212	Ø838	13 22 32	-42 45.7	CENTAURUS-A	AGN Ø65			5	L	MG	Molteni, Dr. D.
84/192	2345	193	Ø126	13 22 48	-Ø2 11.7	H1325-Ø2	MIS Ø35		C	13	L	MG	Lawrence, Dr. A.

84/213	Ø442	.213	1854	13	23	48	-47	13.2	NGC 5139	HLX	-Ø93			165	L MG Verbunt, F.
84/192	2Ø5Ø	.192	2255	13	26	31	-Ø2	33.8	H1325-Ø2	MIS	Ø35		*	13	L MG Lawrence, Dr. A.
84/193	Ø21Ø	.193	Ø439	13	3Ø	16	-Ø2	55.5	H1325-Ø2	MIS	Ø35		C	13	L MG Lawrence, Dr. A.
84/2Ø2	Ø626	.2Ø2	1336	13	33	Ø1	-34	2.8	MCG6-3Ø-15	AGN	Ø36			8	L MG Pounds, Prof. K.A.
84/2Ø1	235Ø	.2Ø2	Ø519	13	46	27	-3Ø	4.1	IC 4329 A	AGN	Ø36			8	L MG Pounds, Prof. K.A.
84/193	1153	.194	Ø439	14	15	43	+25	22.2	NGC 5548	AGN	124			66	L MG De Korte, Dr. P.A.J.
84/21Ø	Ø214	.21Ø	1644	14	44	Ø2	+Ø7	41.6	4C 7.38	AGN	-Ø81			19	L MG McHardy, Dr. I.
84/194	Ø654	.196	Ø123	15	ØØ	47	+1Ø	49.4	DEEP FIELD	DEEP	GI			1Ø3	L MG Culhane, Prof. L.
84/216	1256	.218	ØØ2Ø	15	1Ø	Ø9	-Ø8	55.1	PKS151Ø-Ø8	AGN	Ø69			112	L MG Petre, R.
84/227	Ø5ØØ	.227	1546	15	16	47	-56	58.9	CIRCINUS X-1	HLX	ØØ6			155	L MG Tennant, A. F.
84/228	Ø557	.228	2257	15	16	47	-56	58.9	CIRCINUS X-1	HLX	ØØ6			155	L MG Tennant, A. F.
84/235	1514	.235	19Ø2	15	16	48	-56	59.2	CIRCINUS X-1	HLX	ØØ6			155	L MG Tennant, A. F.
84/223	Ø239	.223	Ø82Ø	15	38	36	-52	13.7	4U1538-52	HLX	F59			5	L MG Molteni, Dr. D.
84/224	1324	.224	19ØØ	15	38	36	-52	13.7	4U1538-52	HLX	F59			5	L MG Molteni, Dr. D.
84/22Ø	2Ø15	.22Ø	2346	15	38	37	-52	13.8	4U1583-52	HLX	Ø2Ø			158	L MG Ohashi, T.
84/238	2155	.239	Ø957	15	43	29	-62	24.9	2S1543-624	HLX	Ø84			Ø	L MG
84/223	1651	.223	23ØØ	15	51	57	-53	8.1	G328.4+Ø.2	SNR	ØØ1			126	L MG Trussoni, E.
84/187	2Ø29	.188	ØØØØ	16	Ø8	52	-52	17.7	16Ø8-522	TOO			C	Ø	L MG
84/216	Ø62Ø	.216	113Ø	16	14	2Ø	-15	56.2	SCORPIUS X-1	HLX	135			68	MG Pollock, Dr. A.M.T.
84/2Ø8	Ø54Ø	.2Ø8	1135	16	26	54	+39	39.7	A2199	AGN	Ø84			19	L MG McHardy, Dr. I.
84/211	1745	.211	212Ø	16	3Ø	13	-47	16.2	163Ø-47	TOO				Ø	L MG
84/183	Ø857	.183	1147	16	3Ø	14	-47	16.4	163Ø-47	TOO				Ø	MG
84/234	12Ø9	.234	1433	16	42	Ø5	+25	2Ø.4	AH HER	LLX	F35			36	L MG Mason, Dr. K.O.
84/237	Ø72Ø	.237	1Ø1Ø	16	5Ø	11	-43	3Ø.Ø	G342.1+Ø.1	SNR	ØØ3			Ø	L MG
84/183	2Ø25	.183	2347	16	52	1Ø	+39	5Ø.Ø	MKN 5Ø1	AGN	Ø34			21	L MG Warwick, Dr. R.S.
84/2Ø1	Ø644	.2Ø1	Ø945	16	52	1Ø	+39	5Ø.Ø	MKN 5Ø1	AGN	Ø34			21	L MG Warwick, Dr. R.S.
84/191	Ø6Ø9	.191	Ø844	16	52	11	+39	5Ø.Ø	MKN 5Ø1	AGN	Ø34		*	21	L MG Warwick, Dr. R.S.
84/2Ø9	2Ø14	.2Ø9	235Ø	16	52	11	+39	5Ø.4	MKN 5Ø1	AGN	Ø34			21	L MG Warwick, Dr. R.S.
84/2Ø7	ØØ24	.2Ø7	Ø337	16	52	15	+39	46.9	MKN 5Ø1	AGN	Ø6Ø			5Ø	L MG Staubert, Dr. R.
84/235	21Ø7	.236	Ø7ØØ	16	56	Ø2	+35	25.Ø	HER X-1	HLX	114	13		167	L MG Voges, W.
84/197	13Ø9	.197	144Ø	16	56	Ø3	+35	25.1	HER X-1	HLX	114			167	L MG Voges, W.
84/238	1635	.238	1944	16	56	Ø4	+25	49.5	GL 649	LLX	148			66	L MG De Korte, Dr. P.A.J.
84/24Ø	Ø915	.24Ø	1109	16	58	52	-29	52.6	XB 1658-298	TOO				Ø	L MG
84/226	1621	.227	Ø3Ø1	17	ØØ	32	-37	46.2	4U17ØØ-37	HLX	G27			96	L MG Brinkmann, Dr. W.
84/227	1817	.228	Ø333	17	ØØ	32	-37	46.2	4U17ØØ-37	HLX	G27			96	L MG Brinkmann, Dr. W.
84/229	ØØ41	.229	Ø6Ø4	17	ØØ	32	-37	46.2	4U17ØØ-37	HLX	G27			96	L MG Brinkmann, Dr. W.
84/221	Ø219	.221	143Ø	17	11	ØØ	-33	59.7	A1711-339	HLX	1Ø5		*	Ø	L MG
84/221	1525	.222	Ø325	17	15	31	-32	7.5	2S1715-321	HLX	1Ø5		C	Ø	L MG
84/181	152Ø	.181	23Ø9	17	27	Ø2	+5Ø	15.2	I ZW 186	AGN	G18			88	L MG Maccagni, Dr. D.
84/238	Ø925	.238	14ØØ	17	28	56	-24	42.7	GX1+4	HLX	Ø82			36	L MG Mason, Dr. K.O.
84/235	Ø925	.235	1247	17	28	58	-24	42.5	GX1+4	HLX	Ø82			36	L MG Mason, Dr. K.O.
84/218	Ø3Ø9	.218	Ø6ØØ	17	29	22	-16	14.Ø	V442 OPH	LLX	Ø89			145	L MG Van der Woerd, H.
84/199	Ø115	.199	Ø545	17	29	38	-32	56.9	173Ø-33	TOO				Ø	MG
84/236	1514	.236	2322	17	35	19	-44	25.3	4U1735-44	HLX	Ø34			43	L MG Charles, Dr. P.A.
84/235	Ø351	.235	Ø652	17	42	25	+43	24.3	GL 694	LLX	148			66	L MG De Korte, Dr. P.A.J.
84/239	1222	.24Ø	Ø512	17	55	18	-33	48.4	4U1755-33	HLX	Ø87			Ø	L MG
84/185	1ØØ2	.185	1Ø12	18	14	54	+49	51.1	AM HER	HLX	Ø63			61	MG Heise, Dr. J.
84/184	Ø927	.184	13Ø8	18	14	55	+49	5Ø.6	AM HER	HLX	Ø63			61	L MG Heise, Dr. J.
84/214	1951	.214	22Ø6	18	14	58	+49	5Ø.6	AM HER	HLX	-Ø63			61	L MG Heise, Dr. J.
84/2Ø8	14Ø6	.2Ø9	Ø4ØØ	18	17	5Ø	+5Ø	29.7	4C 5Ø.44	AGN	Ø81			19	L MG McHardy, Dr. I.
84/189	Ø539	.189	Ø83Ø	18	21	33	+64	2Ø.1	K 1-16	LLX	Ø68			73	L MG Barstow, Dr. M.A.
84/2Ø2	163Ø	.2Ø2	2234	18	46	Ø8	-78	36.1	H1846-786	AGN	Ø36			8	L MG Pounds, Prof. K.A.

84/215	2334..216	Ø4ØØ	19	Ø1	Ø9	+69	52.7	A 2315		CLU	Ø12			3	L MG	McKechnie, Dr. S.P.
84/215	145Ø..215	1818	19	23	5Ø	+42	4Ø.8	RR LYR		LLX	Ø85			133	L MG	Jameson, Dr. R. F.
84/223	1136..223	1344	19	24	Ø2	+27	15.4	NOVA VUL.		TOO				Ø	L MG	
84/189	1Ø44..189	1527	19	56	27	+35	3.7	CYGNUS X-1		TOO				Ø	L MG	
84/19Ø	ØØ42..19Ø	Ø535	19	56	27	+35	3.7	CYGNUS X-1		TOO				Ø	L MG	
84/191	1113..191	1648	19	56	27	+35	3.6	CYGNUS X-1		TOO			C	Ø	L MG	
84/2Ø6	15Ø1..2Ø6	22ØØ	19	56	28	+35	3.9	CYGNUS X-1		CAL	GS-M			Ø	MG	
84/233	1534..233	19ØØ	2Ø	22	Ø8	+46	2Ø.9	LANNING 9Ø		LLX	Ø63			141	L MG	Cook, M. C.
84/2Ø7	Ø614..2Ø7	Ø9ØØ	2Ø	22	Ø9	+46	2Ø.4	LANNING 9Ø		LLX	Ø63	19		141	L MG	Cook, M. C.
84/214	11Ø3..214	1634	2Ø	3Ø	37	+4Ø	46.9	4U2Ø3Ø+4Ø		HLX	-F24			58	L MG	Van der Klis, Dr. M.
84/19Ø	235Ø..191	Ø248	2Ø	37	32	-Ø1	3.Ø	AE AQR		LLX	G15			Ø	L MG	
84/199	Ø9ØØ..199	1229	2Ø	47	15	+45	55.4	HD 198478		LLX	F3			64	L MG	Zwaan, Dr. C.
84/182	1534..182	22ØØ	2Ø	52	43	+31	43.Ø	CYGNUS LOOP		SNR	F24			41	L MG	Arnaud, Dr. M.
84/19Ø	143Ø..19Ø	2Ø33	2Ø	54	Ø4	+3Ø	39.8	CYGNUS LOOP		SNR	F24			41	L MG	Arnaud, Dr. M.
84/2Ø4	Ø4Ø7..2Ø4	Ø6ØØ	21	Ø2	ØØ	+41	25.5	HD 2ØØ723		LLX	G11			64	L MG	Zwaan, Dr. C.
84/182	Ø144..182	1252	21	27	31	+11	56.9	X2127-119		HLX	Ø54			163	L MG	Redfern, R. M.
84/192	Ø444..192	Ø63Ø	21	36	22	+61	51.2	HD 2Ø6165		LLX	F3			64	L MG	Zwaan, Dr. C.
84/241	Ø435..241	18ØØ	21	4Ø	41	+43	22.2	SS CYG		LLX	Ø69		*	57	L MG	Watson, Dr. M.G.
84/241	1829..242	ØØØ1	21	4Ø	43	+43	21.7	SS CYG		LLX	Ø69		C	57	L MG	Watson, Dr. M.G.
84/2Ø5	Ø239..2Ø5	1636	21	42	35	+38	5.4	CYG X-2		CAL	GS-M			Ø	L MG	
84/187	Ø3Ø4..187	13Ø8	22	Ø6	37	+45	29.7	AR LAC	+	LLX	135		C	226	L MG	White, Dr. N.
84/185	1334..187	Ø238	22	Ø6	41	+45	3Ø.5	AR LAC		LLX	135		*	226	L MG	White, Dr. N.
84/222	Ø631..222	Ø937	22	44	39	+44	4.7	GL 873		LLX	171			154	L MG	Schmitt, J. H.
84/192	ØØ23..192	Ø226	22	51	24	-17	5Ø.7	MR2251-179		AGN	F4			8	L MG	Pounds, Prof. K.A.
84/184	Ø25Ø..184	Ø614	23	ØØ	42	+ØØ	36.7	NGC 7469		CAL				Ø	L MG	
84/19Ø	Ø839..19Ø	1134	23	ØØ	42	+ØØ	36.3	NGC 7469		CAL				Ø	L MG	
84/191	1959..191	22Ø3	23	ØØ	42	+ØØ	36.3	NGC 7469		CAL				Ø	L MG	
84/188	Ø415..188	Ø629	23	ØØ	44	+ØØ	36.8	NGC 7469		CAL				Ø	L MG	
84/188	Ø9Ø2..188	1132	23	19	42	+4Ø	34.7	NGC764Ø		EXG	F14			31	L MG	Gregorini, Dr. L.
84/219	1321..219	18Ø6	23	35	Ø5	+46	11.4	LAMDA AND		LLX	F5			84	L MG	Brinkman, Dr. A.C.
84/225	Ø6Ø6..225	1758	23	52	24	+28	21.7	II PEG		LLX	143			Ø	L MG	
84/2ØØ	2239..2Ø1	Ø349	23	55	23	-35	1.2	IH2355-35Ø		MIS	Ø33			124	L MG	Wood, Dr. K. S.

OBSERVATORY TEAM

		Ext.
David Andrews	Observatory Manager	705*
Julian Sternberg	Observatory Software	703
Julian Lewis	System Software/HP Computers	702
Nick White	Senior Observatory Scientist	764
Paul Barr	Duty Scientist/Mission Planning	711
Paolo Giommi	"	710
Manfred Gottwald	"	758
Julian Osborne	"	714
Arvind Parmar	"	763
Luigi Stella	"	715
Anne Fahey	Mission Planning	707
Paolo Ferri	Observatory Controller	716
Maria Gonano	" "	427
Frank Haberl	" "	717
Antonella Nota	" "	717
Mark Sweeney	" "	716
Susanne Ernst	Data Assistant	713
Margit Farkas	" "	709
Grazia Giommi	" "	709
Sandra Andrews	Secretary	704

*Direct dialling to any extension, prefixed by 886, is possible, eg. 06151-886-705

Personnel Changes (1.7.85 - 31.8.85)

G. Mellor has resigned his position as Observatory Controller.

Dr E. Gronenschild has resigned his position as Duty Scientist.

CAMBRIDGE DISCUSSION MEETING

ON

EXOSAT RESULTS

5 and 6 November 1985

At the request of the organisers, it is a pleasure to announce an informal meeting on scientific results from EXOSAT to be held at the Institute of Astronomy, Cambridge. There will be no registration fee or published proceedings. Attendance will be limited to about 80 people. It is hoped to select and schedule 20 contributed talks of half an hour in length. If you wish to give one of these talks, please submit an abstract with your application. It is essential that overnight accommodation (estimated cost approx. 30 pounds per night per person), is booked early and those wishing to attend are urged to return the application form to Professor Fabian at the address below as soon as possible. A further mailing to those who reply will be made in early October.

I hope to attend the Cambridge Discussion Meeting on EXOSAT Results (5/6 November 1985)

NAME: .....

ADDRESS: .....

.....

.....

Overnight accommodation (bed & breakfast) required for:

4, 5, 6 November (Please circle)

Abstract enclosed: YES/NO

TITLE: .....

.....

Professor A. Fabian, Institute of Astronomy, Madingley Road, Cambridge CB3 OHA, United Kingdom.

EUROPEAN SPACE AGENCY

Vacancy at the European Space Operations Centre (ESOC)

at Darmstadt, (Germany)

POST	Supernumerary post in scientific operations - Resident Astronomer/Duty Scientist at the EXOSAT Observatory.
GRADE	A2 in the Coordinated Organisations' salary scale
LOCATION	ESOC, Darmstadt, West Germany.
DUTIES	The Resident Astronomer/Duty Scientist will work within the EXOSAT Observatory team at ESOC and be affiliated to the Astrophysics Division of the Space Science Department in the Scientific Programmes Directorate. Support duties will include operational support to the conduct of real-time operations, support to, and development of, the interactive data analysis system, instrument calibration and performance overview, data base maintenance and archive retrieval. The successful applicant will be required to participate actively in the research activities of the Observatory team and will be expected to propose programmes in response to announcements of opportunity for EXOSAT observations.
QUALIFICATIONS	Applicants should hold a Ph.D or equivalent degree in astronomy and preferably have a thorough knowledge of X-ray astrophysics. They should be experienced in data analysis and scientific programming for mini- and main-frame computers. A good knowledge of either English or French is required together with a working knowledge of the other language.

Applications for this post should be addressed to the Head of Personnel, ESOC, Robert Bosch-Strasse 5, 61 Darmstadt, Germany.

THE EUROPEAN SPACE AGENCY

The European Space Agency has a number of vacancies in Scientific positions as follows:

ASTROPHYSICS DIVISION, SPACE SCIENCE DEPARTMENT

at ESTEC, Noordwijk, The Netherlands

Research Fellowship Positions (PhD or equivalent) in:

Optical Astronomy – Observational astronomy using the ESA photon counting system developed for the Space Telescope and the development of detector systems for future space astronomy missions.

X-ray Astronomy – Development of imaging detectors for future space astronomy missions with participation in the analysis of EXOSAT data.

Submillimetre Astronomy – Development of a super-heterodyne system for ground-based submillimetre astronomy, participation in observational campaigns and data analysis.

Gamma-ray Astronomy – Development of the COMPTEL instrument for the Gamma Ray Observatory mission and data analysis.

The research fellowship positions at ESTEC are normally limited to a duration of two years.

Salary, will depend on qualifications, experience, marital status etc.

A good knowledge of English or French is required, with a working knowledge of the other language.

Applications should be directed to the Head of Personnel, ESTEC, Postbus 299, 2200 AG Noordwijk, The Netherlands, including detailed curriculum vitae and stating for which post(s) they wish to be considered. For enquiries phone 1719-83308 or 1719-83556.

EUROPEAN SPACE AGENCY

Vacancy at the European Space Research and Technology Centre (ESTEC) at Noordwijk, The Netherlands

POST	Scientist in the Astrophysics Division, Space Science Department, Directorate of Scientific Programmes.
GRADE	This post is classified in the A2/A4 grade band of the Coordinated Organisations' scale.
LOCATION	ESTEC, Noordwijk, The Netherlands.
DUTIES	The duties involve: - carrying out project and/or study scientist work in connection with approved ESA scientific missions and studies for future missions in astrophysics. In particular, the scientist would be engaged in the support of the EXOSAT on-going mission and the cornerstone future-mission in high-throughput X-ray spectroscopy. - carrying out research in X-ray astronomy with emphasis on analysis and interpretation.
QUALIFICATIONS	Applicants should hold a Ph.D or equivalent degree in physics or astronomy with some years of post-doctoral experience in X-ray astronomy. Good knowledge of English or French; some knowledge of the other language desirable.
CLOSING DATE	Applications for this post should reach the Head of Personnel, ESTEC, Keplerlaan 1, 2201 AZ Noordwijk ZH, The Netherlands, quoting reference 59/85, not later than the 23rd October 1985.

ESA Regulations exclude the recruitment of personnel aged over 55

EUROPEAN SPACE AGENCY

Vacancy at the European Space Research and Technology Centre (ESTEC) at Noordwijk, The Netherlands

POST	Scientist in the Astrophysics Division, Space Science Department, Directorate of Scientific Programmes.
GRADE	This post is classified in the A2/A4 grade band of the Coordinated Organisations' scale.
LOCATION	ESTEC, Noordwijk, The Netherlands.
DUTIES	The duties involve: - carrying out project and/or study scientist work in connection with approved ESA scientific missions and studies for future missions in astrophysics. In particular, the scientist would be engaged in the support of the ISO mission with regard to the focal plane instruments through all development and operation phases. - carrying out research in infra-red/sub-mm heterodyne astronomy with emphasis on instrument development and observational work.
QUALIFICATIONS	Applicants should hold a Ph.D or equivalent degree in physics or astronomy with experience in infra-red detector technology and cryogenics. Good knowledge of English or French; some knowledge of the other language desirable.
CLOSING DATE	Applications for this post should reach the Head of Personnel, ESTEC, Keplerlaan 1, 2201 AZ Noordwijk ZH, The Netherlands, quoting reference 58/85, not later than the 23rd October 1985.

ESA Regulations exclude the recruitment of personnel aged over 55

QUESTIONNAIRE

☐ There is an error/change of address on the current mailing list; the correct version is given below.

☐ Please add my name and address (printed below) to the EXOSAT Express mailing list.

☐ Please delete my name and address (printed below) from the EXOSAT Express mailing list.

NAME: _____

ADDRESS: _____

_____

_____

_____

Tear off the page and return to: EXOSAT Observatory, ESOC,
Robert Bosch Str. 5,
6100 Darmstadt, W. Germany.